FUNCTIONAL CHARACTERIZATION OF T-TYPE CALCIUM CHANNELS IN AREA CA3 OF THE HIPPOCAMPUS

by

Aqsa Malik

B.Sc., University of Toronto, 2008

M.Sc., University of Toronto, 2010

A DISSERTATION SUBMITTED IN PARTIAL FULFILLMENT OF

THE REQUIREMENTS FOR THE DEGREE OF

DOCTOR OF PHILOSOPHY

in

THE FACULTY OF GRADUATE AND POSTDOCTORAL STUDIES

(Neuroscience)

THE UNIVERSITY OF BRITISH COLUMBIA

(Vancouver)

October 2015

Abstract

Calcium (Ca^{2+}) entry through voltage-gated Ca^{2+} channels in dendrites of hippocampal pyramidal cells (PCs) contributes to synaptic depolarization and activation of downstream pathways that regulate many aspects of synaptic and cellular function. Activated by small depolarizing changes in voltage, T-type Ca^{2+} channels mediate low-threshold spikes (LTS) that drive the resting membrane potential towards action potential threshold. T-type Ca^{2+} channels are hypothesized to contribute to subthreshold synaptic depolarization in the CA3 subfield of the hippocampus due to the stratified nature of inputs on CA3 dendrites. While T-type Ca^{2+} channels are densely expressed in area CA3, their functional characteristics and interactions with postsynaptic receptors are not well understood and LTS have not been reported in CA3 PCs.

In Chapter 3, using whole-cell electrophysiology, we demonstrate that LTS in CA3 PCs can be evoked by somatic current injection. LTS were only evoked when 4AP was applied to depress A-type K^+ channels. Using specific pharmacological blockers, we show that $Ca_v3.2$ channels mediate LTS in CA1 and CA3 PCs. In Chapter 4, using two-photon Ca^{2+} imaging, we map the subcellular distribution of $Ca_v3.2$ channels in hippocampal PCs. Our results show that $Ca_v3.2$ channel expression is restricted to the soma and proximal dendrites in CA1 PCs, while Ca^{2+} influx from $Ca_v3.2$ channel activation occurs in distal (>50 μm) regions of CA3 PC dendrites.

In Chapter 5, we demonstrate that mAChR stimulation potentiates LTS amplitude and such amplification of Ca^{2+} influx through $Ca_v3.2$ channels is dependent on M-current inhibition. Furthermore, we show that application of *t*-ACPD causes potent and rapid inhibition of LTS propagation. This inhibition occurs exclusively through $mGlu_1$ receptors and downstream

activation of PKC is necessary for this process. Lastly, in Chapter 6, we show boosting of subthreshold synaptic signals by T-type Ca^{2+} channels in PCs within area CA3 but not CA1.

Taken together, our data identify a new T-type mediated Ca^{2+} signaling pathway in CA3 PC dendrites that is unlocked by A-type K^+ channel blockade, potentiated by mAChR activation, and inhibited by $mGluR_1$ activation. Furthermore, our study highlights the important involvement of T-type Ca^{2+} channels in enhancing dendritic depolarization in CA3 PCs.

Preface

I was jointly responsible with Dr. Brian MacVicar in the research design; however, I was solely responsible for carrying out all the experiments and data analysis presented in this dissertation.

All animal work conducted for this dissertation was approved by the UBC Animal Care Committee under certificates A11-0031 and A11-0116.

Table of Contents

List of Figures

List of Abbreviations

4AP	4-aminopyridine
bAP	Back-propagating action potential
BAPTA	1,2-bis(o-aminophenoxy)ethane-N,N,N,N-tetraacetic acid
BK	Big conductance K^+ channel
CA1	Cornu Ammonis 1
Ca^{2+}	Calcium
CA3	Cornu Ammonis 3
DG	Dentate Gyrus
EGTA	Ethylene glycol tetraacetic acid
EPSC	Excitatory postsynaptic current
EPSP	Excitatory postsynaptic potential
GABA	Gamma-Aminobutyric acid
GIRK	G-protein-coupled inwardly rectifying K^+ channel
GPCR	G-protein-coupled receptor
HCN	Hyperpolarization-activated cyclic nucleotide-gated
HVA	High voltage-activated
IPSP	Inhibitory postsynaptic potential
I-V	Current-voltage relationship
LTD	Long-term depression
LTP	Long term potentiation
LTS	Low threshold spikes
LVA	Low voltage-activated

mAChR	Muscarinic acetylcholine receptor
mGluR	Metabotropic glutamate receptor
MCO	Metal-catalyzed oxidation
MS-DBB	medial septum-diagonal band of Broca
NMDA	N-methyl-D-aspartate
PC	Pyramidal cell
PKC	Protein Kinase C
PLC	Phospholipase C
sI/O	Subthreshold input-output
SK	Small conductance K^+ channel
TTX	Tetrodotoxin
VGCC	Voltage-gated Ca^{2+} channel

Acknowledgements

I would like to thank my thesis advisor Dr. Brian MacVicar for his excellent guidance and supervision. Your passion for scientific research and dedication towards cultivating a vibrant neuroscience community in Canada is particularly inspiring. I am astounded by how much you have accomplished and how you continue to make meaningful contributions to the field. I am deeply appreciative of your approach towards supervising students. You always make time to discuss data, revise my work, and respond to all my inquiries instantly. I would also like to thank my committee members Dr. Terry Snutch, Dr. Jeremy Seamans, and Dr. Yu Tian Wang for their unrelenting support and innovative advice for my project.

I am grateful of the various organizations that financially supported my PhD training including: NSERC Postgraduate Scholarship, the University of British Columbia Four-Year Fellowship, and the Heart and Stroke Foundation of Canada Doctoral Award.

I had the amazing opportunity to learn from a dedicated group of colleagues throughout the course of my doctoral education. In particular, I am thankful for the support of Eli York, Jasmin Hefendehl, Jingfei Zhang, Lasse Dissing-Olesen, LP Bernier, Ravi Rungta, and Rebecca Ko. My education was enriched through the interesting collaborations and discussions that I had with all of you. Each of you helped me troubleshoot experiments at some point and encouraged me to keep trying when experiments inevitably failed. I would also like to express my sincere gratitude to Jeff LeDue for his enthusiasm towards solving problems and willingness to answer my questions so quickly.

Thank you to my family and friends for supporting all my pursuits, keeping my spirits up, and encouraging me to tackle challenges. Thank you to my parents for instilling my love of learning and giving me the opportunity to obtain an excellent education. Thank you to my siblings for showing me the power of resiliency and being my cheerleaders. Lastly, I would like to thank my husband, Matthew, for giving me invaluable feedback on all my research efforts. Without your patience and unconditional support, I could not have finished this dissertation.

For R.M., T.M., H.M. and my parents.

For always being there.

Chapter 1: Introduction

1.1 Hippocampal circuitry

The work detailed in this thesis was carried out exclusively in the rodent hippocampus, a heavily studied brain region associated with learning and memory, as well as various other behavioural phenotypes. Together with additional brain structures, the hippocampus forms part of the limbic system and is one of the oldest parts of the brain phylogenetically (Cherubini and Miles 2015). The hippocampal formation is a compound structure consisting of the dentate gyrus (DG), the hippocampus proper (comprised of Cornu Ammonis 1 (CA1), CA2, and CA3), the subiculum, presubiculum and parasubiculum, and the entorhinal cortex. CA regions of the hippocampus proper are organized depth-wise in clearly defined strata that include the alveus – one of the major outputs of the hippocampus, stratum oriens – containing basal dendrites of pyramidal cells (PCs) and interneurons, stratum pyramidale – containing cell bodies of PCs, stratum lucidum – containing mossy fibers from dentate gyrus granule cells (only found in CA3), stratum radiatum – containing septal, commissural, and collateral fibers in addition to apical dendrites of PCs, and lastly, stratum lacunosum-moleculare – containing perforant path fibers from the entorhinal cortex.

The hippocampal formation is located in the medial temporal lobe, beneath the cortical surface of the brain. In addition to being critical for learning and memory, the hippocampal formation contributes to various adaptive behaviours by integrating information along the septo-temporal axis via anatomical connections to cortical and subcortical structures. These projections arise from the entorhinal cortex, neocortex, amygdala, basal forebrain, hypothalamus, thalamus, and

brain stem. Inputs to the hippocampus are distributed along the septo-temporal axis in a variable manner such that olfactory and gustatory inputs are distributed evenly, while connections from the visual, auditory, and somatosensory neocortices decline in density from the septal to the temporal pole and are restricted to the septal and intermediate hippocampus (Bast 2007). Similarly, connections from the prefrontal cortex and subcortical structures that link the hippocampus to emotional, motivational, and executive processes are mainly restricted to temporal and intermediate hippocampus (Bast 2007). Thus, the rapid encoding and retrieval of information, a hallmark feature of hippocampal function, is transferred into adaptive behaviours via connections (sometimes reciprocal) to cortical and subcortical sites that govern emotional, executive, and motor processes.

Intrinsic connections between regions of the hippocampus proper have been described in detail (Andersen *et al.* 1971). The unidirectional flow of information from dentate gyrus to CA3, from CA3 to CA1 via Schaffer collaterals, and CA1 to subiculum is a useful organizing principle; however, recent studies show that far from being an excitatory feed-forward loop, communication within the circuit is not exclusively excitatory or unidirectional (Jackson *et al.* 2014). Intrahippocampal synchrony occurs through state-dependent bidirectional communication between CA1, CA3, and the subiculum, and it is mediated by long-range inhibitory connections (Jackson *et al.* 2014, Thuault 2014).

1.1.1 Synaptic connectivity in area CA3

Neocortical information is conveyed directly to hippocampal CA3 PCs via perforant path fibers from the entorhinal cortex making connections in stratum lacunosum-moleculare, and indirectly through mossy fibers of granule cells that synapse in the stratum lucidum (Henze *et al.* 1996). Commissural/associational fibers from contra- and ipsi-lateral CA3 PCs synapse on both the mid-apical and basal dendritic arborization in stratum radiatum and oriens, respectively (Henze *et al.* 1996). In addition, axons of PCs in CA3 region of the hippocampus excite other PCs and interneurons. Before projecting into the ipsilateral (Schaffer collaterals) and contralateral (commissural fibres) CA1 region, axons of CA3 PCs ramify in stratum radiatum and oriens of CA3 and synapse onto the apical and basal dendrites of neighbouring PCs as well as interneurons (Le Duigou *et al.* 2014).

Referred to as recurrent collaterals, these fibres divide into 5-10 collaterals and project in different directions to synapse onto other CA3 PCs. Recurrent collaterals of a given neuron remain predominantly in the same subfield of CA3 as their parent cell but seldom synapse back onto the parent cell (Li *et al.* 1994). The properties of recurrent synapses differ significantly from mossy fiber inputs, which are the other main source of excitation of CA3 PCs. Mossy fibers contact apical dendrites of CA3 PCs close to the soma through specialized giant mossy fiber boutons (5-8 μm), while recurrent collaterals synapse onto more distal dendrites (Amaral and Dent 1981). Further, recurrent collaterals make several thousand connections with a large population of CA3 PCs while mossy fibers only make 10-20 contacts with different CA3 PCs (Claiborne *et al.* 1986). Functionally, this translates into deterministic firing of CA3 PCs by granule cells because the latter can drive firing of CA3 PCs with high reliability. As such, the

mossy fiber synapse is a ‘detonator’ synapse reflecting its ability to control the activity of CA3 PCs without coordinated input from various other synapses on more distal dendritic sites (Engel and Jonas 2005). This activation of CA3 PCs with high temporal precision provides the ‘Hebbian’ postsynaptic depolarization required to strengthen perforant path and/or commissural/associational synapses onto CA3PCs (Magee and Johnston 1997).

1.2 Coherent population synchrony in area CA3

Relative to other hippocampal regions, internal connectivity is denser in the CA3 subfield (Cherubini and Miles 2015). Recurrent excitatory synapses between CA3 cells form an associative network that has critical roles in encoding spatial representations and episodic memories (Le Duigou *et al.* 2014). The associative recurrent network also generates coherent oscillations including gamma, theta and sharp-waves that are implicated in coordinating the firing of disparate neuronal ensembles during specific behavioural conditions. An uncomplicated synchronized electroencephalographic activity easily recorded from the mammalian brain is the rhythmic slow activity (theta) of the limbic system (Kowalczyk *et al.* 2013).

Generally, theta waves (4-7 Hz) are absent during resting states and present during REM sleep and various locomotor activities (e.g. exploratory, orienting, etc.). Theta oscillations can be detected in the dentate gyrus and CA3; however the largest amplitude and most regular frequency theta is measured in stratum lacunosum-moleculare of area CA1 (Buzsaki 2002). Along the longitudinal axis of the hippocampus, theta waves are similar in phase and amplitude within a given strata, but vary depth-wise in both amplitude and phase between different layers (Buzsaki 2002). Oscillations in the theta frequency and neuronal discharge that is phase-locked

to theta waves have been observed in the entorhinal cortex, subiculum, amygdala, and cingulate cortex; however, none of these regions are capable of generating theta activity in isolation and oscillations in these structures are not coherent with hippocampal theta activity. In contrast, hippocampal PCs are capable of generating their own theta fields *in vitro*.

1.2.1 Role of CA3 recurrent collaterals in theta generation

Intact connectivity between the hippocampus and medial septum-diagonal band of Broca (MS-DBB) is required for generation of extracellular theta waves in the hippocampus. Pharmacological blockade or lesions of MS-DBB neurons abolish theta oscillations in the hippocampus and cortical structures, as such, this subcortical nucleus is implicated as the ultimate rhythm generator of theta that modulates activity in the hippocampus (Petsche *et al.* 1962). It is unclear, as of yet, whether MS-DBB has pacemaker properties or whether hippocampal and entorhinal feedback is required for coherent activity in MS-DBB neurons (Buzsaki 2002). The classic theta model posits that all principal cells of the hippocampus receive excitatory input from perforant path fibers (CA1 and CA3 PC also receive respective excitatory inputs from Schaffer and recurrent collaterals) and inhibitory input from the septum. The summed activity of IPSPs in the somata and EPSPs in the dendrites of hippocampal PCs results in two "current generators" – intrinsic membrane conductances that determine the magnitude of the measured theta field (Buzsaki 2002).

In the local CA1 field circuitry, the two current generators include an inhibitory dipole at the soma and an active current sink at the distal dendrites. The coordinated activity between these dipoles underlies the precise amplitude and phase profiles of hippocampal theta waves (Stewart

and Fox 1990). This means that the maximum extracellular current flow results from coincident dendritic excitation and somatic inhibition that corresponds to the trough of theta in stratum lacunosum-moleculare (current sink from perforant path input onto distal dendrites) and the peak of theta in stratum pyramidal/oriens (current source from inhibitory septal input at the soma). In addition, cholinergic neurons of the MS-DBB act as "rhythm generators" – cooperative mechanisms that lead to rhythm generation and control the frequency and pattern of oscillations (Buzsaki 2002). Cholinergic MS-DBB neurons have a slow depolarizing influence on both PCs and interneurons. Specifically, tonic cholinergic excitation combined with phasic septal inhibition leads to rhythmic activity in interneurons, which in turn, results in the generation of rhythmic IPSPs in hippocampal PCs that are targeted by interneurons (Toth *et al.* 1997).

This model fails to take into account the cell-specific intrinsic resonant properties that allow neurons to oscillate independent of postsynaptic potentials. Further, recent research has shed light on the importance of CA3 recurrent collateral system in theta generation. Occurrence of theta fields in CA1 neurons coincides with a measurable current sink in stratum radiatum of CA1 region, implicating the direct contribution of CA3 PCs to theta activity recorded in CA1. Activity in a small percentage of CA3 PCs is sufficient to induce theta fields in CA1 neurons because the magnitude of the sink observed in CA1 stratum radiatum is small and CA3 PCs discharge in the same theta phase as CA1 PCs (Fox *et al.* 1986). This is further demonstrated by the observation that theta oscillations are dependent on an intact CA3 after surgical removal of the entorhinal cortex. Under these conditions, theta activity in all layers of the CA1 and CA3 subfields are highly coherent with each other (Bragin *et al.* 1995). Comparison of theta signals between strata in the intact brain shows that coherence between CA1 stratum radiatum and stratum lacunosum-

moleculare is low and inversely correlated, while the inner third of dentate molecular layer and CA1 stratum radiatum are highly coherent (Kocsis *et al.* 1999). Because intrahippocampal associational fibers project to CA1 stratum radiatum, it is suggested that the recurrent collateral network of CA3 with a possible contribution from hilar mossy cells comprises an intrahippocampal oscillator (Buzsaki 2002). This intrinsic hippocampal oscillator is dependent on input from the entorhinal cortex and MS-DBB because theta oscillations in CA3 neurons are abolished by atropine. Atropine-sensitive intrahippocampal theta is observed during the complete absence of movement and occurs during autonomic activities that include licking and chewing (Kowalczyk *et al.* 2013).

Theta activity has been studied in detail in isolated hippocampal slice preparations. The muscarinic antagonist atropine sulphate but not the nicotinic blocker tubocurarine can block carbachol-induced theta *in vitro* (Konopacki *et al.* 1987). Further, carbachol concentrations that are not sufficient to produce theta *in vitro*, when combined with $GABA_A$ antagonists, can induce theta activity in isolated hippocampal slices (Konopacki and Golebiewski 1993). Theta induction by combined carbachol and $GABA_A$ antagonist treatment is blocked by both atropine sulphate and muscimol – a selective agonist of $GABA_A$ receptors (Konopacki and Golebiewski 1993). This presents the main difference between theta recorded *in vitro* and *in vivo* – activity in interneurons is not essential for maintenance of theta rhythm *in vitro* (MacVicar and Tse 1989). Theta oscillations have also been observed in organotypic hippocampal slice cultures and in co-cultures of the hippocampus and septum (Fischer *et al.* 1999). In the latter preparation, simply enhancing spontaneous release of acetylcholine by blocking the enzyme acetylcholine esterase generates theta-like rhythmic activity (Fischer *et al.* 1999). The magnitude of theta activity

recorded *in vitro* is much larger compared to observations *in vivo* (Traub *et al.* 1992). Further, theta oscillations observed *in vivo* are continuous; in contrast, theta activity *in vitro* is restricted to a limited number of cycles. It has been suggested that acetylcholine diminishes glutamate release from recurrent and Schaffer collaterals and the ensuing break on collateral excitation may explain the short number of theta cycles observed *in vitro* (Konopacki *et al.* 1987). These differences between theta activity observed *in vitro* and *in vivo* raise doubts about the existence of an intrahippocampal theta oscillator; however, CA3 oscillations observed in the awake behaving rat change frequency and phase independently of entorhinal inputs (Kocsis *et al.* 1999). This observation, combined with numerous other studies strengthens the notion of an intrinsic CA3 hippocampal oscillator.

1.2.2 Theta oscillations and synaptic plasticity

Long-term potentiation (LTP) and long-term depression (LTD) are activity-dependent cellular mechanisms that underlie learning and memory. Generally, the frequency and pattern of stimulation are determining factors in whether synapses undergo LTP or LTD; however, synapses can be modified such that the threshold for plasticity induction is reduced under certain conditions and several studies highlight the involvement of theta oscillations in synaptic plasticity. For example, stimulation of Schaffer collateral/commissural inputs in the presence of carbachol leads to long-term enhancement of synaptic efficacy in CA1 neurons (Huerta and Lisman 1993). This modification of synaptic efficacy failed to occur when the stimulation protocol was used without simultaneous application of carbachol. The authors also showed that synaptic enhancement was coupled with robust carbachol-induced theta oscillations and in instances where small or no oscillations were observed, synaptic enhancement was minimal.

Further, timing stimulation delivery at positive peaks of theta (in-phase) waves led to an even larger synaptic enhancement, while stimulation that was not synchronized with theta oscillations (out-of-phase) failed to produce an enhancement. Thus, the electrical and not just biochemical consequences of carbachol application, namely the oscillatory state of the network, determined the level of enhancement and magnitude of synaptic efficacy.

Bidirectional plasticity that requires NMDA and muscarinic receptors during cholinergic theta oscillation in CA1 has also been observed *in vitro* (Huerta and Lisman 1995). In this case, a very brief burst (4 pulses, 100 Hz) given at the peak of theta induced LTP, while the same protocol delivered out-of-phase in relation to theta induced LTD. These studies suggest that the requirement of high frequency stimulation for LTP induction is removed when incoming stimuli are phase-synchronized with hippocampal oscillatory activity and the timing of excitatory inputs during theta cycles holds deterministic value for synaptic strengthening or weakening. These findings bolster work carried out in other labs showing that plasticity in the hippocampus is especially sensitive (heightened) to theta-frequency inputs independent of the occurrence of intrinsic rhythmic activity (Christie and Abraham 1992).

1.2.3 Theta phase precession

Place cells in the hippocampus and grid cells in the medial entorhinal cortex of freely moving rodents have spatially regulated firing patterns. A place cell becomes active when an animal enters that cell's place field – a particular space in the environment. Place cells, along with other neurons of the hippocampus and neighbouring regions create a cognitive representation of a specific location in space. This spatial processing, unlike processing in the visual cortex, takes

place without any apparent topography of place fields – neighbouring cells are as likely to have distant place fields as adjacent ones. A place cell fires action potentials when an animal traverses its place field, since the maximum discharge rate of the cell occurs at the center of the field, and this firing activity shifts systematically in relation to the ongoing theta rhythm. This theta oscillation of the local field potential that is associated with locomotion, exploration, REM sleep, or attention to external stimuli is atropine-resistant (Kowalczyk *et al.* 2013) and the combined spiking activity of principal neurons in the hippocampus is phase-locked to this rhythm (Maurer and McNaughton 2007).

On average, hippocampal PCs fire on the negative phase of theta recorded extracellularly in the pyramidal cell layer although spike-to-phase relationship can vary considerably between individual neurons. Further, phase fluctuation of place cell spiking is not stochastic; rather, theta phase relationship shifts predictably as the animal traverses the place field of the recorded unit. When the animal enters the field, firing consistently begins late in phase but the first spike and the median of spikes advance progressively forward on each theta cycle as the animal further traverses the field (O'Keefe and Recce 1993). This precession of the phase can vary between 100° and 355° between cells due to a burst frequency that is slightly higher than theta oscillation in the local field (O'Keefe and Recce 1993) and the phase offset provides a measurement or representation of the distance covered. As the animal leaves the field, spiking occurs near the beginning of theta cycle so the timing of spiking in relation to theta oscillation encodes spatial information. Spiking precesses almost 360°, but never more, as the animal traverses a typical place field of the dorsal hippocampus, occupying 25 cm of space, in its entirety (Maurer and McNaughton 2007). This occurs over the course of 8-12 theta cycles (Maurer and McNaughton

2007), thus, spatial location is encoded by hippocampal neurons by not just firing rate but also timing of the rate in relation to the phase of on-going theta. Although spike to phase relationship fails to provide any information about absolute location, because phase always precesses from late to early as the place field is traversed from any given direction, it does provide information about position relative to the centre of a place field (Maurer and McNaughton 2007).

The timing of place cell firing is shifted in an experience-dependent manner. As the animal enters the place field, the rate of firing of place cells is symmetric around the place field; however, the negative correlation of spike phase to position in a place field (theta phase precession), occurs with experience. Shifting spike rate to earlier phases over subsequent theta cycles transforms the rate code into a temporal code enabling the use of Hebbian learning mechanisms for encoding sequential spatial information (Skaggs *et al.* 1996). Behavioural sequences associated with traversing a place field occur on the magnitude of seconds, while NMDA receptor-dependent plasticity mechanisms are constrained by channel open times that are in the magnitude of milliseconds (Monyer *et al.* 1994). Through phase precession, behavioural sequences are compressed on a temporal scale because during each theta cycle the sequence of activity between neuronal ensembles with overlapping place fields corresponds to the sequence of place fields that the animal is traversing. The first spikes of each theta cycle are from cells whose place fields the animal is exiting, while the late phase spikes are from cells whose place fields the rat is about to enter (Maurer and McNaughton 2007), and the time lag between the activity of respective place cells encodes the spatial distance between place field centers. Thus behavioural time scales of seconds become compressed to the time scale of a theta cycle (~125 msec) allowing for a neural mechanism that encodes sequential spatial information in a temporal

order. Further, because place cells can have overlapping place fields, activity of sequentially ordered place fields could also overlap leading to neural representation of sequential information that is correlated (Gupta *et al.* 2012). From a sequence encoding perspective, this would be ineffective because instead of allowing for progressive waves of activity through a sequence of cell assemblies that is required during recall, it would lock neuronal ensembles together (Maurer and McNaughton 2007). In other words, even though place cell spiking is correlated in space between cells with overlapping place fields, phase precession transforms the rate code into a temporal code ensuring that 1) the activity of cells with overlapping place fields does not correlate in time and 2) timing of spikes satisfies the temporal constraints of Hebbian learning.

Spatial position of an animal can be determined by using both firing rate and spike-theta phase relationship; however, the mechanisms underlying both phenomena are unclear. Activity-dependent theta phase advancement might arise from interference effects between two different oscillators because the burst frequency of place cells must be slightly higher than the local field potential in order for phase precession to occur (O'Keefe and Recce 1993). Two oscillators with slightly different frequencies can emerge from interactions between extrinsic inputs to the hippocampus and synaptically mediated membrane currents that are intrinsic to hippocampal principal cells (Maurer and McNaughton 2007). Inputs from the medial septum can produce a slow oscillator and place-related spiking in CA1PCs can be induced by CA3 input leading to phase advancement by a full cycle by the fast CA3 theta oscillator (Buzsaki 2002). In agreement with this hypothesis, it is known that the extrahippocampal (entorhinal) and intrahippocampal (CA3) oscillations can occur independently (Kocsis *et al.* 1999), CA3 input is the primary induction source of spiking in CA1 PCs, and lastly, both CA1 and CA3 PCs discharge on the

same phase of theta (Fox *et al.* 1986). Together these mechanisms can form the basis of a model wherein intrinsic or synaptically mediated membrane currents interact with extrinsic inputs to account for phase advancement.

In this model, dendritic depolarization during background theta oscillation leads to somatic hyperpolarization and an oscillation that is equal to or greater than the frequency of theta recorded extracelluarly (Kamondi *et al.* 1998). The size of dendritic depolarization correlates with the magnitude of phase advancement and with the spike rate (Kamondi *et al.* 1998). The maximum dendritic depolarization also correlates with maximum extracellular current flow resulting in a negative peak theta in stratum lacuonosum-moleculare and positive in stratum pyramidale/oriens (Buzsaki 2002). Therefore, inhibition of the soma and excitation of dendrites compete with each other to produce phase advancement. Somatic hyperpolarization can arise from septal inputs and/or modulation of intrahippocampal interneurons by theta (Maurer and McNaughton 2007), as discussed earlier. Various sensory inputs, including entorhinal input, which is constant over a large spatial area (Barnes *et al.* 1990), can produce the dendritic membrane potential oscillation. In addition, cooperativity between entorhinal and CA3 inputs can activate neurons strongly, resulting in spikes that are earlier in phase (Buzsaki 2002). When the animal is outside of the place field of a cell, the dendritic oscillation is anti-phase relative to the extracellular theta and the somatic oscillation (Lengyel *et al.* 2003) leading to zero net excitation. When phases of somatic and dendritic oscillations coincide, the probability of cell firing increases (Maurer and McNaughton 2007). If the animal enters and stops in the place field of a given neuron, dendritic excitation will be sustained and the cell will maintain its firing rate and firing phase (Maurer and McNaughton 2007). Thus, phase precession is a consequence of

competition between excitatory and inhibitory inputs and the modulation of those inputs by theta rhythm allowing spatial information to be encoded in a manner that satisfies the rules of Hebbian learning through synaptic plasticity.

1.2.4 Pattern completion in CA3

The pattern of feedforward hippocampal connectivity (entorhinal cortex – DG – CA3 – CA1) described in section **1.2.1** has led to the development of various theories about the role of each hippocampal subregion in spatial and contextual learning. It is thought that the hippocampus creates context-specific neural representations by integrating external sensory information from the lateral entorhinal cortex and spatial information relative to the body (self-motion) from the medial entorhinal cortex (Knierim *et al.* 2006). Characteristics of hippocampal connectivity patterns include widespread recurrent connections in CA3, as detailed previously, but also strong divergence of connections at the first step between dentate gyrus and inputs from the entorhinal cortex. A small number, in fact five times smaller (200,000 in rat), of entorhinal cells project into a large number of dentate granule cells (1,000,000) (Amaral *et al.* 1990). This divergent connectivity, combined with sparse activity in granule cells (Chawla *et al.* 2005) has led to the hypothesis that the dentate gyrus is a preprocessing region that performs pattern separation on entorhinal cortex inputs (Yassa and Stark 2011). Pattern separation refers to the process of amplifying small changes into large differences resulting in the ability to differentiate one memory from many other stored memories (Newman and Hasselmo 2014). Pattern separation allows for similar representations to be stored in a distinct, non-overlapping manner (Yassa and Stark 2011).

David Marr was the first to suggest that because CA3 projects to itself, it is capable of autoassociation and thus pattern completion (Marr 1971). Pattern completion is the process of reactivating previous representations given noisy or partial sensory inputs (Yassa and Stark 2011). It is hypothesized that through autoassociation, a group of coactive neurons in CA3 can strengthen connections between each other via canonical synaptic plasticity mechanisms and subsequent activation of a small subset of neurons can provide enough excitatory drive to the remaining portion and thereby, activate, or pattern complete the entire original ensemble (Newman and Hasselmo 2014). On the basis of autoassociation in CA3, it has been postulated that 'detonator synapses' between mossy fibers and proximal apical dendrites of CA3 PCs are used to create new pattern separated representations in CA3 neurons in order to avoid noise in the system and support new memory formation (Rolls 2007). Balanced against this, direct input from layer II entorhinal neurons, that are weaker in comparison to mossy fiber inputs, function to provide a cue for accurate recall (Rolls 2007). In agreement with this theory, reversible inactivation of mossy fiber synapses impairs new spatial learning without affecting memory recall or consolidation (Lassalle *et al.* 2000). Further, lesioning dentate gyrus interferes with encoding but not retrieval, and lesioning perforant path input to CA3 leads to deficits in retrieval but not encoding (Lee and Kesner 2004). Therefore, discharge from mossy fiber inputs is 'associated' by CA3 with direct inputs from entorhinal cortex leading to pattern completion.

Several studies have shown convincing evidence of pattern separation in the dentate gyrus and pattern completion in CA3 (Gold and Kesner 2005, McHugh *et al.* 2007). A recent study (Neunuebel and Knierim 2014) employed simultaneous single unit recordings of CA3 and dentate gyrus cells from freely moving rats while distorting the testing environment ever so

slightly. The testing environment consisted of a circular track that was placed in the centre of a black curtained enclosure. Salient cues were presented locally in the form of texture on the track that was divided into four 90° segments, and distally in the curtained area. Post-surgery and training, rats ran five track sessions as they foraged for chocolate sprinkles in a clockwise direction. The sessions were interleaved between three standard and two mismatched sessions. In standard sessions, local and global cues remained constant, while local and global cues were rotated by equal increments in opposite directions for the mismatched sessions. The degree of conflict between spatial cues in this "double-rotation task" was used to test whether the cue-conflict environment resulted in degraded dentate gyrus input patterns to CA3 and whether representations in CA3 were more similar to the original environment, when compared to DG inputs. The authors found that dentate gyrus showed significant decorrelation following any changes in the testing enclosure, while CA3 output resembled the originally stored representation better than the degraded input patterns from dentate gyrus. CA3 representation remained coherent relative to the position of local cues despite noisy sensory inputs and this was not the case for upstream areas. These findings are consistent with previous studies showing the CA3 collateral network performs pattern completion when input representations are similar to stored memories (Guzowski *et al.* 2004). A particular strength of the study detailed above is that measuring both the input and output representations provides conclusive evidence for whether putative pattern separation or completion is inherent to the area being tested or a result of upstream processing by a different brain structure (Newman and Hasselmo 2014). Together with other studies (Deshmukh and Knierim 2011, Neunuebel *et al.* 2013), these findings confirm computational modeling predictions that attribute specific information processing functions to different regions of the hippocampus.

1.3 Dendritic integration in principal cells of the hippocampus

An important function of central neurons is to transform thousands of individual synaptic inputs into specific patterns of output. When integration of multiple synaptic inputs results in a net depolarization that is greater than spike threshold, an output signal (action potential) with varying firing patterns occurs. Decoding synaptic input patterns is the primary function of central neurons and it is dependent on a multitude of dendritic characteristics. Integrative properties of dendrites are determined by not just their passive cable properties, but also by the combined activity of post-synaptic voltage-gated channels. Active forms of dendritic integration that are produced through various voltage-dependent conductances allow neurons to preferentially respond to spatiotemporally clustered input patterns (Magee and Johnston 2005). Morphological, passive, and active properties of dendrites govern the rules of synaptic integration such that synaptic inputs summate linearly, sublinearly, or supralinearly.

Quantification of dendritic integration requires comparisons between the observed EPSP response from simultaneous activation of synaptic inputs and arithmetic, expected sum of individual EPSP responses (Tran-Van-Minh *et al.* 2015). Plotting the observed and expected EPSPs results in a dendritic subthreshold input-output relationship (sI/O) (Tran-Van-Minh *et al.* 2015). sI/O relationships are 1) linear when the expected response is equal to the observed response; 2) sublinear when the expected depolarization is more than the observed depolarization; and 3) supralinear when the expected depolarization is less than the observed depolarization. Supralinear summation, or amplification of postsynaptic potentials, results from activation of voltage-gated channels in spines. In certain cases, the coincident activation of

synaptic inputs leads to not just EPSP boosting but also a threshold-dependent, regenerative dendritic spike mediated by the combined activity of voltage-dependent channels in spines (Tran-Van-Minh *et al.* 2015). There is an uneven distribution of voltage-gated channels along the length of dendrites (Hell *et al.* 1993) and this further facilitates modification of synaptic currents by dendritic conductances. Evoked subthreshold synaptic potentials can activate Na^+ and Ca^{2+} channels leading to increase in spine Ca^{2+}concentrations and the size of EPSPs (Lipowsky *et al.* 1996, Gillessen and Alzheimer 1997). These actions are counteracted by dendritic K^+ channels that decrease synaptic currents and contribute to sublinear summation of synaptic inputs (Hoffman *et al.* 1997). Further, the relative size, location, and timing of inputs affects cross-talk between conductances and modulates dendritic spike dynamics (Konig *et al.* 1996).

1.3.1 Influence of passive membrane properties on signal propagation

In a passive, single compartment cell that does not have dendrites, synaptic summation is sublinear due to the decrease in driving force when membrane voltage approaches the reversal potential for a given synaptic conductance (Tran-Van-Minh *et al.* 2015). Accounting for neuronal morphology, such as dendritic arborization, results in a more complicated model wherein dendrites are viewed as electrical cables. This notion was first put forth by Rall (Rall 1967) who, using cable theory, included axial resistance in a multi-compartmental circuit model to show that progressive reduction in current from the site of injection across electrically coupled membranes results in attenuation and slower time course of voltage responses because adjoining compartments allow current to leak across the membrane. Referred to as dendritic filtering, this phenomenon explains why local voltage responses tend to be larger and faster when compared to those recorded in the soma (Tran-Van-Minh *et al.* 2015). Rall also provided the concept of space

constant, which succinctly describes dendritic filtering. Space constant is the distance along a cable where the change in membrane potential is 37% of the initial magnitude, as measured at the site of current injection (Rall 1967).

Space constant provides a rough indication for the size of effective dendritic compartments (Tran-Van-Minh *et al.* 2015). For example, substantial cable filtering can be expected in a dendrite length that is longer than the space constant (Tran-Van-Minh *et al.* 2015). Conversely, EPSP propagation occurs without significant filtering in dendrites that are shorter than the space constant (Tran-Van-Minh *et al.* 2015). Increasing distance of the synapse from the soma results in higher distance-dependent impedance and this contributes to sublinear sI/O relationships (Tran-Van-Minh *et al.* 2015). Space constant is also proportional to dendrite diameter; however, values of length constant within the same dendritic branch can vary considerably between steady state conditions and during rapid synaptic conductances due to an alteration in space constant by capacitative currents that mimic frequency-dependent shunts (Abrahamsson *et al.* 2012). Thus, summation of EPSPs in wider dendrites tends to favour sublinear sI/O relationships. Dendritic branching on the other hand shortens the space constant because increased current flow reduces membrane resistance such that higher branch points result in linear sI/O relationships despite increased dendritic filtering (Abrahamsson *et al.* 2012, Tran-Van-Minh *et al.* 2015).

1.3.2 Influence of active dendrites on signal propagation

Large local synaptic conductances can either reduce driving force or cause downstream activation of voltage-gated conductances that may include NMDA receptors, Na^+, Ca^{2+}, K^+, and hyperpolarization-activated cyclic nucleotide-gated (HCN) channels (Tran-Van-Minh *et al.*

2015). As mentioned previously, the impact of active conductances on changes in sI/O relationships is dependent on myriad factors including, biophysical properties of channel gating, relative channel density along the somato-dendritic axis, passive dendritic properties, and the amplitude/time course of the synaptic conductance (Tran-Van-Minh *et al.* 2015). For example, variable distribution of HCN channels in mitral cells boosts EPSP amplitude and promotes action potential generation (Angelo and Margrie 2011). Even small local depolarization brought about by NMDA receptors can activate other voltage-dependent conductances leading to supralinear summation of EPSPs (Makara *et al.* 2009). In addition to NMDA receptors, voltage-gated Na^{+} and Ca^{2+} channels can mediate dendritic spiking activity locally depending on the cell type and brain region being studied (Golding and Spruston 1998, Chiovini *et al.* 2014).

The ability to generate spikes by dendrites of pyramidal cells was documented more than a decade ago (Nettleton and Spain 2000); however, the mechanisms that support spike generation have been discovered recently. Not surprisingly, these mechanisms vary between different regions of the hippocampus to accommodate the computational requirements that arise from differential input patterns between regions.

1.3.3 Dendritic integration in dentate gyrus granule cells

Dendritic integration in granule cells is critical for processing input from the entorhinal cortex and relaying this information to the hippocampus proper. Modeling, based on passive properties, of morphologically restructured granule cells highlights the critical influence of dendritic and cellular morphology on precise dendritic signal processing and coincidence detection (Schmidt-Hieber *et al.* 2007). Dendrites of granule cells arborize extensively within the inner region of

molecular layer, in close proximity to the soma, and give rise to higher order dendrites that extend throughout the entire molecular layer (Amaral *et al.* 2007). The dendritic arbors of granule cells have a cone-shape and the majority of synapses are located on spines in distal dendrites residing within the outer two-thirds of the molecular layer (Amaral *et al.* 2007). Krueppel *et al*. used a combination of dual somatodendritic patch recordings and multiphoton glutamate uncaging to study integrative properties of small-diameter (~0.8 μm in distal and medial molecular layer) granule cell dendrites (Krueppel *et al.* 2011).

The authors found that backpropagating action potentials (bAPs) evoked by somatic current injection attenuated more strongly compared to other principal cells in the hippocampus. There was also a complete absence of regenerative dendritic potentials during invasion of bursts of bAPs into dendrites. The authors also studied EPSP attenuation by injecting mock EPSCs into the dendritic electrode and recording the result at the somatic electrode. At all dendritic recordings sites, beyond the initial proximal region, voltage attenuation was significant with the somatic EPSP being 10-20% of the dendritic EPSP. Similarly, steady-state forward and backward voltage attenuation was stronger when current was injected into dendrites compared to prolonged current injection at the soma. Such asymmetric voltage propagation arises from variable input impedances between the soma and dendrites and complements computational modeling data (Krueppel *et al.* 2011). Voltage attenuation was also frequency-dependent such that stronger attenuation was observed at higher frequencies suggesting that granule cells have a propensity for integrating inputs with low synchrony. EPSP attenuation at dendritic distances greater than 100 μm from the soma was uniform in nature indicating that the majority of voltage decrement occurs in proximal regions of the dendritic arbor.

Using two-photon uncaging of MNI-glutamate, Krueppel *et al*. studied integration of spatiotemporal input patterns. Up to 13 spines on individual dendritic branches were stimulated to measure EPSPs induced by glutamate uncaging. The relationship between summed measured EPSPs to expected EPSPs that were summed arithmetically was fitted with a linear function, however, the average gain was greater than one in most experiments. Synchronous uncaging failed to elicit dendritic spikes; thus, granule cells are incapable of supralinear integration, rather they invariably exhibit linear integration with amplification capabilities over a wide range of input strengths. In order to examine the underlying factors responsible for linear integration, the authors used blockers of glutamate receptors and voltage-gated receptors. When the number of spines that were stimulated synchronously was increased in the presence of NMDA receptor blocker, D-APV, the ratio of measured versus computed EPSPs decreased. This also occurred, but to a lesser extent, when experiments were repeated in the presence of TTX and nickel, blockers of voltage-gated Na^+ and Ca^{2+} channels. Thus, voltage-dependent mechanisms are responsible for voltage boosting that underlies linear integration in granule cell dendrites. Next, using a computational model, the authors studied the contribution of a single spine to the voltage boosting that was observed in summed EPSPs. Krueppel *et al*. found that voltage boosting occurs at the single spine level and a subsequent boosting effect occurs when asynchronous inputs are summed. Further, spatial distribution of stimulated spines did not impact dendritic integration in granule cells.

The inability of granule cells to integrate synchronous inputs, combined with a preference for computing the influence of individual synapses on somatic potential makes them inefficient

coincident detectors (Krueppel *et al.* 2011). Granule cells also have a markedly hyperpolarized membrane potential compared to other principal neurons of the hippocampus (Kress *et al.* 2008) and this, combined with strong voltage attenuation, further exacerbates the sparse activity observed in these cells (Chawla *et al.* 2005). The larger gap between resting membrane potential and action potential threshold can be compensated by dendritic spikes; however, regenerative, threshold-dependent dendritic spikes are completely absent in granule cells (Krueppel *et al.* 2011). Using unitary EPSP size, and resting/threshold potentials, Krueppel *et al*. estimate that approximately 55 distal synapses would have to be concurrently active in order to produce an action potential output in granule cells. These dendritic properties have a profound impact on the function and information storage capabilities of granule cells. Weights of individual synaptic inputs are not modulated by location or timing and the frequency-dependent voltage transfer properties make granule cell dendrites less prone to temporal interference (Krueppel *et al.* 2011).

Generally, synaptic plasticity mechanisms are emphasized as primary mediators of information storage capacity in hippocampal cells; however, local state-dependent modifications of membrane excitability can also result in long-term strengthening or weakening of synapses. Dendritic excitability is not a static phenomenon and plasticity of individual branches in the dendritic arbor can be used to store recent experience (Losonczy *et al.* 2008). Such experience-dependent dendritic plasticity is subserved by modulation of voltage-gated conductances. Specifically, the ability to enhance previously weak compartmentalized dendritic segments is an important way of storing input features (Losonczy *et al.* 2008) and because granule cells lack this ability, it is thought that storage of input features through dendritic spikes is not utilized by

granule cells and they must employ different synaptic computational strategies for this operation (Krueppel *et al.* 2011).

1.3.4 Dendritic integration in CA1 PCs

In contrast with dentate granule cells, dendrites of CA1 PCs are efficient coincident detectors that respond to synchronous input patterns with a precisely timed action potential mediated by local regenerative spikes. The first study to show this in acute slices used whole-cell dendritic recordings of the distal and proximal apical tufts of CA1 PCs (Gasparini *et al.* 2004). Gasparini *et al*. injected EPSC-shaped currents through a whole-cell electrode placed on the distal apical tuft (>250 μm) and measured the voltage response with an electrode placed <20 μm away. The EPSP responses to injected current of increasing amplitude were generally linear for low current intensities, while higher current intensities (≥3 nA) resulted in a dendritic spike. Threshold for eliciting dendritic spikes was nearly 10 mV higher than that for somatic regions and threshold for dendritic spike initiation was inversely correlated with the rate of membrane depolarization reflecting the differential balance between inward and outward currents that is required for spike generation in different subcellular compartments. Local dendritic spikes in CA1 PCs were dependent on voltage-gated Na^+ channels and A-type K^+ currents because they were blocked by TTX and 4-AP lowered the intensity of current required for spike generation and also increased spike amplitude. Previous studies have shown that A-type K^+ channels provide a breaking mechanism for regenerative Ca^{2+} channel activation in CA1 PCs (Magee and Carruth 1999), and consistent with this, Gasprini *et al*. found that dendritic spikes lacked contribution from Ca^{2+} channels and were primarily mediated by voltage-gated Na^+ channels.

The timing of spikes was critical for dendritic spike generation, as the EPSP response increased linearly with the number of inputs that had an interval of 1 msec, while inputs with 5 msec intervals results in sublinear sI/O relationships. Inputs with intervals of <0.5 msec were required to elicit a dendritic spike. Spatial clustering was also important for spike generation because current threshold for spike generation increased as the distance between two inputs increased such that 30-50% more current was needed to compensate for input separation of approximately 100 μm. Combining spatiotemporal dynamics, the authors found that synchronous, arriving in less than a 3 msec window, and clustered inputs (<100 μm) were required for dendritic spiking activity. Further, dendritic spikes showed weak voltage attenuation with distance in the forward direction (dendrite-to-soma); however, this was dependent on the holding membrane potential with weaker attenuation at more depolarized potentials. Effective spike propagation to the soma, where it resulted in an action potential with a short latency, was achieved when spikes were elicited in the main apical trunk. In addition to membrane potential, spike propagation was modulated by distance of the spike initiation site from the soma and extracellular ion concentrations. Thus, dendrites of CA1 PCs, unlike granule cells can integrate spatially clustered and highly synchronous inputs via dendritic spikes that propagate to the soma and have a modulatory effect on neuronal output.

In addition to the large diameter apical trunk and its apical tufts, dendritic integration has also been studied in short thin terminal dendrites that branch off the trunk or soma. Using two-photon uncaging and patch clamp recordings, Losonczy and Magee studied responses of single radial oblique branches to different spatiotemporal input patterns (Losonczy and Magee 2006). They examined uncaged glutamate on 7-20 spines that covered approximately 20 μm of an oblique

branch with varying interstimulus intervals. They found that synchronous inputs (0.1 msec interval, total input duration of 3 msec) resulted in an EPSP with fast time course at the soma that was mediated by dendritic spikes generated locally at the site of uncaging. The sI/O relationship recorded at the soma in response to asynchronous inputs was linear and there was no evidence of dendritic spike generation. To determine the threshold requirement for state shift between linear and supralinear integration, the authors determined the level of depolarization required for oblique spike generation. Although dependent on distance of dendrite from the soma, the mean threshold depolarization for all branch locations was 3.4 mV, which corresponds to synchronous activation of approximately 20 Schaffer collateral synapses within a 6 msec temporal time window. Further, the likelihood of spike generation was equal between spatially clustered inputs and inputs that were distributed across the length of a single oblique branch, indicating that these dendrites act as independent integrative units that summate inputs without favouring their spatial distribution.

Examining ionic conductances underlying dendritic spikes showed that voltage-gated Na^+ channels contributed to the fast component of the somatic EPSP and transient K^+ currents modulated the duration of the slow component in addition to the temporal window over which synchronous inputs must be delivered for initiation of the Na^+ spike. The slow component of the somatic EPSP was dependent on secondary activation of NMDA receptors and although the majority of local Ca^{2+} influx at the site of uncaging was mediated by VGCCs, they failed to have a significant impact on somatic depolarization. The fast Na^+ spike evoked in oblique dendrites is very similar to that observed in the apical trunk of CA1 PCs (Gasparini *et al.* 2004), except that the threshold for generating spikes is higher in apical trunks due to a combination of

morphological and passive properties (e.g. lower resistance and increased branching). Poor spike propagation in both regions is likely due to the ionic nature of spikes, as fast Na^+ spikes propagate poorly and require very rapid depolarization for initiation compared to slow NMDA receptor or VGCC spikes that not only propagate throughout the dendritic arbor efficiently, but also have lower initiation requirements (Larkum *et al.* 1999, Schiller *et al.* 2000). These findings show that, unlike dentate granule cells, dendrites of CA1 PCs can distinguish between synchronous and asynchronous input patterns by varying their sI/O profiles and specific input patterns can have a measurable impact on somatic output through the generation of dendritic spikes.

Dendritic spikes can be modulated under conditions that are known to underlie functional plasticity. For example, Losoncsy *et al*. (Losonczy *et al.* 2008) have shown that repeated activation of spines, resulting in dendritic spikes, leads to an increase in voltage measured at the cell body. This enhancement of somatic voltage is mediated by more efficient spike propagation that is dependent on downregulation of $K_v4.2$ voltage-gated K^+ channels. Such 'branch-specific plasticity', that is distinct from synaptic plasticity, allows CA1 dendrites to encode specific features of synaptic input (Losonczy *et al.* 2008) and because it is experience-dependent, it can be modulated by physiologically relevant factors including input patterns with varying spatiotemporal characteristics (Losonczy *et al.* 2008, Spruston 2008). Thus, dendritic spikes can trigger long-term changes in intrinsic excitability that "tune" neuronal responses to specific input patterns.

In addition, dendritic spikes generated within a single branch can affect how future input patterns are summated locally and globally through changes in biophysical properties of voltage-gated channels (Remy *et al.* 2009). In CA1 PCs, temporally and spatially clustered inputs to various spines of basal dendrites at low frequencies (1 Hz) consistently evoke Na^+ channel-dependent dendritic spikes that have been reported by multiple groups. Critically, Remy *et al*. (Remy *et al.* 2009) have shown that inputs delivered at theta frequencies (5-10 Hz) that mimic activity during behaviour, result in a significant reduction of spike amplitude that lasts several hundred milliseconds and converts branches that could previously summate supralinearly into a linear processing state. This spike attenuation was not observed in the absence of supralinear summation, meaning that inputs leading to a linear sI/O profile do not affect future summation capabilities of a given branch. Further, local attenuation of future spiking activity is branch specific – a dendritic spike in one branch does not alter summation properties of other daughter branches from the same parent dendrite.

In contrast, triggering of action potentials that was elicited by either somatic current injection or uncaging glutamate on multiple spines attenuated dendritic spikes globally in all branches and reduced subsequent action potential output. Spike attenuation was less severe after an action potential burst when compared to a single action potential, likely because of the extended dendritic depolarization induced by a burst. Recording currents from basal dendrites in response to 5 Hz stimulation showed that prolonged inactivation constrains the availability of Na^+ channels for future spike generation. Highly synchronous inputs can therefore depress dendrite excitability by prolonging the temporal window within which subsequent inputs can cause supralinear summation (Remy *et al.* 2009). Also, spike attenuation creates a frequency range that

determines optimal input processing by placing an upper limit on the rate at which information can be processed. This implies that dendritic inputs must be sparse if dampening of information retrieval by frequency-dependent spike attenuation is to be avoided (Remy *et al.* 2009). These results demonstrate that dendritic information processing modes are not static phenomena and biophysical properties of voltage-gated conductances can shape output profiles of neurons in an experience-dependent manner. In the case of CA1 PCs, modulation of Na^+-mediated dendritic spikes through changes in K^+ and Na^+ conductances results in functional strengthening or weakening of not just synapses but entire dendritic branches/arbors (Losonczy *et al.* 2008, Remy *et al.* 2009).

1.3.5 Dendritic integration in CA3 PCs

Unlike CA1 dendrites, relatively little is known about input integration patterns of CA3 PCs despite the critical role of this region in information processing, theta oscillations, and pattern completion. Using somatodendritic recordings, Kim *et al*. have shown that near-threshold current injection at the soma initiates trains of action potentials in CA3 PCs that consistently back propagate in the proximal domain (Kim *et al.* 2012). Amplitude of backpropagating action potentials at distances of 100 μm from the soma was almost 90% of the maximal amplitude recorded at the soma. Action potential backpropagation was sustained over a wide range of stimulus frequencies (20-100 Hz) and this was dependent on active conductances with voltage-gated Na^+ channels providing the largest contribution. Current density analysis employed by Kim *et al*. showed that Na^+ channels decreased in density from the soma to the proximal dendrites and then increased again towards the distal dendrites, while A-type K^+ currents increased progressively from the soma to the distal dendrite regions (Kim *et al.* 2012). Further, Na^+-

channel dependent dendritic spikes were easily elicited by short current pulses and they propagated to the soma when a higher stimulation was used. Surprisingly, the threshold for eliciting spikes was lower in distal dendrites when compared to the soma indicating that a small number of coincident inputs may be enough to elicit spiking activity in distal dendrites of CA3 PCs (Kim *et al.* 2012).

Direct comparison of the effects of dendritic spikes on somatic output between CA3 and CA1 PCs showed dramatic differences. Action potential propagation in CA1 PCs was attenuated to a higher degree compared to CA3 PCs and it was also frequency-dependent. The probability of dendritic spiking was also lower in CA1 PCs and this was due to lower, more uniform density of Na^+ channels. In contrast, even though dendritic spike attenuation occurred in the forward (dendrite-to-soma) direction, it was represented as an overshoot with an accelerating rising phase of the EPSP in the soma of CA3 PCs (Kim *et al.* 2012). These findings show that relative to dentate granule cells and CA1 PCs, dendritic spikes might be the primary computational parameter used by PCs in area CA3. Further, the inverse relationship between dendritic spike threshold and distance from the soma, combined with the high Na^+-to-K^+ channel ratio across the dendritic arbor, may contribute to reduced voltage attenuation of inputs received at more distal sites in CA3PCs (Kim *et al.* 2012).

In order to study integration properties of CA3 basal and apical dendrites, Makara and Magee used two-photon glutamate uncaging to measure sI/O profiles after synchronous stimulation (Makara and Magee 2013). The authors found that synchronous activation of increasing number of synapses resulted in supralinear integration that was largest in the apical dendrite and

mediated by a slow component, although fast spikelets were observed predominantly in basal dendrites. Using patch recordings of the apical trunk to examine this discrepancy between basal and apical arbors, Makara and Magee found that although small Na^+ spikes could be initiated in all apical oblique branches, dendritic filtering and significant voltage attenuation yielded undetectable effects of dendritic Na^+ spikes at the soma. This is inconsistent with the observations discussed above that were made by Kim *et al*.; however, the stimulation paradigm and location vary considerably between the two studies. Kim *et al*. studied dendritic spike propagation by direct current stimulation of thick CA3 dendrites, while Makara and Magee used two-photon glutamate uncaging in thin dendrites. As mentioned in section **1.3.1**, morphological features, such as dendrite diameter and extent of branching, can dramatically alter input impedance of dendrites leading to variable voltage attenuation between dendritic arbors of the same cell.

Unlike the Na^+-dependent supralinear integration observed in CA1 PCs, NMDA receptors were responsible for the slow component of dendritic spikes in CA3. NMDA-mediated spikes also had a lower requirement for spatial clustering of inputs – voltage amplification occurred in response to synchronous activation of 15 synapses. The temporal window for eliciting NMDA spikes was also lower compared to Na^+ spikes, stimulation of 20 inputs with 2 msec intervals was sufficient to generate NMDA spikes. The time course of NMDA spikes was regulated predominantly by G-protein-coupled inwardly-rectifying potassium (GIRK) channels and to a lesser extent, by A-type K^+ currents. Next, Makara and Magee tested the impact of theta stimulation on CA3 PC output. They discovered that theta stimulation of NMDA spikes consistently resulted in an action potential at the soma and the efficacy of action potential output was dependent on NMDA spike

decay kinetics that are determined primarily by GIRK channels. These findings demonstrate that NMDA spikes act as a dendritic gain, amplifying coincident inputs with specific spatiotemporal characteristics (Makara and Magee 2013).

The spatial and temporal requirements for dendritic spikes in CA3 are lower than those in CA1 and this is a direct consequence of the mechanisms underlying spike initiation and regulation. Broad and slow NMDA spikes in CA3 PCs, unlike fast Na^+ spikes in CA1 PCs, propagate more efficiently because they have lower voltage initiation requirements. As discussed previously, dentate granule cells are only capable of linear integration (Krueppel *et al.* 2011) and supralinear integration in PCs of CA1 and CA3 are subserved by different ionic conductances (Losonczy and Magee 2006, Makara and Magee 2013). Based on these differences, it is possible that specific types of dendritic integration may facilitate different computational functions. Linear integration and frequency-dependent voltage transfer in the dentate gyrus essentially leads to integration of asynchronous inputs. Fast Na^+ spike-mediated voltage amplification in CA1 PCs enables storage of specific features of input (Losonczy *et al.* 2008), while NMDA spikes in CA3 PCs may be important for flexible organization of information-encoding ensembles that is required for pattern completion and autoassociative storage of memories (Makara and Magee 2013).

1.4 Neuronal voltage-gated Ca^{2+} channels

Neuronal membrane depolarization leads to activation of Ca^{2+}channels that in turn, depolarize the neuron further by mediating Ca^{2+} influx into the cell and facilitate action potentials or subthreshold depolarization. Ca^{2+} is an important secondary messenger that can modulate various processes including, synaptic transmission, gene expression, synaptic plasticity, apoptosis, and regulation of membrane proteins. Mechanisms such as Ca^{2+}-buffering proteins and sequestration

of Ca^{2+} in intracellular stores keep resting neuronal Ca^{2+} concentrations in the 100 nM range, while opening of VGCCs results in Ca^{2+} influx down its electrochemical gradient driving local intracellular Ca^{2+} concentrations into the high micromolar range (Clapham 2007). Because unregulated Ca^{2+} entry is neurotoxic, activation of VGCCs is highly regulated by intrinsic gating mechanisms and intracellular pathways that coordinate trafficking of channels to and from the plasma membrane (Simms and Zamponi 2012). Genetic alterations resulting in changes in the biophysical properties of VGCCs or altered expression of channels results in pathophysiological changes that underlie various chronic diseases including chronic pain, epilepsy, and migraines (Cain and Snutch 2011). Thus, tight regulation of channel activity and expression is critical for maintaining intracellular Ca^{2+} homeostasis and preventing neurotoxic signaling.

1.4.1 Biophysical and pharmacological properties of voltage-gated Ca^{2+} channel

Since 1975, it has been recognized that there are two distinct general classes of VGCCs: high voltage-activated (HVA) channels that activate upon large depolarizations from the resting membrane potential and low voltage-activated (LVA) channels that open in response to smaller changes in membrane voltage (Hagiwara *et al.* 1975). In addition to high voltage activation, the first HVA channels were distinguished by their large single channel conductance, slow voltage-dependent inactivation, and specific inhibition by dihydropyridines, phenylalkylamines, and benzothiazepines (Reuter *et al.* 1983, Catterall 2000). Because currents from these channels are long-lasting when Ba^{2+} is the current carrier, these channels were designated L-type (Nowycky *et al.* 1985). Voltage-clamp studies of Ca^{2+} currents in starfish eggs (Hagiwara *et al.* 1975) and cerebellar Purkinje neurons (Llinas and Yarom 1981) revealed Ca^{2+} currents with different properties from L-type including: activation at more negative potentials that are closer to

neuronal resting membrane potential, rapid inactivation, slow deactivation, small single channel conductance, and insensitivity to typical Ca^{2+} channel antagonists (Catterall 2000). Because of their transient kinetics, these LVA channels were designated T-type (Nowycky *et al.* 1985). According to a new nomenclature scheme based upon molecular cloning, L-type channels belong to the Ca_v1 family of proteins, whereas T-type belong to Ca_v3 family of VGCCs (Catterall *et al.* 2005).

VGCC recordings from dissociated dorsal root ganglion neurons revealed an additional Ca^{2+} current, termed N-type ($Ca_v2.2$) for neuronal (Nowycky *et al.* 1985). The voltage dependence and rate of inactivation of these channels is lower and faster than L-type channels but higher and slower compared to T-type channels. N-type channels also exhibit insensitivity to organic L-type channel blockers; however, they have a specific sensitivity to the cone snail peptide ω-conotoxin GVIA (McCleskey *et al.* 1987). Since the voltage dependence and kinetics of N-type channels vary significantly between neuronal populations, blockade by ω-conotoxin is the distinguishing feature of N-type channels from other Ca^{2+} currents (Catterall 2000). Further recordings from different types of neurons revealed three additional Ca^{2+} currents. P-type Ca^{2+} currents ($Ca_v2.1$), first recorded from Purkinje neurons (Llinas *et al.* 1989), and Q-type currents ($Ca_v2.1$), first recorded from cerebellar granule cells (Randall and Tsien 1995), both sensitive to the spider toxin ω-agatoxin IVA but with different affinities (Mintz *et al.* 1992, Adams *et al.* 1993). R-type currents ($Ca_v2.3$), also recorded from cerebellar granule cells initially, are blocked by SNX-482, a peptide derived from Tarantula venom (Newcomb *et al.* 1998). Although L- and T-type currents have been recorded from a wide variety of cell types, N-, P-, Q-, and R-type currents are found primarily in neurons (Catterall 2000).

1.4.2 Subunit structure of voltage-gated Ca^{2+} channels

HVA channels are heteromultimeric protein complexes that are comprised of a pore-forming α1 subunit, plus ancillary β and α2δ subunits, while LVA channels appear to lack ancillary subunits and function as monomers (Catterall 2010). The α1 subunit is the defining feature of different VGCC subtypes and in mammals there are 10 different genes that encode α1 subunits (Catterall 2000). The three major families of $Ca_v\alpha1$ subunits (Ca_v1, Ca_v2, and Ca_v3) each have a number of subtypes and it is has been suggested that gene duplication and divergence of an ancestral Ca^{2+} channel gene gave rise to HVA and LVA subfamilies (Perez-Reyes 2003). Ca_v1 and Ca_v2 arose from further gene duplication of the HVA gene, which must have occurred over 500 million years ago because the nematode *Caenorhabditis elegans* retains a member of each subclass (Perez-Reyes 2003). Over time, the Ca_v1 subfamily evolved into four L-type genes (the broadly expressed $Ca_v1.2$, $Ca_v1.3$, $Ca_v1.4$, and a skeletal muscle specific subtype, $Ca_v1.1$.), while the Ca_v2 subfamily (Ca_v 2.1, $Ca_v2.2$, $Ca_v2.3$) and the Ca_v3 subfamily ($Ca_v3.1$, $Ca_v3.2$, $Ca_v3.3$) each evolved into three genes (Perez-Reyes 2003).

The α1 subunits are large proteins comprised of ~2000 amino acid residues and with sequence alignment studies predicting a transmembrane structure resembling the pore-forming α subunit of Na^+ channels (Catterall 2000). The amino acid sequences of all ten α1 subunits are organized in four repeating structural domains, each of which contains six transmembrane helices (S1 to S6) and a reentrant P loop between S5 and S6 (Catterall 2000). Positive charges in every third or fourth position on the S4 segments determine voltage-dependent activation and the membrane-associated loop between S5 and S6 lines the permeation pathway (Catterall 2000). The four P loop regions combine to form the pore that determines ion selectivity of VGCCs, S5-S6 linkers

(P-loops) line the pore extracellularly; whereas, the S6 segments line the pore intracellularly (Catterall 2000). Each P loop region contains highly conserved negatively charged amino acid residues that render VGCCs permeable to cations including Ca^{2+}, barium and strontium, and allow certain VGCC subtypes to interact with nonpermeant divalent cations (e.g. cadmium) (Simms and Zamponi 2014). Large cytoplasmic linker regions connect the primary membrane domains, while both the N and C termini are located intracellularly (Simms and Zamponi 2014). The greatest sequence variation between subtypes is found within the cytoplasmic linker regions, which serve as substrates for subtype-specific regulation by secondary messengers (e.g. PKC and calmodulin) and protein-protein interactions (e.g. G proteins) (Zamponi *et al.* 1997) (Hall *et al.* 2013). Functional diversity of each of the ten α1 subunits also occurs via alternative splicing in a cell-dependent manner (Tan *et al.* 2012), and functional variation can also arise from RNA editing (Bazzazi *et al.* 2013).

Structural and functional diversity of the HVA VGCCs is further enhanced by various ancillary β subunits. Four genes encoding β subunits have been reported, each of which is subject to alternative splicing, and further the neuronal HVA α1 subunits can be associated with multiple types of β subunits (Catterall 2000). The different β subunit isoforms, by modulating current kinetics and voltage-dependence of activation, can significantly alter functional properties of α1 subunits (Catterall 2000). Association of β subunits with the I-II linker regions of α1 subunits results in increased trafficking of channels to the cell surface by masking of intrinsic endoplasmic reticulum signals in the α1 subunit by the β subunit (Bichet *et al.* 2000, Waithe *et al.* 2011). Four different types of α2δ subunits are found in association with the extracellular domain of HVA channels, connecting to the extracellular leaflet of the plasma membrane

through a glycophosphatidylinositol (GPI) anchor (Davies *et al.* 2010). Following transcription and translation as a single protein, the α2 and δ subunits are posttranslationally cleaved and then rejoined by a disulfide bond (Dolphin 2013). Unlike β subunits, α2δ subunits do not appear to significantly alter channel gating or function; however, they do promote channel targeting to presynaptic terminals, which results in increased neurotransmitter release probability (Hoppa *et al.* 2012). Such enhancement of channel cell surface density is mediated by an α2 metal-ion-dependent adhesion site in a conserved Von Willebrand factor-A domain and possibly via interactions with thrombospondin receptors (Canti *et al.* 2005, Eroglu *et al.* 2009). Distinct from the HVA channels, the functional activity of LVA channel α1 subunits alone in heterologous systems is remarkably similar to endogenous LVA channels, suggesting that these channels are made up of α1 subunits exclusively (Perez-Reyes 2003).

The amino acid sequence and predicted secondary structure of T-type channels show that, similar to HVA channels, they are evolutionarily related to the α subunits of Na^+ and K^+ channels (Jan and Jan 1990). The most highly conserved sequence resides in the S4 segments predicted to move outward when the neuronal membrane is depolarized. The pore loops are also well-conserved and amongst VGCCs, containing the distinguishing sequence: T-x-E/D-x-W. In HVA channels, all four domains have a glutamate residue in the pore (EEEE), while glutamate in the third and fourth domains of T-type channels has been replaced with aspartate (EEDD) (Perez-Reyes 2003). These residues in the pore control selectivity and permeation of both LVA and HVA channels. The EEDD pore locus is responsible for the lower single channel conductance of LVA channels to Ba^{2+} and decreased sensitivity to Cd^{2+} with respect to HVA channels (Ellinor *et al.* 1995). Other than the extracellular loop connecting S5 of domain I to the pore loop, all

extracellular loops are predicted to be very short. The S5 extracellular loop on domain I contains six cysteine residues that are highly conserved within the T-type family and are substrates for glycosylation (Perez-Reyes 2003). It has been shown that glycosylation inhibits the activity of T-type but not L-type channels in cardiac myocytes (Fermini and Nathan 1991). The amino termini of Ca_v3 family of channels are <100 amino acids, while the carboxy termini are 433-493 amino acids (Perez-Reyes 2003). As described previously, these loops are important for binding ancillary subunits in HVA channel; however, their role in T-type channel function is currently contested (Perez-Reyes 2003).

1.4.3 Unique biophysical properties of T-type Ca^{2+} channels

T-type channels exhibit a higher selectivity for Ca^{2+} than other cations such as Na^+ and K^+. T-type channels do not employ the selectivity by rejection mechanism to discriminate between Ca^{2+} and Na^+, because their pore diameter is 5.1 angstrom and the hydration diameter of Ca^{2+} is larger than Na^+, thus Ca^{2+} selectivity over Na^+ cannot occur by sieving (Talavera and Nilius 2006). Instead, Ca^{2+} selectivity occurs through affinity of the ions to certain binding sites within the channel pore. Ca^{2+} ions bind to the T-type channel pore with high affinity and this occludes the access of monovalent cations to the channel pore by electrostatic repulsion (Talavera and Nilius 2006). Ca^{2+} ions flow through the channel pore at a rate of millions per second because of repulsion between ions when two or more occupy the space at millimolar Ca^{2+} concentrations (Talavera and Nilius 2006). The permeation of monovalent cations is promoted at low extracellular pH levels and reduced with increasing external Ca^{2+} concentrations (Talavera and Nilius 2006).

Characterization of T-type currents is usually done with voltage-clamp whole-cell recordings of isolated neurons. T-type channels have single channel conductances between 6 and 8 pS in the presence of Ca^{2+} and Ba^{2+} (Talavera and Nilius 2006). *I-V* relationships are generally constructed by holding cells at –90 mV to -100 mV and then depolarizing with pulses of 10 mV increments. The threshold potential for T-type current activation is typically –60 mV in isolated neurons (Perez-Reyes 2003). Closer to threshold potentials, currents require several milliseconds to reach their peak because they activate and inactivate slowly (Perez-Reyes 2003). At more depolarized potentials, both activation and inactivation kinetics are faster resulting in a stereotypical pattern wherein successive steps activate currents that cross each other (Perez-Reyes 2003). This pattern is not observed in recordings of HVA channels because their inactivation rates are slower than activation rates.

The time constant of activation for T-type channels is between 8 and 15 msec at potentials near threshold and decreases exponentially with depolarization to 1-2 msec at voltages of maximum activation (–20 mV or greater) (Talavera and Nilius 2006). *I-V* curves of T-type channels show a peak and then decrease at more depolarized potentials because of the reduction in driving force for Ca^{2+} ions as the test pulse approaches the theoretical reversal potential (+40 mV) (Perez-Reyes 2003). A hallmark feature of T-type channels is that they are transient with whole cell currents rapidly decaying after peaking. This decay is due to channel inactivation - membrane depolarization shifts T-type channels into an inactivated state where channels are in a closed conformation (Perez-Reyes 2003). The voltage dependence of steady-state inactivation is –80 mV in neuronal tissues and –72 mV when measured in HEK293 cells (Klockner *et al.* 1999). This value is more hyperpolarized than the activation threshold, suggesting that T-type channels

exist in a closed conformation at potentials where they do not appear to be activated (Perez-Reyes 2003). The time constant of inactivation varies between 50 to 100 msec at the threshold for activation and decreases exponentially with increasing depolarization to 10-20 msec at voltages of maximum activation (Talavera and Nilius 2006). Current inactivation varies with channel subtype: $Ca_v3.1$ and $Ca_v3.2$ show the fastest inactivation, while currents mediated by $Ca_v3.3$ channels are more slowly inactivating (Talavera and Nilius 2006).

Hyperpolarization of the membrane back to negative potentials removes the voltage-dependent inactivation of T-type channels in a process called deinactivation or reactivation. The time course of reactivation decreases as the duration of channel state in inactivation increases (Kuo and Yang 2001). $Ca_v3.1$ recovers from inactivation faster (120-140 msec) than $Ca_v3.2$ (400-440 msec) and $Ca_v3.3$ (260-350 msec) (Kuo and Yang 2001, Talavera and Nilius 2006). T-type channels do not recover directly from an inactivated to an open state, instead deinactivation occurs through the deactivation-first pathway (Frazier *et al.* 2001). Deactivation refers to the transition of channels from the open state to the nearest closed state. Deactivation kinetics can be studied by repolarizing the membrane after a short activation pulse, resulting in a tail current that decays reflecting the time course of the closing of channels as the voltage is returned to rest (Talavera and Nilius 2006). Relatively slow deactivation kinetics are a distinguishing feature of T-type channel gating (Perez-Reyes 2003). The rate of deactivation increases exponentially with hyperpolarization (Chemin *et al.* 2002), deactivation kinetics also vary between subtypes with $Ca_v3.1$ showing slower kinetics and $Ca_v3.3$ displaying faster rates of deactivation (Klockner *et al.* 1999).

1.4.4 Role of T-type Ca^{2+} channels in neurotransmitter release

In part due to their unique biophysical characteristics, T-type channels are particularly well-suited to facilitate neurotransmitter release and their role in low-threshold exocytosis has been reported in various cell types. Pan *et al*. showed that retinal bipolar cells, second order neurons in the retina, express functional T-type channels (Pan *et al.* 2001). Brief activation of these channels resulted in Ca^{2+} transients in axonal termini that could be visualized with Ca^{2+} sensitive dyes. The authors also found that Ca^{2+} influx in terminals led to a detectable increase in capacitance, indicating the occurrence of exocytosis and transmitter release. Similarly, Egger *et al*. found that *I-V* relationships and inactivation kinetics of Ca^{2+} transients in olfactory bulb granule cells, interneurons that form dendrodendritic synapses with principles cells, were consistent with T-type channel properties (Egger *et al.* 2003). Further, action-potential evoked Ca^{2+} transients in dendrites and spines of granule cells were responsible for neurotransmitter release from granule cells to mitral cells (Egger *et al.* 2003).

T-type channels have also been implicated in GABA release from cortical interneurons. Tang *et al*. showed that subthreshold depolarization induced by nicotinic receptor activation leads to Ca^{2+} influx through presynaptic T-type channels in GABAergic neurons (Tang *et al.* 2011). This Ca^{2+} influx results in asynchronous release of GABA from cortical interneurons to hippocampal CA1 pyramidal cells (Tang *et al.* 2011). In addition to evoked release, a recent report showed that T-type channels contribute to spontaneous synaptic release in nociceptive dorsal horn neurons. Jacus *et al*. reported that specific pharmacological antagonism of T-type channels in dorsal horn neurons inhibits spontaneous glutamate, but not GABA release, and recordings from acute spinal cord preparations of knock-out mice, along with immunohistochemistry, implicate presynaptic

$Ca_v3.2$ channels in this process (Jacus *et al.* 2012). These studies provide convincing evidence regarding the role of presynaptic T-type channels in synaptic transmission in various different cell types.

1.4.5 T-type Ca^{2+} channels and neuronal firing

At resting neuronal membrane potentials, T-type Ca^{2+} channels are unavailable for opening due to voltage-dependent inactivation; however, a small hyperpolarization (e.g. caused by an IPSP) allows T-type channels to enter a deactivated state and permit Ca^{2+} entry from a subsequent depolarization that is in the voltage range of T-type channel activation. If sufficient channels recover from inactivation during the transient hyperpolarization, then a low-threshold spike (LTS) can depolarize neurons to action potential threshold leading to burst firing (Alvina *et al.* 2009). This phenomenon of "rebound bursting" shapes the output profiles of many neurons, particularly thalamocortical relay neurons and thalamic reticular neurons (Ulrich and Huguenard 1997).

Detailed studies of thalamic neurons indicate that T-type Ca^{2+} channels underlie the neuronal property of membrane potential bistability – the existence of two resting membrane potentials that is facilitated by the window current generated by T-type channels (Crunelli *et al.* 2005). The window current is the steady state current that originates within the range of voltages where the activation and inactivation curves of T-type channels overlap. Within this voltage region, a small fraction of channels do not inactivate and remain available for opening, although the number of these channels and the magnitude of current mediated by their opening is strongly dependent on recording conditions. Investigations on recombinant T-type channels have indicated that $Ca_v3.3$ channels exhibit the largest window current (Klockner *et al.* 1999). The window current-

mediated bistability underlies slow wave (< I Hz) non-REM sleep that organizes other sleep rhythms such as spindle and delta waves into coordinated repetitive episodes (Crunelli and Hughes 2010). The intracellular correlates of slow wave sleep are repeating segments of sustained action potential firing interleaved with periods of inactivity that result in "up" and "down" states of the membrane potential that differ by 15-20 mV (Crunelli and Hughes 2010). Such patterns of activity are observed in all cortical neurons and they are the result of intrinsic resonant properties of neurons combined with extensive cortical interconnectivity (Crunelli *et al.* 2005).

In thalamocortical (TC) neurons, the shift from down to up state is marked by a LTS and subsequent high-frequency bursts of action potentials (Hughes *et al.* 2002). The up state corresponds to window current activation and the down state to window current inactivation (Hughes *et al.* 2002). Background leak currents modulate the activity of window currents such that bistability occurs when leak conductance is below a certain threshold. In addition, other channels (e.g. HCN) determine the duration of up and down states in the absence of other synaptic inputs (Hughes *et al.* 2002). The slow oscillation cannot be observed in thalamic neurons if the cortical afferent have been removed; however, stimulation of metabotropic glutamate receptors (mGluR), that reduces background leak currents, can activate membrane bistability and intrinsic slow oscillations (Hughes *et al.* 2002). T-type channel window currents also underlie the high frequency bursts of thalamocortical neurons in the awake animal (Crunelli *et al.* 2005).

In addition to controlling neuronal firing by virtue of their biophysical properties, T-type Ca^{2+} channels also modify neuronal output by altering the activity of other channels. In stellate cells, interneurons in the cerebellum, $Ca_v3.2$ and $Ca_v3.3$ form a signaling complex with $K_v4.2$ channels and K_v channel interacting proteins (KChIPs) (Anderson *et al.* 2010). Ca^{2+} entry through T-type channels shifts the inactivation voltage of $K_v4.2$ to more depolarized potentials, enabling them to regulate firing properties of cerebellar stellate cells. Further, the Ca_v3-K_v4 complex acts a voltage sensor and responds to a decrease in extracellular Ca^{2+} by reducing K_v4 and Ca_v3 conductance, thereby elevating the rate of stellate cell firing (Anderson *et al.* 2013). Similarly, $Ca_v3.2$ channels interact with intermediate conductance Ca^{2+}-activated potassium channels ($K_{Ca}3.1$) in cerebellar Purkinje cells. Ca^{2+} entry through $Ca_v3.2$ channels in response to subthreshold activation triggers $K_{Ca}3.1$-mediated control over temporal summation of synaptic inputs (Engbers *et al.* 2012). Additionally, a physical signaling complex between large conductance Ca^{2+} activated potassium channels ($K_{Ca}1.1$) in medial vestibular neurons reduces firing frequency (Rehak *et al.* 2013) and Ca^{2+} entry through T-type channels modulates the activity of small conductance Ca^{2+}-activated potassium channels ($K_{Ca}2.1$) to ultimately regulate sleep-related oscillations in dendrites of thalamic reticular neurons (Cueni *et al.* 2008). These studies show the ability of T-type channels to modulate neuronal output through downstream regulation of K^+ channel activity.

1.4.6 Regulation of T-type channel function

Although T-type channel gating and activation is primarily determined by changes in membrane potential, their function can also be modulated by a variety of G protein-coupled receptors (GPCRs) and downstream intracellular protein kinases. Sequence analysis of the α1 subunit of T-type Ca^{2+} channels reveal the existence of several phosphorylation consensus sites for protein kinases (Perez-Reyes 2003). One of the first reports documenting T-type channel targeting by protein kinases implicated the role of Ca^{2+}/CaM-dependent protein kinase II (CaMKII) in potentiating recombinant $Ca_v3.2$ currents (Wolfe *et al.* 2002). CaMKII is abundantly distributed in the postsynaptic densities of excitatory synapses, where it modulates synaptic transmission (Braun and Schulman 1995). CaMKII causes a hyperpolarizing shift in the half-maximal potential for activation, leading to increased $Ca_v3.2$ activity at negative potentials (Wolfe *et al.* 2002). This shift in the channel activation curve increases the proportion of channels that are available for opening by increasing the magnitude of window current. The potentiation depends on phosphorylation of a serine residue on the intracellular linker domain II and III that is absent in other T-type channels (Welsby *et al.* 2003). This structural requirement results in preferential targeting of $Ca_v3.2$ channels by CaMKII. Similarly, in Xenopus oocytes protein kinase C (PKC) augments the current amplitude of all three T-type channel subtypes through interactions with the cytoplasmic linker II-III region of the channels (Park *et al.* 2006). Protein kinase A (PKA) also increases the current amplitude of all three channel subtypes without affecting cell surface expression in various mammalian cell lines (Chemin *et al.* 2007).

In contrast, Rho-associated kinase (ROCK) reversibly inhibits peak current amplitudes of $Ca_v3.1$ and $Ca_v3.3$ channels and causes a depolarizing shift in the voltage dependence of activation in

$Ca_v3.2$ channels (Iftinca *et al.* 2007). ROCK-mediated inhibition is dependent on intracellular GTP and serine/threonine residues sites within the domain II-III linker regions (Iftinca *et al.* 2007). The intracellular loop connecting transmembrane domain II and III is also the mediating factor in $Ca_v3.2$ inhibition by G-protein beta-gamma subunits (DePuy *et al.* 2006). Beta-gamma subunits reduce the open channel probability and current density of $Ca_v3.2$ channels, but not $Ca_v3.1$ or $Ca_v3.3$, at all potentials tested without changing surface expression or activation gating of the channel (Wolfe *et al.* 2003). Thus, the domain II-III linker region renders T-type Ca^{2+} channels sensitive to regulation by a variety of intracellular second messengers.

Given that T-type channel activity can be regulated by kinases that are coupled to G proteins, GPCRs are expected to influence T-type channel function. Several studies have detailed the involvement of muscarinic acetylcholine receptors (mAChR) in regulating T-type channel activity. Permberton and colleagues (Pemberton *et al.* 2000) studied modulation of nickel-sensitive T-type Ca^{2+} currents by five mAChR subtypes in NIH 3T3 cells. They found that activation of M3 and M5 receptors enhances T-type currents through increased cAMP levels and subsequent activation of PKA; however, application of acetylcholine to cells stably transfected with M2 or M4 receptors had no effect on T-type channel activity. Similarly, application of carbachol, a nonhydrolyzable cholinergic agonist, increases T-type currents in CA1 lacunosum-moleculare neurons (Fraser and MacVicar 1991), and increases open channel probability in CA3 pyramidal cells of the guinea pig hippocampus (Fisher and Johnston 1990). Hildebrand and colleagues have shown that M1 mAChRs selectively inhibit $Ca_v3.3$ but not $Ca_v3.1$ or $Ca_v3.2$ channel activity in HEK293T cells (Hildebrand *et al.* 2007). In this study, inhibition was mediated by both $G\alpha_q$/ $G\alpha_{11}$- and $G\beta\gamma$-linked pathways; however, none of the downstream

secondary messenger proteins such as PKC, PKA, or CAMK were involved. This points to a novel M1-mediated regulatory pathway that modulates T-type channel activity and fine-tuning of T-type channel function that is dependent on the specific isoform and modulatory pathways expressed in a given cell.

T-type channel activity is also subject to regulation by mGluRs. Pre- and postsynaptically expressed mGluRs frequently modulate synaptic communication between neurons and various studies have shown that regulation of synaptic transmission by mGluRs fine-tunes the output a circuit (Cosgrove *et al.* 2011). mGluRs are categorized into three different groups based on sensitivity to specific pharmacological agonists, receptor structure, physiological activity, and gene products (Conn and Pin 1997). Group I mGluRs are composed of splice variants of mGluR1 and mGluR5 subtypes. These receptors are coupled to G_q proteins that initiate a second messenger pathway involving phosphatidylinositol hydrolysis via phospholipase C, which elevates intracellular Ca^{2+} concentration, activates ryanodine-sensitive Ca^{2+} stores, and modulates voltage-gated channel activity (Swartz and Bean 1992, Guerineau *et al.* 1994, Guerineau *et al.* 1995). Activation of $mGluR_1$ by glutamate causes potentiation of $Ca_v3.1$ and $Ca_v3.2$, but an inhibition of $Ca_v3.3$ currents in HEK293 cells (Hildebrand *et al.* 2009). This selective inhibition of $Ca_v3.3$ by $mGluR_1$ is similar to that shown by mAChRs in the same exogenous system (Hildebrand *et al.* 2007). Heterogeneous T-type channel modulation by a metabotropic receptor coupled to the same $G\alpha_q/11$ protein indicates that the combined repertoire of downstream transduction pathways and specific channel subtypes expressed in a given system determine the extent and modality of T-type regulation.

In addition to G proteins and GPCRs, T-type channels are also sensitive to changes in cellular redox state. Redox regulation of T-type channels via oxidation of histidine residues has been reported in multiple cell types and it underlies both peripheral and central pain processing (Todorovic and Jevtovic-Todorovic 2006). In dorsal root ganglion neurons, the endogenous reducing agent L-cysteine shifts gating properties of T-type channels causing an increase in T-type channel amplitude and inducing burst firing (Nelson *et al.* 2005). This sensitizes a subset of peripheral nociceptors by decreasing the threshold for cellular excitability such that injection of L-cysteine into the receptive fields of these neurons produces thermal and mechanical sensitization in vivo (Todorovic *et al.* 2001). Similarly, reducing agents, including L-cysteine, increase T-type channel currents in rat reticular thalamic neurons and recombinant $Ca_v3.2$ currents without having an effect on currents generated by $Ca_v3.1$ or $Ca_v3.3$ (Joksovic *et al.* 2006).

$Ca_v3.2$ is the molecular substrate for redox regulation that occurs through modulation of a histidine residue in domain I S3-S4 region of the channel (Joksovic *et al.* 2006). Sulfur-containing reducing agents, such as L-cysteine, chelate heavy metals that normally inhibit $Ca_v3.2$ channel activity (Nelson *et al.* 2007). Specifically, endogenous zinc tonically inhibits $Ca_v3.2$ activity by modulating a high-affinity metal-binding site on the extracellular surface of $Ca_v3.2$ (Nelson *et al.* 2007). A histidine residue at position 191 (H191) is a critical component of this metal-binding site and L-cysteine-mediated zinc chelation removes this inhibition leading to enhancement of $Ca_v3.2$ currents and nociceptor sensitization (Nelson *et al.* 2007). Mutation of the histidine residue in position 191 to glutamine (H191Q) completely removes $Ca_v3.2$ sensitivity to reducing agents without changing biophysical properties of the channel suggesting

that modulation of $Ca_v3.2$ by reducing agents occurs independent of channel gating (Nelson *et al.* 2007).

H191 also underlies inhibition of $Ca_v3.2$ channels by ascorbate. Ascorbate can function as an antioxidant scavenging reactive oxygen and nitrogen species; however, it can also catalyze the formation of reactive oxygen species (ROS) by reducing transition metals via electron transfer mechanisms (Nelson *et al.* 2007). The process of ROS formation at metal binding sites is termed metal-catalyzed oxidation (MCO) and ROS generated directly at metal-binding sites can modify functional groups of neighbouring residues (Stadtman 1993). Ascorbate inhibits $Ca_v3.2$ channels specifically by initiating MCO of metal-binding H191 in domain I of the channel (Nelson *et al.* 2007). Ascorbate reduces $Ca_v3.2$-, but not $Ca_v3.1$ or $Ca_v3.3$-mediated currents in both thalamic and recombinant HEK293 cells (Nelson *et al.* 2007). Ascorbate induced reduction in amplitude of $Ca_v3.2$ currents occurs over a wide range of potentials without measurable changes in voltage dependence of activation or inactivation (Nelson *et al.* 2007). Physiologically relevant concentrations of ascorbate also reduce the amplitude of LTS and abolish burst firing in reticular thalamic neurons (Nelson *et al.* 2007).

In addition to reducing agents, divalent metal ions such as nickel and zinc selectively inhibit $Ca_v3.2$ over the other two T-type channel subtypes (Jeong *et al.* 2003, Traboulsie *et al.* 2007). Pharmacological studies using sinoatrial nodal cells (Hagiwara *et al.* 1988) and dorsal root ganglion neurons (Todorovic and Lingle 1998) show that low concentrations of nickel (<50 μM) preferentially block $Ca_v3.2$ channels, while block of $Ca_v3.1$ and $Ca_v3.3$ channels requires much higher concentrations (>100 μM) (Zamponi *et al.* 1996). Nickel block of $Ca_v3.2$ channels is also

dependent on H191 in the short extracellular loop (9 amino acids long) connecting S3 and S4 of domain I of the channel. Consistent with this, mutations replacing histidine at position 191 with alanine or glutamine in $Ca_v3.2$ lower its nickel sensitivity to that measured for $Ca_v3.1$ (Kang *et al.* 2006). Comparisons between amino acid sequences of all 10 VGCC $\alpha 1$ subunits reveal that only $Ca_v3.2$ and $Ca_v2.3$ (R-type) contain a histidine residue in the region connecting S3 to S4, which might explain higher sensitivity of $Ca_v2.3$ to nickel compared to other HVA channels (Kang *et al.* 2006). In the case of $Ca_v3.2$, it is proposed that nickel binding to H191 prevents coupling between S4, the voltage sensor, and the channel pore, thereby blocking channel gating to the open state and stabilizing channels in closed states (Kang *et al.* 2006). Thus, nickel along with reducing agents, block $Ca_v3.2$ with high affinity and independent of voltage by taking advantage of the histidine residue in a metal-binding site that is unique to this subtype of T-type channels.

1.4.7 Contributions of voltage-gated Ca^{2+} channels to synaptic potentials in neuronal dendrites and spines

Cytosolic Ca^{2+} increase in response to synaptic activation can arise from three distinct sources: VGCCs, glutamate receptors, and release from internal stores (Bloodgood and Sabatini 2008). The relative contribution of each source to intracellular Ca^{2+} elevation is dependent on the brain region, neuronal type, and subcellular compartment (Bloodgood and Sabatini 2007). In pyramidal neurons of the hippocampus, NMDA receptors are major contributors to synaptic Ca^{2+} influx and AMPA receptors, although typically Ca^{2+} impermeable, provide a significant membrane depolarization that removes the Mg^{2+} block of NMDA receptors and activates various voltage sensitive conductances. Physiological conditions that change the number or properties of

NMDAR and AMPA receptors underlie many forms of synaptic plasticity because they result in long-term changes of synaptic potential and Ca^{2+} transient amplitude (Higley and Sabatini 2008). Recent data from different labs highlights the important contribution of VGCCs to glutamate-receptor independent mechanisms of synaptic plasticity.

The distribution of VGCCs in dendritic shafts and spines differs between a given region of the dendrite and across different types of neurons. In CA1 pyramidal neurons, T-type, L-type, N-type Ca^{2+} channels are found both in dendrites and spines; while, R-type channels are present exclusively in spines (Sabatini and Svoboda 2000, Bloodgood and Sabatini 2007). The relative contribution of each VGCC subclass to cytosolic Ca^{2+} elevation induced by back-propagating action potentials is roughly equal (Magee *et al.* 1995, Magee and Johnston 1995); however, subthreshold synaptic activation leads to a local Ca^{2+} influx that is independent of L-type and N-type channels but requires SNX-482-sensitive R-type ($Ca_v2.3$) channels (Bloodgood and Sabatini 2008). Unexpectedly, blockade of R-type channels with SNX-482 ultimately increases synaptic potential and Ca^{2+} transient amplitude (Bloodgood and Sabatini 2008). Such boosting of synaptic potentials with SNX-482 occurs through prevention of downstream activation of apamin-sensitive small conductance Ca^{2+}-activated K^+ (SK) channels and 4-aminopyridine (4AP)-sensitive A-type potassium channels (Wang *et al.* 2014).

Studies utilizing multiple pharmacological antagonists show that VGCCs and voltage-activated K^+ channels act in concert to regulate synaptic potentials and NMDA receptor-mediated Ca^{2+} influx. Specifically, Ca^{2+} entry through NMDA receptors is required for activating synaptic SK channels in CA1 spines, while boosting of synaptic potentials with SNX-482 is dependent on A-

type K^+ channel availability (Wang *et al.* 2014). Consistent with this idea, blocking either apamin-sensitive SK channels or SNX-sensitive Ca^{2+} channels increases the amplitude of synaptically evoked potentials; however, the effects of apamin and SNX are not mutually exclusive (Wang *et al.* 2014). Inhibition of NMDA receptors occludes the boosting effect of apamin but not SNX, suggesting that Ca^{2+} entry through NMDA receptors is sufficient to activate SK channels (Wang *et al.* 2014). Instead, the boosting effect of SNX on synaptic potentials requires 4AP-sensitive $K_v4.2$ channels and KChIPs indicating that the influence of R-type channels on spine Ca^{2+} levels is constrained by A-type K^+ channels (Wang *et al.* 2014). Together, these observations have been incorporated into a model of synaptic signaling regulation that is influenced by the coordinated activity of voltage-gated ion channels and glutamate receptors.

In this model, the amplitude of synaptic potentials and Ca^{2+} transients is determined by the sequential activation of both voltage-gated and ligand-gated ion channels (Bloodgood and Sabatini 2008). First, the activation of SNX-sensitive Ca^{2+} channels independent of NMDA receptors indicates that local subthreshold synaptic activation through glutamate uncaging or Schaffer collateral stimulation is sufficient to open VGCCs (Bloodgood and Sabatini 2008). Subsequent activation of SK channels repolarizes the spine potential and terminates Ca^{2+} entry from NMDA receptors. Second, the boosting of synaptic potentials by SNX is not prevented by NMDA receptor inhibition (Wang *et al.* 2014), indicating that instead of functioning as a single Ca^{2+} signaling domain, spines in pyramidal cells contain various Ca^{2+} signaling microdomains (Bloodgood and Sabatini 2008). This idea is further bolstered by the observation that Ca^{2+} influx through R-type channels is not sufficient for SK channel activation; instead it is dependent on

Ca^{2+} entry through NMDA receptors (Wang *et al.* 2014). Further, the boosting effects of SNX on synaptic potential amplitude are not mediated through Ca^{2+}-activated K^+ channels, but rather, voltage-gated K^+ channels. This reflects a tight coupling between R-type Ca^{2+} and A-type K^+ channels leading to their sustained activation during synaptic transmission (Wang *et al.* 2014). This coupling is reminiscent of the molecular complex between T-type Ca^{2+} channels and $K_V4.2$-containing channels in cerebellar stellate cells (Anderson *et al.* 2010). Thus, concerted activity of K^+ channels and VGCCs regulates the amplitude of synaptic potentials and Ca^{2+} transients in spines, reflecting the importance of non-glutamatergic ion channels in modulating synaptic transmission.

1.5 Rationale and hypothesis

The rapid activation of T-type Ca^{2+} channels at low voltages results in LTS that underlie normal physiological (e.g. burst-firing patterns observed during sleep) (Beenhakker and Huguenard 2009) and pathological conditions, such as neuropathic pain and epilepsy (Khosravani and Zamponi 2006). T-type Ca^{2+} channels play a variety of different and important roles in almost every type of neuronal oscillation observed in thalamic neurons including non-rapid eye movement sleep, alpha/theta waves, the K complex and slow (<1 Hz) sleep rhythm, sleep spindles, and delta waves (Crunelli *et al.* 2006). In hippocampal CA1 pyramidal neurons, activation of nickel-sensitive Ca^{2+} channels by backpropagating large-amplitude spikes leads to a persistent inward current that generates a burst firing pattern reflecting the ability of these channels to regulate the processing and storage of information by switching the firing mode of neurons from single spikes to burst firing (Magee and Carruth 1999). Upon muscarinic activation, hippocampal CA3 pyramidal neurons exhibit a distinctive rhythmic slow network

activity that results in oscillations at theta frequency (Buzsaki 2002). Further, synaptic stimulation of theta frequency induces LTP in the CA1 region and complex spike bursting is required for the induction of LTP (Thomas *et al.* 1998).

Complex spikes require highly synchronous synaptic activation *in vivo* and are observed under physiological conditions that cause different regions of the hippocampal network to discharge in synchrony (Kamondi *et al.* 1998). Complex spikes observed *in vitro* occur as a series of fast sodium-dependent action potentials that give rise to a slower Ca^{2+}-dependent spike. Golding *et al*. have shown that in the CA1 region, complex spikes can be observed at the soma only under specific ionic conditions because the underlying Ca^{2+} currents are under the strong repolarizing influence of various K^+ conductances (Golding *et al.* 1999). To our knowledge, LTS have not been reported in CA3 PCs even though low-threshold currents have been observed in these cells (Avery and Johnston 1996). We hypothesize that LTS in CA3 PCs have a dendritic origin and that somatic recordings have precluded their observation because activation of K^+ channels in dendrites terminates Ca^{2+} channel-mediated depolarization before it can be detected at the soma. Given that dendritic integration in CA3 PCs is highly dependent on Ca^{2+} signaling, it is important to investigate the precise interactions between voltage-gated ion channels that govern Ca^{2+}-mediated signal propagation.

In addition to both demonstrating and investigating the conditions under which LTS are generated in CA3 PCs, we aim to study the regulation of LTS by mechanisms that alter intrinsic activity of T-type channels (e.g. gating kinetics) and postsynaptic receptors that affect T-type function indirectly by activating opposing K conductances (e.g. M-current). Dendritic

depolarization from T-type Ca^{2+} channels combined with enhanced Ca^{2+} entry would change membrane excitability and dramatically modify Ca^{2+}-dependent synaptic plasticity. There is a large body of evidence showing T-type regulation by GPCRs in different brain areas and the reciprocal influence of voltage/Ca^{2+}-gated K^+ channels on T-type channel activity (Perez-Reyes 2003). We hypothesize that the high dendritic expression of non-inactivating, low-threshold, muscarinic-sensitive K^+ channels in CA3 PCs (Safiulina *et al.* 2008, Qi *et al.* 2014) constrains LTS to discrete spatial events and that inhibition of these channels by muscarinic activation will greatly facilitate LTS propagation in CA3 PCs. Further, because $mGlu_1$ receptors potentiate T-type channel activity through secondary messenger pathways (Hildebrand *et al.* 2009) and their effects on A-type K^+ channel gating (Otsu *et al.* 2014), we hypothesize that $mGluR_1$ activation will also augment LTS propagation in CA3 PCs.

T-type channels have a prominent role in synaptic transmission and can support neurotransmitter release independent of HVA Ca^{2+} channels in various brain areas (Carbone *et al.* 2014). In contrast, the contribution of T-type channels to synaptic depolarization by subthreshold stimulation has yet to be examined; however, it has been shown that spontaneous neurotransmitter release from mossy fibers blocks a nickel-sensitive inward current in CA3 PCs. Selective blockade of neurotransmitter release from mossy fiber terminals reveals a large Ca^{2+} transient in the proximal apical dendrite that leads to increased cell excitability (Reid *et al.* 2008). In contrast, R-type channel blockade in CA1 PCs removes the dendritic depolarization required for A-type K^+ channel activation, thereby increasing the amplitude of synaptic potentials elicited by Schaffer collateral stimulation (Wang *et al.* 2014). Taken together, these data suggest that the spatial location of VGCCs in a given dendrite, combined with their

influence on nearby Ca^{2+}/voltage-activated K^+ conductances, determines the relative contribution of these channels to dendritic depolarization. **Given the potential for significant attenuation of distal inputs by dendritic filtering in CA3 PCs, we hypothesize that dendritic T-type channels act to amplify synaptic transmission by increasing the amplitude of EPSPs elicited by subthreshold stimulation of CA3 PCs.**

1.5.1 Objective 1: Functional characterization of T-type Ca^{2+} channels in CA3 PCs using whole-cell recordings and two-photon Ca^{2+} imaging.

T-type Ca^{2+} channels are ubiquitously expressed in different brain regions and combinations of some or all three subtypes of Ca_v3 can contribute to LTS in various cell types (Perez-Reyes 2003). Previous studies have elucidated the role of T-type Ca^{2+} channels in CA1 PCs under both physiological and pathophysiological conditions. Using whole-cell recordings in acute hippocampal slices, Ekstein *et al*. (Ekstein *et al.* 2012) found that T-type currents in CA1 PCs are predominantly generated by $Ca_v3.2$ channels due to sensitivity of the current to low concentrations of nickel. As discussed in **section 1.4.6**, nickel blocks recombinant expressed $Ca_v3.2$ T-type channels (EC_{50} = 30 μM) more potently than $Ca_v3.1$ (EC_{50} = 216 μM) and $Ca_v3.3$ (EC_{50} = 250 μM) (Lee *et al.* 1999). In contrast to area CA1, reports investigating the functional distribution of T-type Ca^{2+} channels in the CA3 subfield are scarce.

An immunolabeling study reports a gradient of expression of Ca_v3 channel isoforms in somatic and dendritic regions of CA1 and CA3 PCs that is relatively low in the CA3 subfield and high in CA1 (McKay *et al.* 2006). This study reports subcellular distribution of all three Ca_v3 isoforms in PCs with $Ca_v3.1$ exclusively expressed in the soma/proximal dendritic region and $Ca_v3.2/3.3$

expressed widely in the soma and apical dendrites (McKay *et al.* 2006). Apical dendritic labeling of PCs was found primarily in main dendritic shafts without discernible labeling in oblique apical dendrites or anywhere in basal dendrites (McKay *et al.* 2006). Electrophysiological studies of T-type channel activity in CA3 PCs are limited to acutely isolated rat (Avery and Johnston 1996) and guinea pig hippocampal cells (Mogul and Fox 1991), in addition to guinea pig hippocampal slices (Fisher and Johnston 1990). To our knowledge, there are no studies of CA3 PCs that have: 1) systematically examined T-type channel activity in acute slices using a comprehensive repertoire of pharmacological blockers targeting Ca_v3 channels; 2) reported LTS in CA3 PCs; or 3) investigated the nature of Ca^{2+} transients associated with LTS in CA3 PCs. We will combine current-clamp whole-cell recordings with two-photon Ca^{2+} imaging to determine the conditions that allow LTS detection at the soma and the subcellular localization of T-type channels in CA3 PCs.

1.5.2 Objective 2: Regulation of T-type channel activity by GPCRs and K^+ channels

The modulatory effects of GPCRs on T-type channel activity have been reported extensively, including lysophosphatidic acid receptors, corticotropin releasing factor receptor 1 (Iftinca *et al.* 2007), serotonin receptors (Gilmore *et al.* 2012), mAChRs (Pemberton *et al.* 2000), mGluRs (Hildebrand *et al.* 2009) and $GABA_B$ receptors (Young *et al.* 2010),. Enhancement of T-type channel currents by muscarinic receptor activation has been reported in both isolated rat CA1 lacunosum-moleculare neurons (Fraser and MacVicar 1991) and acutely exposed CA3 neurons of adult guinea pig (Fisher and Johnston 1990). The interaction of specific Ca_v3 subtypes with muscarinic receptors was not examined in the aforementioned studies; however, using HEK293 cells, Hildebrand *et al*. reported M1 $G\alpha_{q/11}$-coupled mAChR-mediated inhibition of $Ca_v3.3$

channels without an effect on the $Ca_v3.1$ and $Ca_v3.2$ subtypes (Hildebrand *et al.* 2009). Given that pyramidal neurons of the hippocampus express high levels of all mAChRs (Levey *et al.* 1995, Rouse *et al.* 1999), we will examine the effects of muscarinic activation on T-type channel activity in CA3 PCs.

Recent studies have also provided detailed modes of interaction between mGluRs and VGCCs. Using electrophysiological recordings of cerebellar Purkinje cells, Otsu *et al*. showed that $mGluR_1$ activation shifts the inactivation curve of A-type K^+ channels towards hyperpolarized potentials, thereby decreasing the availability of these channels at Purkinje cell resting membrane potentials (Otsu *et al.* 2014). This reduces the capacity of these channels to control spike backpropagation and results in distal dendritic Ca^{2+} spikes mediated by P/Q-type Ca^{2+} channels (Otsu *et al.* 2014). Similarly, Hildebrand *et al*. have shown that $mGluR_1$ activation potentiates $Ca_v3.1$ currents through a G-protein- and tyrosine-phosphatase-mediated pathway in cerebellar Purkinje cells (Hildebrand *et al.* 2009). Such potentiation is activity-dependent as it occurs selectively during bursts of excitatory input (Hildebrand *et al.* 2009). Distribution of mGluRs has been determined by the use of pharmacological and electrophysiological techniques and show that group I mGluRs are heavily expressed postsynaptically in pyramidal cells of area CA3, while group II and III mGluRs are distributed presynaptically (Conn and Pin 1997). Further, multiple intracellular signaling cascades are known to be associated with mGluRs in the hippocampus (Cosgrove *et al.* 2011), and we aim to identify the pathways associated with regulatory influence, if any, of mGluR activation on T-type channel function in CA3 PCs. Lastly, we will investigate the effects of G protein-coupled inwardly rectifying K^+ (GIRK) channels and Ca^{2+}-activated K^+ channels on LTS initiation and afterhyperpolarization.

1.5.3 Objective 3: Contribution of T-type Ca^{2+} channels to synaptic transmission

The role of T-type channels in neurotransmitter release has been discussed in **Chapter 1.4.4**. Although T-type-mediated neurotransmitter release has not yet been reported in area CA3, using rat organotypic hippocampal slices Reid *et al*. showed that spontaneous release from mossy fiber terminals inhibits T-type Ca^{2+} channels in CA3 PCs (Reid *et al.* 2008). The inhibition is mediated by CNQX-sensitive postsynaptic channels and it influences CA3 PC excitability because in the presence of CNQX, the magnitude of depolarization required to elicit an action potential is reduced (Reid *et al.* 2008). The authors showed that changes in cell excitability were completely reversed by the addition of nickel reflecting the diminished impact of VGCCs on membrane depolarization at a "detonator" synapse (see **section 1.1.1**) where large synaptic events are highly prevalent (Reid *et al.* 2008).

The inhibitory effect of R-type channel activity on postsynaptic potentials in CA1 PCs is well documented (Wang *et al.* 2014). By activating 4AP-sensitive A-type K^+ conductance, R-type channels significantly reduce CA1 dendritic depolarization arising from Schaffer collateral stimulation (Wang *et al.* 2014). K^+ channels play an important role in dendritic integration (Cai *et al.* 2004) and T-type channels are found in microdomains with various K^+ channels (Bloodgood and Sabatini 2007, Bloodgood and Sabatini 2008, Anderson *et al.* 2010). As such, we predict that T-type Ca^{2+} channels have the capacity to tune various characteristics of synaptic potentials. Given the widespread pre- and postsynaptic role of VGCCs in synaptic transmission, we will examine EPSP kinetics of CA3 PCs in response to afferent stimulation before and after T-type channel blockade.

Chapter 2: Materials and methods

2.1 Hippocampal slice preparation

Sprague Dawley rats (postnatal day 10-18) were anesthetized with isoflurane or halothane and decapitated according to standards approved by the University of British Columbia committee on animal care. Brains were removed rapidly and placed into chilled slicing solution saturated with carbogen (95% O_2/5% CO_2). The slicing solution contained (in mM): N-methyl-D- glucamine, 120; KCl, 2.5; NaH_2PO_4, 1.2; $NaHCO_3$, 25; $CaC1_2$, 1.0; $MgCl_2$, 7.0; sodium pyruvate, 2.4; sodium ascorbate, 1.3; glucose, 20. 400 μm thick transverse hippocampal slices were cut using a Leica VT 1200S vibratome and recovered in artificial cerebrospinal fluid (aCSF) saturated with carbogen at 32°C for 30 minutes. aCSF contained (in mM): NaCl, 126; $NaHCO_3$, 26; KCl, 2.5; glucose, 10; NaH_2PO_4, 1.25; $MgCl_2$, 2; $CaCl_2$, 2.0. Slices were allowed to recover in carbogen-saturated aCSF at room temperature for 1 hr prior to experimentation.

2.2 Whole-cell recordings

Whole-cell patch-clamp recordings were performed on CA1 or CA3 pyramidal cells within hippocampal slices. Individual slices were transferred to a recording chamber located on an upright Zeiss microscope fitted with IR-DIC capabilities and a charge-coupled device camera (Bosch) for light-guided whole-cell recordings. After transfer, slices were perfused with aCSF saturated with carbogen (95% O_2/5% CO_2) at a rate of 2 mL/min. Patch electrodes were pulled from borosilicate glass capillaries using a P-97 Sutter puller. Patch electrode resistance ranged from 4-7 mΩ. The intracellular solution for voltage-clamp recordings contained (in mM): potassium ATP, 4; sodium GTP, 0.3; cesium methanesulfonate, 108; tetraethylammonium

chloride, 8; sodium gluconate, 8; cesium EGTA, 1; HEPES, 10; $MgCl_2$, 2; pH 7.2 adjusted with cesium hydroxide; osmolarity adjusted to 285-290 mOsm. The intracellular solution for current-clamp recordings contained (in mM): potassium ATP, 4; sodium GTP, 0.3; potassium gluconate, 108; potassium chloride, 8; sodium gluconate, 8; potassium EGTA, 1; HEPES, 10; $MgCl_2$, 2; pH 7.2 adjusted with potassium hydroxide; osmolarity adjusted to 285-290 mOsm. For imaging experiments, internal solution was supplemented with 400 μM Fluo-4, pentapotassium salt, cell-impermeant and 50 μM Alexa Fluor 594 hydrazide.

All experiments were performed at room temperature (22°C—25°C). Cells used for current clamp recordings had stable input resistance (120-320 MΩ) and access resistance (12-30 MΩ). Access resistance was monitored throughout the course of all whole-cell recordings and access resistance changes greater than 20% resulted in exclusion of the recording from a given data set. All recordings were from cells with a resting membrane potential between –56 and –75 mV. Current was injected to maintain the membrane potential at –60 mV. Series resistance was not electronically compensated. Cells were allowed to dialyse for a minimum of 10 minutes prior to commencing experimentation. Electrophysiological signals were amplified using a MultiClamp 700B amplifier (Axon Instruments, Foster City, CA). Data were low-pass filtered at 1 KHz, and digitized at 10 KHz using a 1440A Digidata (Axon Instruments) and analyzed using pClamp 10 software (Molecular Devices, Sunnyvale, CA).

2.3 Two-photon Ca^{2+} imaging

A two-photon laser-scanning microscope (Zeiss LSM510-Axioskop-2 fitted with a 40X-W/0.80 numerical aperture objective lens) directly coupled to a tunable Ti:sapphire laser (~100-fs pulses and 76MHz, pumped by a 5W Verdi laser, Coherent) provided excitation of Fluo-4 and Alexa Fluor 594. Cells were patched at depths between 30-50 μm into the brain slice to avoid damaged tissue at more superficial depths and to increase the probability of dye-filling in dendrites above and below the cell. Fluo-4 and Alexa Fluor 594 were excited at 800 nm and the emission was detected with a photomultiplier tube after passing through a 500-550 nm and 600-660 nm emission filters, respectively. Frame images for the time-lapse analysis were collected at 250 x 300 pixels using 2-line averaging. Line scan images for the time-lapse analysis were collected at 256 x 256 pixels using 2-line averaging. To obtain z-stacks of cells showing dendrite morphology above and below the surface of the soma, 35-50 images using 8-line averaging were collected by stepping 1 μm in the z-axis between frames.

2.4 Synaptic stimulation

Presynaptic axons in stratum radiatum were stimulated using a concentric bipolar microelectrode (FHC-co, Bowdoin, Maine), connected to SIU-V constant voltage stimulus isolation unit and S88X dual output square pulse stimulator (Grass Technologies, Warwick, Rhode Island). Stimulation electrodes were placed at ~500 μm from the soma of the recorded cell. Internal solution was supplemented with 1 mM QX314-chloride to block voltage gated sodium channels and 10 μM picrotoxin to block Gamma-aminobutyric acid (GABA) receptors internally. Subthreshold EPSPs were elicited by 0.1 msec stimulation of 5 V.

2.5 Chemicals and reagents

2-APB (Tocris); (2R-4R)-APDC (Tocris); 4-aminopyridine (Sigma); Alexa Fluor 594 (Life Technologies); apamin (Tocris); ascorbate (Sigma); cadmium chloride (Sigma); chelerythrine chloride (Tocris); CHPG (Tocris); CNQX (Abcam); carbachol (Sigma); D-AP5 (Abcam); DHPG (Tocris); iberiotoxin (Tocris); Fluo-4 (Life Technologies); L-AP4 (Tocris); L-Cysteine (Sigma); linopirdine (Sigma); LY456236 (Tocris); nickelous chloride (J.T. Baker); paxilline (Tocris); picrotoxin (Sigma); t-ACPD (Tocris); staurosporine (Tocris); tertiapin-Q (Tocris); TTX (Abcam); U73122 (Tocris); Z944 (gift from Terry Snutch).

2.6 Data analysis and statistics

All values shown in figures are mean ± SEM. Statistical significance was determined using paired and unpaired t-tests (*: $p<0.05$; **: $p<0.01$; ***: $p<0.0001$). For imaging experiments, ΔF/F was computed as follows: fluorescence in the green channel was subtracted from background and the fluorescence values prior to voltage or current steps were averaged as "baseline values". Changes in fluorescence in response to current or voltage steps were set as "Measured values". ΔF/F was then calculated as (measured value – baseline value) / baseline value.

Chapter 3: $Ca_v3.2$-mediated LTS in CA3 PCs are unlocked by A-type K^+ channel inhibition

3.1 Overview

The existence of LTS in thalamocortical neurons has been known for quite some time and recent evidence suggests that in addition to generating synchronous activity, LTS are also required for the induction of spike-timing-dependent plasticity in these cells (Hsu *et al.* 2012). In nucleus reticularis thalami (NRT) neurons, current injection from a hyperpolarized potential results in a transient LTS that is crowned by a burst of action potentials (Coulon *et al.* 2009). Recovery to the hyperpolarized state by GABAergic connections within the NRT allows T-type channels to de-inactivate and that triggers another LTS ultimately causing neurotransmitter release (Coulon *et al.* 2009). A similar sequence of events leading to LTS has been observed in relay neurons of the thalamus, deep cerebellar nuclei, and inferior olive neurons (Contreras 2006).

The presence of low-threshold Ca^{2+} channels in CA3 PCs suggests that these cells are capable of generating LTS. Avery and Johnston have shown that LVA currents in CA3 PCs have a transient and a sustained component (Avery and Johnston 1996). Using different pharmacological blockers, they reported that T-type channels mediated the transient component of LVA currents; while, the sustained current was carried by nickel-insensitive, dihydropyridine-sensitive Ca^{2+} channels (Avery and Johnston 1996). This led them to conclude that subthreshold Ca^{2+} signaling can occur independently of T-type channels, at least in CA3 PCs. This concept of multiple channel types contributing to LVA currents in CA3 PCs has yet to be further explored and there are currently no reports of LTS in CA3 PCs. Work on backpropagating action potentials and complex spikes shows that the distribution and density of VGCCs, combined with the repertoire

of voltage-gated ion channels in a given neuron, determine the initiation, propagation, and kinetics of Ca^{2+} spikes. In this chapter, we aimed to: 1) test the assertion that multiple channel subtypes contribute to LVA currents, and 2) explore the interaction between T-type Ca^{2+} channels and voltage-gated K^+ channels that enables LTS generation in CA3 PCs.

3.2 Results

3.2.1 T-type Ca^{2+} current in CA3PCs is sensitive to Z944 and nickel

To determine the functional characteristics of T-type channels in CA3 PCs, we recorded Ca^{2+} currents from cells in slices of the CA3 region using the whole-cell voltage-clamp technique. We tested the contribution of T-type channels to the recorded Ca^{2+} currents by bath-applying well-established pharmacological blockers that specifically target the T-type family of VGCCs. The protocol used to record Ca^{2+} currents is shown in **Fig. 3-1a**. CA3 PCs were held at –100 mV, stepped to –80 mV, and then depolarized to a maximum of +30 mV in 10 mV increments. The duration of each depolarization step was 300 msec. Recordings were done in the presence of 1 μM TTX, 60 μM cadmium chloride, and 50 μM D-APV to block voltage-gated sodium channels, high threshold VGCCs, and N-methyl-D-aspartate (NMDA) receptors, respectively. The activation threshold for the Ca^{2+} currents elicited using the protocol in **Fig. 3-1a** was –40 mV. The current peaked between –30 and –20 mV and was completely inactivated at potentials of –10 mV and higher. We then applied 50 μM nickel to specifically block $Ca_v3.2$ channels (Kang *et al.* 2006) and recorded Ca^{2+} currents using the protocol described above. This completely blocked the Ca^{2+} currents recorded previously from the same cell and resulted in a linear *I-V* relationship.

To reveal the nickel-sensitive component of the current, we subtracted the currents recorded under control conditions from the currents measured after nickel perfusion (**Fig. 3-1b**). The linear current profile in response to voltages –10 mV and above is not shown in the subtracted current for clarity. The first four depolarizing steps between –80 and –50 mV passively charged the membrane without activating any currents. The *I-V* relationship of the subtracted current shows the voltage threshold for activation and the linearity of the response at voltages of –10 mV and above (n=5; **Fig. 3-1c**). We also recorded Ca^{2+} currents before and after application of 2 μM Z944, a high affinity pan T-type channel blocker (Tringham *et al.* 2012). The Z944 subtracted current had similar characteristics to that of the nickel-sensitive current (n=5; **Fig. 3-1d and e**). The peak amplitude of both nickel- and Z944-subtracted currents was between 200-250 pA. Together, these data indicate the presence of T-type Ca^{2+} channels in CA3 PCs.

3.2.2 T-type Ca^{2+} current in CA3 PCs is mediated by $Ca_v3.2$ channels

As detailed in **3.2.1**., T-type Ca^{2+} currents were sensitive to 50 μM nickel. Nickel used at this concentration preferentially blocks $Ca_v3.2$ channels (Kang *et al.* 2006). To confirm this notion, we further tested the sensitivity of the currents to pharmacological agents that selectively target $Ca_v3.2$ channels by taking advantage of the susceptibility of this subtype to redox modulation via a specific histidine residue in the $Ca_v3.2$ domain I extracellular S3-S4 linker region (Zhang *et al.* 2013).

T-type Ca^{2+} currents were recorded before and after application of $Ca_v3.2$ blocker ascorbate (1 mM) (Nelson *et al.* 2007). The threshold for voltage activation and peak amplitude of the ascorbate-sensitive current was comparable to that of the nickel- and Z944-sensitive currents

(**Fig. 3-2a and b**). Next, we tested the sensitivity of T-type Ca^{2+} currents to L-cysteine. L-cysteine chelates trace amounts of heavy metals in acute brain slices and potentiates $Ca_v3.2$ currents because the histidine residue in the S3-S4 linker region increases the susceptibility of these channels to inhibition by zinc and other heavy metals (Nelson *et al.* 2005).

We attempted to measure T-type Ca^{2+} currents using the protocol depicted in Figure 3-1a; however, we were unable to clamp the cell effectively due to increased influx of Ca^{2+} that resulted in large fluctuations of holding current required to maintain the voltage at –100 mV. As such, we opted to measure the current response to a single depolarizing step to –40 mV from a holding potential of –100 mV before and after 500 μM L-cysteine application. We chose a depolarization of –40 mV as this was the threshold for voltage activation and also the voltage that elicited the smallest current amplitude. L-cysteine increased the peak amplitude of the current and decreased the time to peak current (**Fig. 3-2c**). L-cysteine increased the current amplitude at –40 mV in every cell tested (**Fig. 3-2d**). The peak current amplitude at –40 mV under control conditions was –58.20 ± 13.34 pA and after 500 μM L-cysteine application increased to –294.07 ± 88.86 pA (n=5; paired *t*-test; $p = 0.0395$; **Fig. 3-2de**). Modulation of the whole cell T-type Ca^{2+} current by both ascorbate and L-cysteine confirms the major contribution of $Ca_v3.2$ channels to the measured currents.

3.2.3 Slower kinetics of T-type Ca^{2+} currents are characteristic of CA3 PCs

T-type Ca^{2+} currents measured from CA3 PCs have slower activation and decay kinetics when compared to T-type currents recorded from HEK-293 cells and principal cells in other brain areas (Perez-Reyes 2003, Cain and Snutch 2013). We reasoned that opening of T-type channels

and the resulting depolarization and/or Ca^{2+} influx could cause activation of a secondary cation conductance that is obscuring the fast decay typically associated with T-type channels. The primary mediators of this secondary current in the CA3 region of the hippocampus are transient receptor potential cation channels of the subfamily C (TRPC) (Li *et al.* 2010). TRPC channels can be effectively blocked by 100 μM 2APB (Lievremont *et al.* 2005). Thus, we repeated our voltage-clamp experiments in the presence of 100 μM 2APB in addition to the blockers detailed in **3.2.1**. The kinetics of the Z944-sensitive currents were not altered appreciably in the presence of 100 μM 2APB (**Fig. 3-3a**). Similarly, the *I-V* relationship of the Z944-sensitive current remained unchanged after addition of 2APB to the bath (data not shown). We repeated these experiments at the more physiological temperature of 32°C and did not observe any changes in T-type Ca^{2+} current kinetics, peak amplitude, or threshold for voltage activation (data not shown).

Next, we recorded T-type Ca^{2+} currents at room temperature in region CA1 of the hippocampus to determine whether our recording conditions were altering T-type channel kinetics. Ca^{2+} currents measured from CA1 PCs were sensitive to Z944, thus T-type-mediated, and also closely resembled the fast kinetics typical of T-type channels as reported pervasively in the literature (**Fig. 3-3b**) (Perez-Reyes 2003). The *I-V* relationship of Z944-sensitive current in CA1 PCs showed that the threshold for voltage activation was –40 mV and the current peaked between –30 and –20 mV (**Fig. 3-3c**). Recordings from CA3 and CA1 regions were made under identical conditions and in several instances cells were patched consecutively from the two regions in the same slice to ensure consistency in experimental set-up.

3.2.4 LTS is gated by 4AP-sensitive A-type K^+ channels in hippocampal PCs

Comparison of voltage-clamp experiments between CA1 and CA3 PCs reflects the greater space clamp issues associated with measuring T-type Ca^{2+} currents in region CA3 versus CA1 of the hippocampus. Voltage-clamp recordings were performed using a cesium based internal solution to increase the input resistance of the cell and achieve a better clamp; however, this did not rectify the voltage errors associated with a poorly clamped CA3 cell. We next tested a more physiological recording paradigm of current clamp by using a potassium based internal solution. This allows for examining the influence of ongoing background K^+ channel activity near the resting membrane potential. By using whole-cell current clamp, we could also test the impact of background conductances on T-type channel function by measuring LTS instead of blocking these active conductances to isolate T-type Ca^{2+} currents.

In current clamp mode, we tested the occurrence of a LTS in response to somatic current injection. Current was injected to hold cells between –70 and –75 mV and then an initial depolarizing step of 30 pA was applied, followed by a series of depolarizing steps in 10 pA increments to a maximum of 140 pA. These experiments were performed in presence of 1 μM TTX, 60 μM cadmium chloride, and 50 μM D-APV to block voltage-gated sodium channels, high threshold VGCCs, and N-methyl-D-aspartate (NMDA) receptors, respectively. Under control conditions, we failed to observe a subthreshold depolarization or a LTS in recordings from CA3 PCs (**Fig. 3-4a**). We reasoned that background K^+ conductances must have a significant impact on T-type channel activity under current-clamp conditions, especially if the latter are mainly and/or densely expressed in the dendrites of CA3 PCs. We tested the effects of cesium (100 mM) and found that current injection failed to elicit a LTS and cells were too slow

to repolarize after a given depolarizing step reflecting the broad blockade of K^+ channels by addition of cesium to the aCSF (data not shown). Adding 1 mM 4AP, a specific blocker of A-type K^+ channels (Yao and Tseng 1994), resulted in large over-shooting LTS in the same CA3 cell that previously displayed no spikes in response to current injection (**Fig. 3-4b**). In slight contrast, CA1 PCs responded to current injection with subthreshold depolarization that could underlie LTS in control conditions (**Fig. 3-4c**). Similar to CA3 PCs, addition of 1 mM 4AP to the bath solution unlocked LTS in CA1 PCs (**Fig. 3-4d**). These data show that expression of LTS in both CA3 and CA1 PCs is gated by 4AP-sensitive K^+ channels.

3.2.5 LTS in hippocampal PCs is mediated by T-type Ca^{2+} channels

In order to determine whether LTS observed in CA3 PCs are mediated by T-type channels, we tested the sensitivity of LTS to pharmacological blockers of T-type channels. Addition of 50 μM nickel to the bath blocked LTS although a small subthreshold depolarization in response to current injection of 100 pA remained (**Fig. 3-5a**). This small depolarization could be the result of an incomplete block of $Ca_v3.2$ by nickel for the time course employed in our experiments (maximum of 20 minutes) and/or the contribution of $Ca_v3.1/3.3$ channels to subthreshold depolarization. Nonetheless, the complete block of LTS by a concentration of nickel that specifically blocks $Ca_v3.2$ channels shows that LTS are primarily mediated by these channels in CA3 PCs. Both LTS and residual subthreshold depolarization were blocked by 2 μM Z944, reflecting a lack of contribution by non-T-type VGCC to LTS in CA3 PCs (**Fig. 3-5b**).

To confirm our results, we examined the sensitivity of LTS to nickel and Z944 in $Ca_v3.2$ knockout mouse pups (P12-18). In 6 out of 13 recordings in 4AP, voltage responses to current

injection were linear indicating that $Ca_v3.2$ channels fully contributed to LTS in the 6 CA3 PCs tested from $Ca_v3.2^{-/-}$ mice. In the other 7 cells, although we failed to elicit a LTS in response to current injection of any magnitude (data not shown), we did observe a subthreshold depolarization after significant current injection. Nickel failed to block subthreshold depolarization in these cells (**Fig. 3-5c**), whereas Z944 blocked subthreshold depolarization completely (data not shown). In order to compare the results obtained in $Ca_v3.2^{-/-}$ mice, we also tested the sensitivity of wild-type P12-18 mice and found that LTS was reliably produced in every cell tested and was blocked by both nickel and Z944 in both CA1 and CA3 PCs (data not shown). Consistent with our CA3 data, in CA1 PCs 50 μM nickel resulted in inhibition of LTS (**Fig. 3-5d**).

Because both nickel and Z944 completely blocked LTS in CA3 and CA1 PCs, we could not quantify or make comparisons between LTS parameters before and after treatment with blockers. Instead, we quantified the increase in current magnitude required to achieve subthreshold depolarization after treatment with T-type channel blockers. In CA3 PCs, current injection amplitude required for subthreshold depolarization under control conditions was 58.23 ± 4.0 pA and increased to 96.48 ± 5.1 pA after nickel perfusion (n=5; paired *t*-test; $p < 0.0001$; **Fig. 3-5d**). In control conditions for paired recordings where Z944 was added to the aCSF, current injection required for subthreshold depolarization was 56.04 ± 10.2 pA and adding Z944 resulted in a linear voltage response to current injection (i.e. no amount of current injection could elicit a depolarization, therefore there is no bar in the chart for this dataset in **Fig. 3-5d**). In $Ca_v3.2^{-/-}$ CA3 PCs, current injections under control conditions were 86.8 ± 3.4 pA and nickel failed to have an effect on subthreshold depolarizations (88.2 ± 6.3 pA; n=4; paired *t*-test; $p = 0.0231$;

Fig. 3-5d). In contrast, current injections required for subthreshold depolarization in $Ca_v3.2^{-/-}$ CA3 PCs under control condition were 89.5 ± 5.4 and application of Z944 to slices resulted in a linear voltage responses to current injection (**Fig. 3-5d**). In CA1 PCs, current injections required for subthreshold depolarization under control conditions were 55.18 ± 5.0 pA, and increased to 100.32 ± 7.0 pA after nickel perfusion (n=4; paired *t*-test; $p = 0.0324$; **Fig. 3-5d**).

3.2.6 LTS in CA3 PCs is mediated by $Ca_v3.2$ channels

To ascertain that $Ca_v3.2$ channels underlie LTS generation in CA3 PCs, we tested spike sensitivity to ascorbate and L-cysteine due to their respective inhibition and enhancement of $Ca_v3.2$ channels. Addition of 500 μM L-cysteine to the bath increased LTS amplitude and reduced time-to-peak (Fig. 3-6a). Similar to voltage recordings in section **3.2.1**, ascorbate decreased LTS amplitude and increased threshold for LTS activation (Fig. 3-6b). Under control conditions, LTS threshold was 55.0 ± 13.0 pA and after L-cysteine application, it increased slightly to 57.5 ± 11.8 pA (n=5; paired *t*-test; $p = 0.2663$; **Fig. 3-6c**). In contrast, ascorbate significantly increased LTS threshold from 52.0 ± 6.0 pA to 96.5 ± 10.0 pA (n=5; paired *t*-test; $p = 0.0219$; **Fig. 3-6c**). L-cysteine increased LTS amplitude from 52.78 ± 2.83 mV to 75.65 ± 5.49 mV (n=5; paired *t*-test; $p = 0.0397$; **Fig. 3-6d**) and ascorbate decreased mean LTS amplitude from 60.98 ± 2.51 mV to 41.57 ± 2.77 mV (n=5; paired *t*-test; $p = 0.0141$; **Fig. 3-6d**). Combined, these data confirm that $Ca_v3.2$ channels mediate LTS in CA3 PCs.

3.3 Discussion

The data indicate that LVA currents in CA3 PCs are principally due to $Ca_v3.2$ channel expression because of the sensitivity to 50 μM nickel. In addition, we show T-type channels are

the only contributors to LVA currents in CA3 PCs because application of Z944 results in a complete block of T-type currents. Sensitivity of LVA currents to both L-cysteine and ascorbate further supports the functional expression of $Ca_v3.2$ channels in CA3 neurons since this is the only subtype in the Ca_v3 family of channels that is redox-sensitive. Finally, examination of $Ca_v3.2^{-/-}$ mice, further supports our pharmacological data indicating that LTS in CA3 PCs are mediated by $Ca_v3.2$ channels.

Our data do not support the assertion that non-LVA VGCCs contribute to LVA currents in CA3 PCs (Avery and Johnston 1996) because under the conditions employed in our experiments to measure LVA currents, HVA currents were blocked completely by cadmium chloride. The data presented do show some differences between LVA currents recorded from CA1 and CA3 PCs. The average peak amplitude of T-type currents recorded at –30 mV was comparable between both regions. Similarly, the activation, peak, and inactivation parameters of T-type currents did not differ between CA3 and CA1 PCs. However, the time course of currents and the rates of inactivation varied significantly between the two hippocampal areas.

In CA1 PCs, T-type currents displayed faster activation and decay kinetics – the current peak occurred within 50 msec of test pulse initiation consistent with previous reports (Ekstein *et al.* 2012). In contrast, T-type currents recorded from CA3 PCs had slower activation and decay kinetics – the current peak occurred at approximately 150 msec and decayed at a much slower rate, if at all, when compared to CA1 PCs. T-type currents in both CA1 and CA3 were abolished by 2 μM Z944, thus we can conclude that T-type channels underlie LVA currents in both areas. Although we did not test LVA current sensitivity to nickel in CA1 PCs, previous studies have

shown that T-type currents in CA1 PCs are completely blocked by nickel (Ekstein *et al.* 2012), suggesting that T-type currents in both regions are mediated by $Ca_v3.2$ channels. The divergent nature of the two currents could arise from several possibilities: 1) the cellular distribution of the channels (e.g. proportion in somatic versus dendritic compartments) varies between CA1 and CA3; 2) differences in the combination of passive (e.g. dendritic arbor diameter/branching) and active dendritic properties between the two regions giving rise to variable T-type current kinetics independent of channel distribution *per se*; 3) that there exist different isoforms of $Ca_v3.2$ channels in CA1 and CA3. Alternative splicing from each of the three T-type genes can generate functionally distinct T-type channel isoforms and specific splice variants of $Ca_v3.2$ channels are also associated with changes in developmental states (David *et al.* 2010). Alternatively, differential posttranslational modification of T-type channels between the two hippocampal areas could also lead to divergent channel kinetics. To address the possibility of heterogeneous channel distribution, we utilized two-photon Ca^{2+} imaging in CA1 and CA3 PCs, as detailed in Chapter 4. Alternatively, it is also possible that T-type channels in CA3 PCs have different gating properties than CA1 PCs as has been shown for T-type currents in rat sensory neurons (Bossu and Feltz 1986) and GH_3 pituitary cells (Herrington and Lingle 1992). In these instances a voltage-dependent fast component causes the majority of current decline, whereas a slower phase occurring over a time course of seconds is Ca^{2+}-dependent.

We also investigated the precise conditions under which LTS are generated in CA3 PCs. Previous studies have shown that simply blocking sodium-dependent action potentials with TTX is sufficient for activating dendritic VGCCs and detecting Ca^{2+} spikes at the soma. Golding *et al*. showed that the current required for Ca^{2+} spike initiation in CA1 PCs was lower in dendrites than

the soma and this disparity was eliminated after TTX application (Golding *et al.* 1999). This reflects the control of D-type low-threshold K^+ channels that are activated by backpropagating action potentials, on Ca^{2+}spike initiation. We failed to elicit LTS after TTX application and inhibition of HVA channels with cadmium; instead, we found that inhibition of A-type K^+ channels with 4AP was sufficient to unlock LTS in both CA3 and CA1 PCs. This finding highlights the tight control by K^+ channels over dendritic depolarization that prohibits LTS from propagating to the soma. Consistent with our voltage-clamp data, we found that LTS in CA3 PCs were sensitive to nickel, Z944, ascorbate, and L-cysteine, indicating that $Ca_v3.2$ channels underlie the majority of depolarization that supports LTS. Further, in 50% of recordings made from $Ca_v3.2^{-/-}$ mice, we did not observe LTS or subthreshold depolarization in current-clamp mode. In the remaining cells, a subthreshold depolarization was observed after current injection of a large magnitude and it was sensitive to Z944 but not nickel. The increase in current magnitude required to elicit a subthreshold depolarization in $Ca_v3.2^{-/-}$ mice could also occur through a compensatory mechanism whereby upregulation of K^+ channels increases the depolarization requirement for T-type channel activation. Despite this possibility, the findings presented in this Chapter reveal the major contribution of $Ca_v3.2$ channels to LTS in area CA3 of the hippocampus.

Considering that the distribution of voltage-gated K^+ channels in dendrites of PCs is non-uniform, it is expected that their effects on membrane excitability will differ depending on the region of interest. For example, the distribution of A-type K^+ channels is highest in the distal dendrites while the non-inactivating class of K^+ channels is expressed with a uniform density throughout the dendritic arbor (Hoffman *et al.* 1997, Johnston *et al.* 2003). Extensive work

exploring mechanisms of dendritic Ca^{2+} signaling has revealed that L- and N-type Ca^{2+} channels are densely expressed in the soma and apical dendrite, whereas, the distribution of R- and T-type channels is highest in the distal dendrites (Magee *et al.* 1995, Sabatini and Svoboda 2000). Consistent with these reports, we found that A-type K^+ channels suppress membrane excitability and spatially constrain LTS such that rapid membrane repolarization prevents significant T-type-mediated signal propagation. Stimuli, such as EPSPs with fast kinetics (~15 msec) that can directly inactivate A-type K^+ channels (Johnston *et al.* 2000) will have an indirect, but significant impact on dendritic Ca^{2+} influx mediated by T-type Ca^{2+} channels. In addition, patterned synaptic inputs capable of inactivating these channels may give rise to efficient spatiotemporal summation mediated by T-type Ca^{2+} channels in CA3 PCs.

Figure 3-1 T-type Ca^{2+} current in CA3 PCs.

(**a**) Step protocol used to measure T-type current. Passive component of the current in response to voltages –10 mV and above (in red) is not shown in b and d for the purpose of clarity. (**b**) Representative nickel (50 μM)-sensitive current. (**c**) *I-V* relationship of the nickel-sensitive current showing the T-type current activating at –40 mV and peaking at –30 mV. (**d**) Representative Z944 (2 μM)-sensitive current. (**e**) *I-V* relationship of the Z944-sensitive current showing the T-type current activating at –40 mV and peaking at –30 mV. Control currents were subtracted from T-type blocker-treated currents to obtain representative traces and *I-V* relationships. Scale in (b) applies to the current trace in (d) as well.

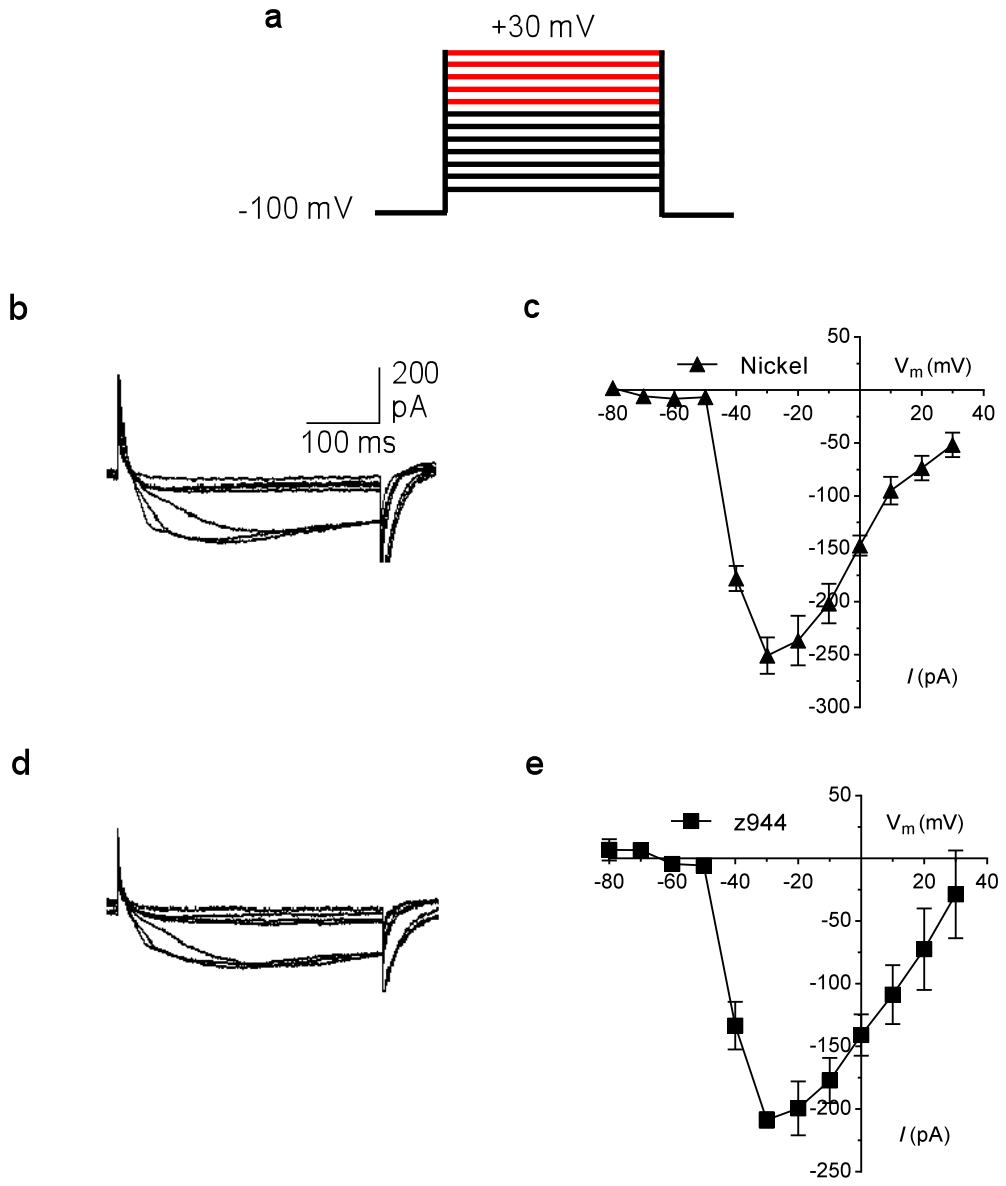
a
+30 mV
-100 mV
b
200
pA
100 ms
c
Nickel
V_m (mV)
50
-80
-60
-40
-20
20
40
-50
-100
-150
-200
-250
-300
I (pA)
d
e
z944
V_m (mV)
50
-80
-60
-40
-20
20
40
-50
-100
-150
-200
-250
I (pA)

Figure 3-2 T-type Ca^{2+} currents in CA3 PCs are mediated by $Ca_v3.2$ channels.

(**a**) Representative ascorbate (1 mM)-sensitive current in voltage clamp mode. (**b**) *I-V* relationship of ascorbate-sensitive current. (**c**) Representative current obtained in response to depolarizing the cell to –40 mV from holding potential of –100 mV before (black) and after 500 μM L-cysteine application (red). (**d**) Pooled data from 5 cells showing the increase in peak current amplitude at –40 mV after L-Cysteine application. (**e**) L-cysteine increased the peak current amplitude at –40 mV (n=5; paired *t*-test; $p = 0.0395$).

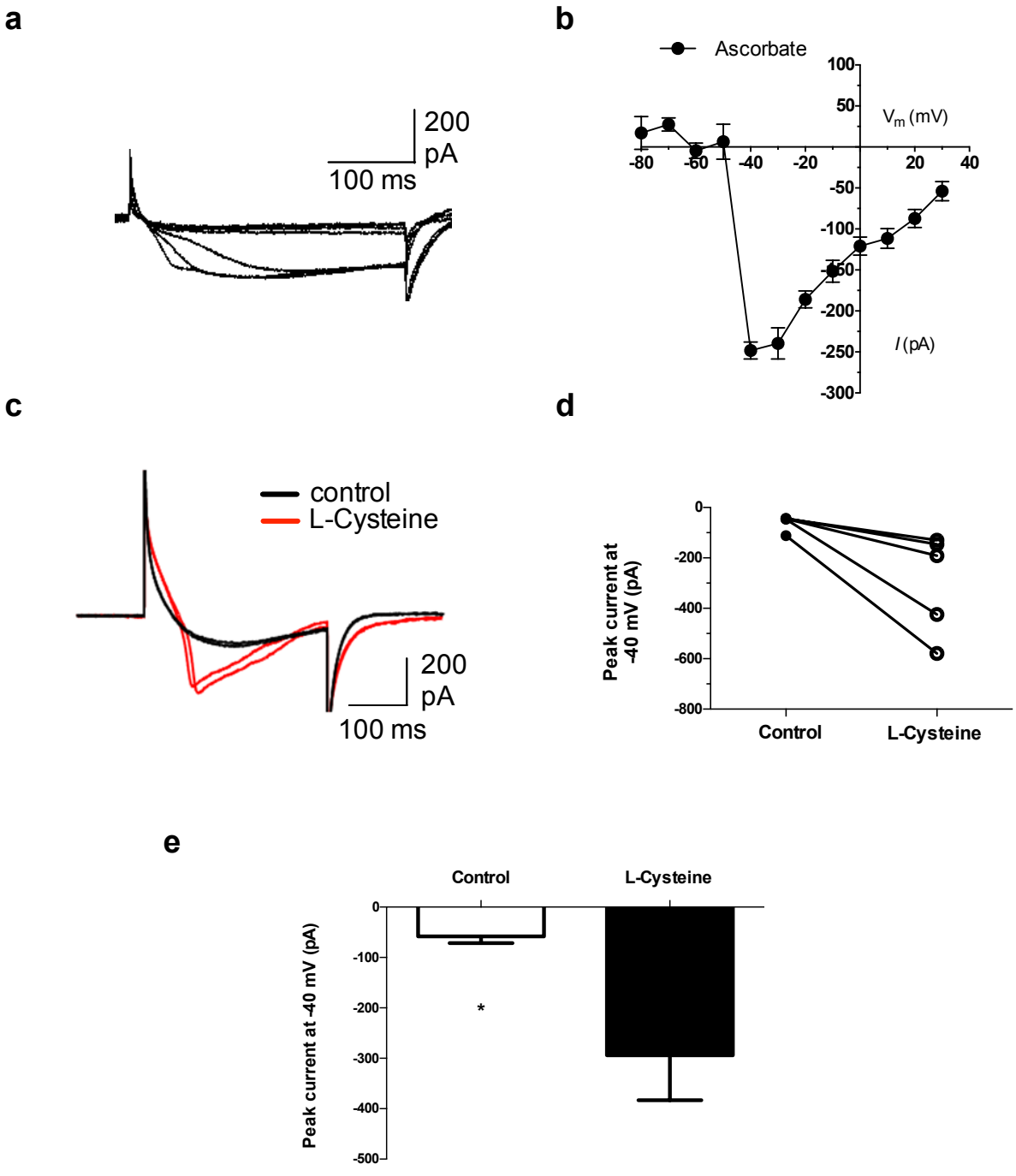
a
200
pA
100 ms
b
Ascorbate
100
50
V_m (mV)
-80
-60
-40
-20
20
40
-50
-100
-150
-200
-250
-300
I (pA)
c
control
L-Cysteine
200
pA
100 ms
d
Peak current at
-40 mV (pA)
0
-200
-400
-600
-800
Control
L-Cysteine
e
Control
L-Cysteine
Peak current at -40 mV (pA)
0
-100
-200
-300
-400
-500
*

Figure 3-3 Slower kinetics of T-type Ca^{2+} currents are characteristic of CA3 PCs.

(**a**) Representative Z944 (2 μM)-sensitive current in the presence of non-selective cation channel blocker 2APB (100 μM). (**b**) Representative Z944 (2 μM)-sensitive current recorded from CA1 PCs. (**c**) *I-V* relationship of Z944 (2 μM)-sensitive current in CA1 PCs showing the T-type current activating at –40 mV and peaking at –30 mV. Scale in (a) applies to (b) as well.

a

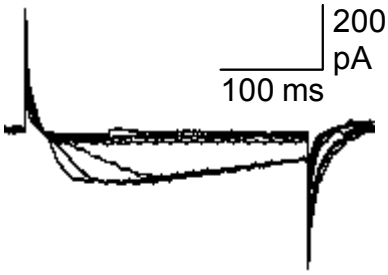

CA3 - z944-sensitive current in 2APB

b

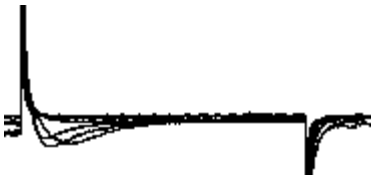

CA1 - z944-sensitive current

c

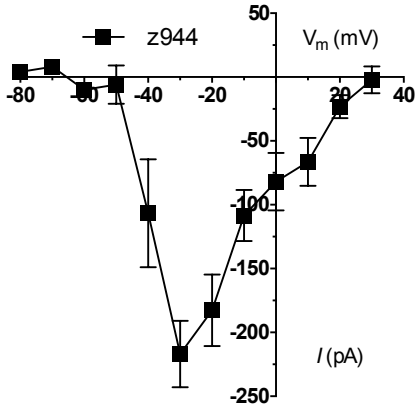

I-V relationship of z944-sensitive current in CA1

Figure 3-4 LTS is gated by 4AP-sensitive A-type K^+ channels in hippocampal PCs.

(**a**) Representative trace of evoked LTS in current-clamped CA3 PC held at –75 mV and depolarized by current injection of 10 pA increments. (**b**) Representative trace of the same CA3 PC in (a) after 1 mM 4AP application. (**c**) Representative trace of a current-clamped CA1 PC held at –75 mV and depolarized by current injection of 10 pA increments. (**d**) Representative trace of the same CA1 PC in (c) after 1 mM 4AP application. Scale in (b) applies to all traces.

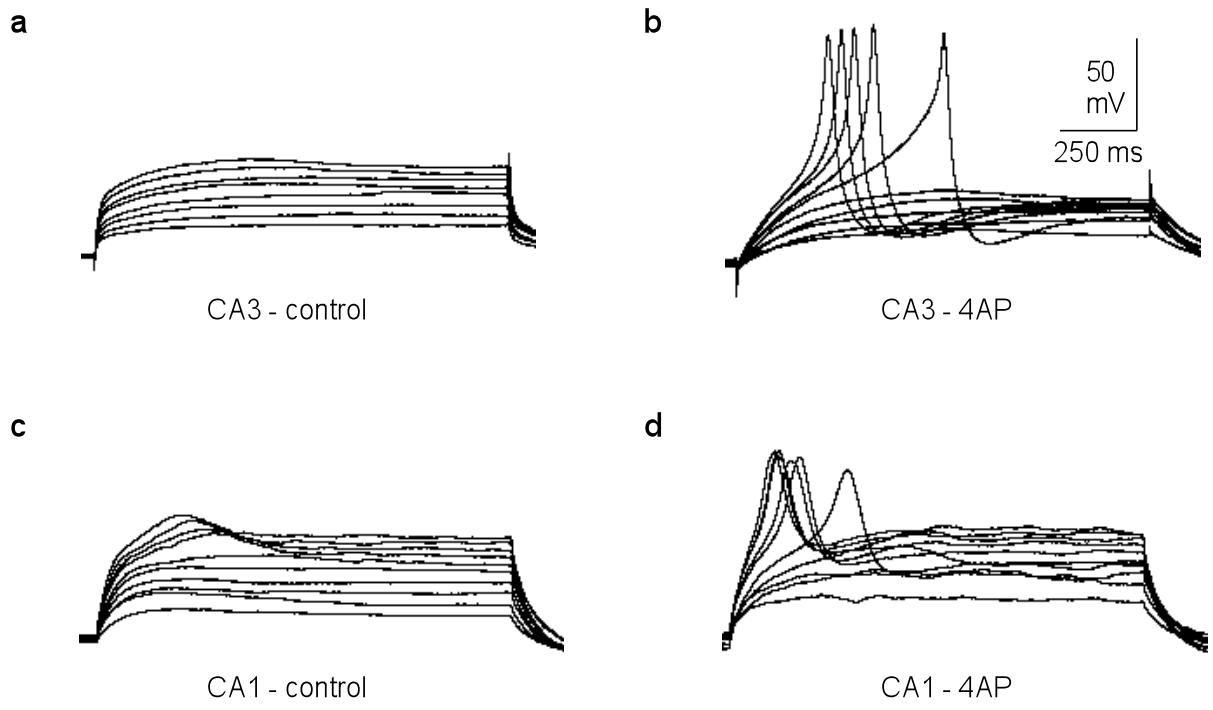

Figure 3-5 LTS in hippocampal PCs is abolished by Z944 and nickel.

(**a**) Representative trace of LTS evoked in a current-clamped CA3 PC by somatic current injection before (top) and after 50 μM nickel application (bottom). (**b**) Representative trace of LTS evoked in a current-clamped CA3 PC by somatic current injection before (top) and after 2 μM Z994 application (bottom). (**c**) Representative trace of subthreshold depolarization (lack of LTS) in a current-clamped $Ca_v3.2^{-/-}$ CA3 PCs before (top) and after nickel (bottom) application. (**d**) Representative trace of a LTS evoked in a current-clamped CA1 PC by somatic current injection before (top) and after 50 μM nickel application (bottom (**e**) Nickel blocked LTS in CA3 PCs and increased the amount of current injection required for subthreshold depolarization (n=5; paired *t*-test; $p < 0.0001$). Z944 blocked LTS and any amount of current injection failed to elicit a subthreshold depolarization in CA3 PCs; therefore, there is no treatment bar accompanying this data. Nickel had no effect on subthreshold depolarization in CA3 PCs patched from $Ca_v3.2^{-/-}$ mice. Z944 blocked subthreshold depolarization in $Ca_v3.2^{-/-}$ CA3 PCs and current injection resulted in a linear voltage response, which is why there is no treatment bar accompanying this data set. Nickel blocked LTS in CA1 PCs and increased the current required for subthreshold depolarization (n=4; paired *t*-test; $p = 0.0324$). Scale in (a) applies to all representative traces.

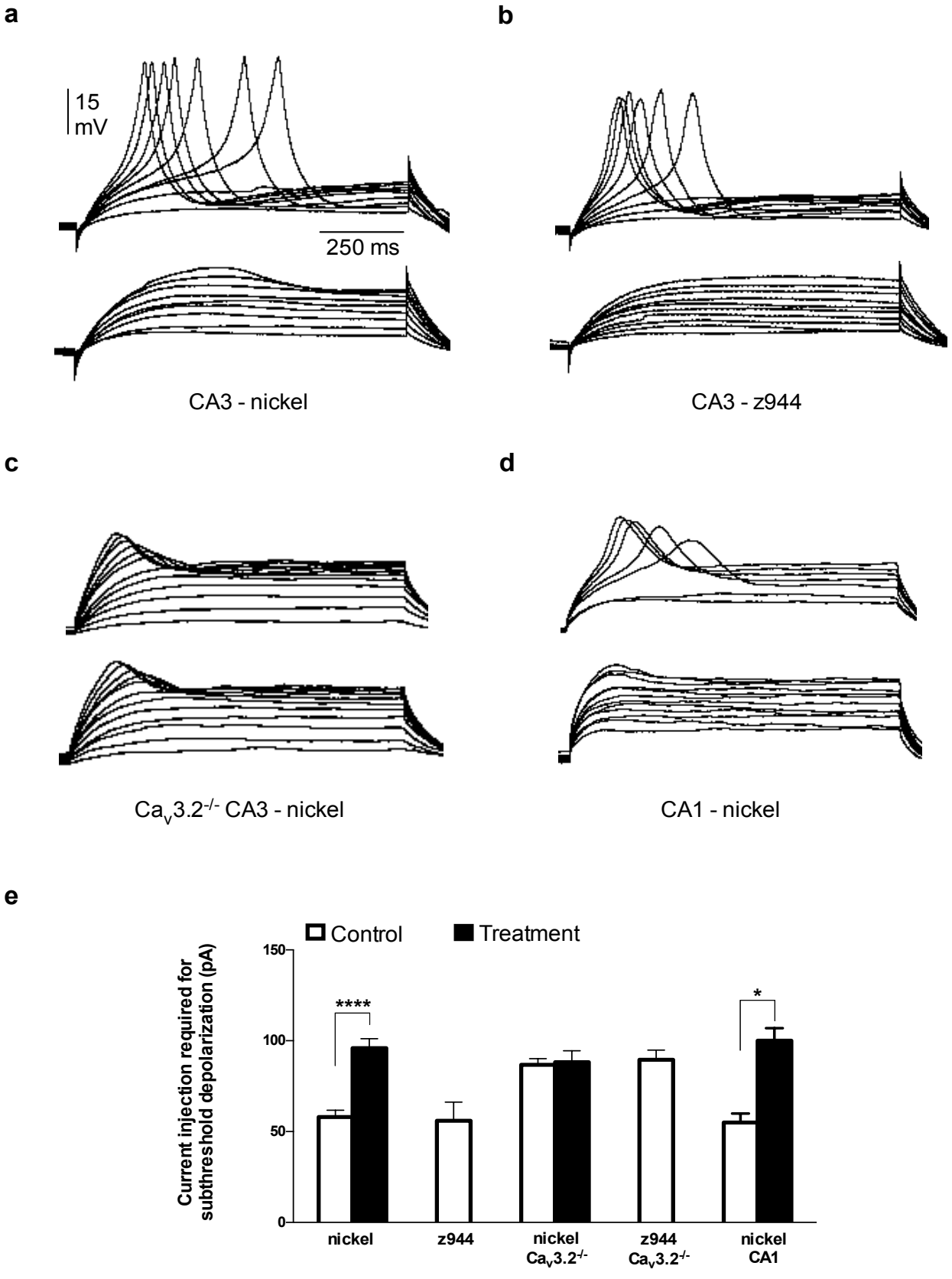
a
15
mV
250 ms
CA3 - nickel
b
CA3 - z944
c
Ca$_v$3.2$^{-/-}$ CA3 - nickel
d
CA1 - nickel
e
Control
Treatment
Current injection required for subthreshold depolarization (pA)
150
100
50
0
****
*
nickel
z944
nickel Ca$_v$3.2$^{-/-}$
z944 Ca$_v$3.2$^{-/-}$
nickel CA1

Figure 3-6 LTS in CA3 PCs is mediated by $Ca_v3.2$ channels.

(**a**) Representative trace of a LTS evoked in a current-clamped CA3 PC by somatic current injection before (top) and after 500 μM L-cysteine application (bottom). (**b**) Representative trace of a LTS evoked in a current-clamped CA3 PC by somatic current injection before (top) and after 1 mM ascorbate application (bottom). (**c**) L-cysteine did not change LTS threshold (n=5; paired *t*-test; $p = 0.2663$), ascorbate increased LTS threshold (n=5; paired *t*-test; $p = 0.0219$). (**d**) L-cysteine increased mean LTS amplitude (n=5; paired *t*-test; $p = 0.0397$) and ascorbate decreased mean LTS amplitude (n=5; paired *t*-test; $p = 0.0141$). Scale in (a) applies to all representative traces.

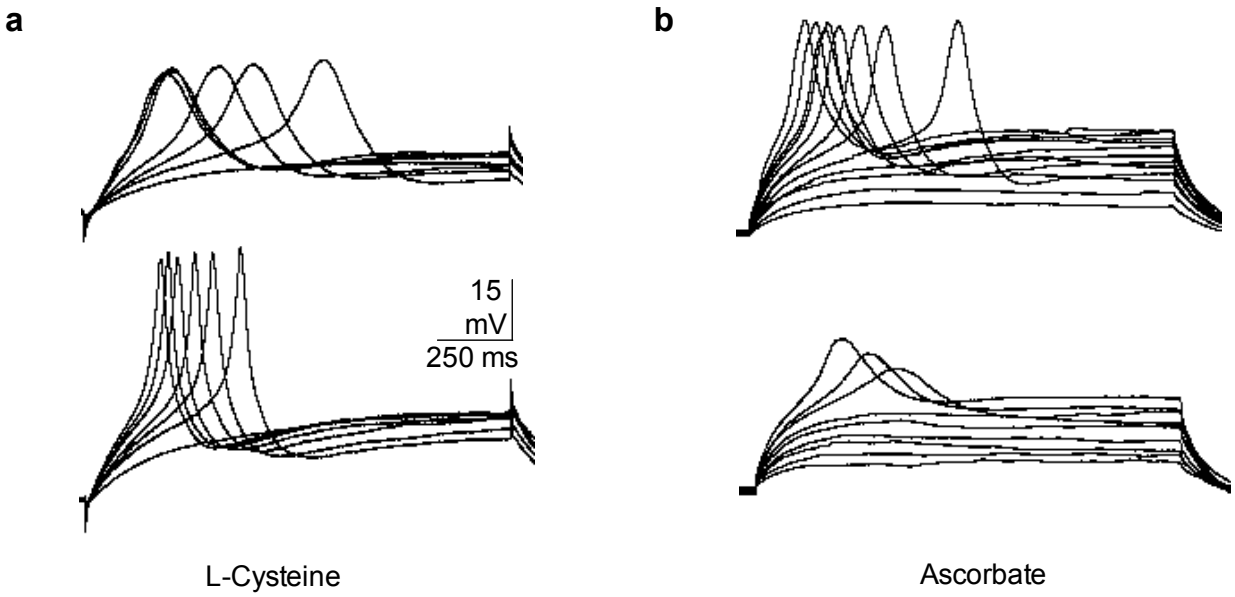
a
b
15
mV
250 ms
L-Cysteine
Ascorbate

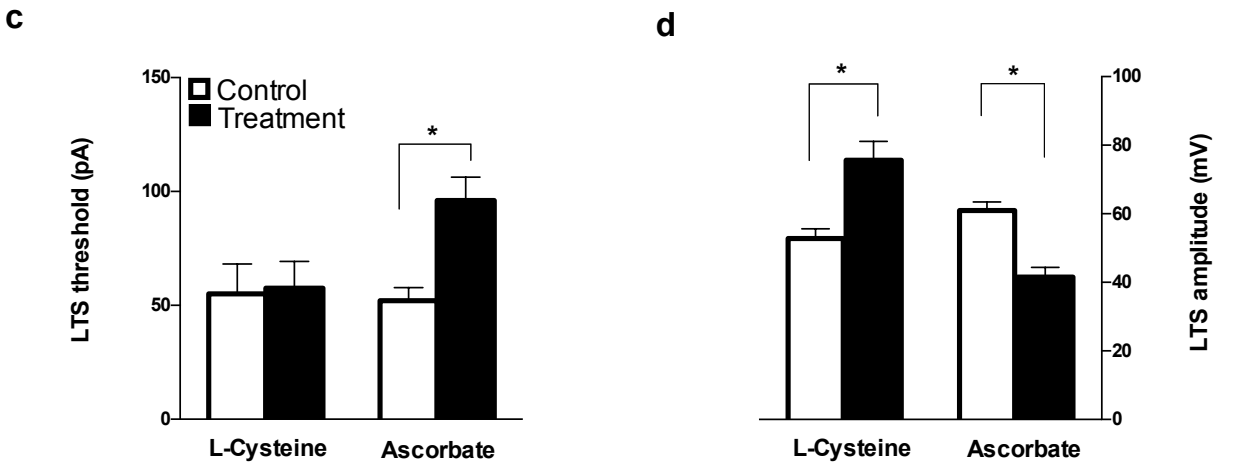
c
d
Control
Treatment
LTS threshold (pA)
150
100
50
0
*
L-Cysteine
Ascorbate
LTS amplitude (mV)
100
80
60
40
20
0
*
*
L-Cysteine
Ascorbate

Chapter 4: LTS-evoked Ca^{2+} influx in dendrites of CA1 and CA3 PCs

4.1 Overview

LVA and HVA Ca^{2+} channels are not distributed uniformly in dendritic arbors of CA1 PCs based on two-photon imaging studies of dendritic Ca^{2+} influx. Trains of backpropagating action potentials evoke Ca^{2+} influx through VGCCs in proximal and distal regions of both apical and basal arbors of CA1 PCs (Christie *et al.* 1995). Ca^{2+} influx in the soma and proximal dendritic region occurs primarily through HVA Ca^{2+} channels; while, nickel-sensitive, presumably LVA Ca^{2+} channels, make the greatest contribution to Ca^{2+} influx in distal dendrites (Christie *et al.* 1995). Consistent with this, the majority of Ca^{2+} influx in distal spines of CA1 PCs also occurs through nickel-sensitive VGCCs (Sabatini and Svoboda 2000). In contrast, climbing fiber stimulation evokes LTS in proximal dendrites of cerebellar Purkinje cells and activity-dependent stimulation initiates P/Q channel-mediated Ca^{2+} spikes at distal sites (Otsu *et al.* 2014).

Contribution of LVA Ca^{2+} channels to dendritic Ca^{2+} influx in CA3 PCs has yet to be determined; however, it is known that K^+ channels in distal basal dendrites spatially compartmentalize voltage responses to synaptic stimulation by shaping the time course of membrane repolarization (Makara and Magee 2013). High K^+ conductance under resting conditions also shortens the length constant by reducing input resistance and prevents integration of dispersed synaptic inputs (Makara and Magee 2013). Our current-clamp data reveals a similar phenomenon in both CA1 and CA3 PCs – LTS propagation is under the restraining influence of A-type K^+ conductance. On the other hand, the voltage-clamp data reveal a significant issue –

namely that the depolarization underlying LTS in CA3 PCs cannot be controlled effectively using patch-clamp recordings of the somatic membrane. We hypothesize that the divergent nature of T-type currents in CA1 and CA3 PCs arises from variable distribution and/or density of channels in the dendrites of PCs in the two regions. In this chapter, we sought to profile in detail the Ca^{2+} transients associated with evoked LTS in subcellular compartments of CA1 and CA3 PCs.

4.2 Results

4.2.1 Two-photon imaging of T-type Ca^{2+} transients in CA3 PCs

Given the differences between characteristics of T-type Ca^{2+} currents observed in CA3 and CA1 PCs, we examined the spatial distribution of Ca^{2+} entry T-type Ca^{2+} channels in hippocampal PCs. To do this, we included a potassium-salt derivative of Fluo-4 in the patch pipette and employed the whole-cell voltage clamp technique to inject this cell-impermeable dye into neurons. Fluo-4 exhibits an increase in fluorescence upon binding Ca^{2+}. To image the Ca^{2+} influx associated with T-type currents, we scanned three sequential frames with the cell held at –100 mV to determine baseline fluorescence. The frame immediately prior to T-type current activation is shown in the left panel of **Fig. 4-1a**. Cells were depolarized using a single voltage step (300 msec) to –30 mV (right panel, **Fig. 4-1a**). Depolarization to –30 mV elicited a T-type Ca^{2+} current that was 200 pA in amplitude (data not shown) and the associated Ca^{2+} influx was observed as an increase in fluorescence of the Fluo-4 dye. We depolarized to –30 mV because this was the voltage at which the amplitude of T-type current was highest (as shown in *I-V* relationships of T-type currents in Chapter 3.2.1). For each experiment, we added 2 μM Z944 to

the bath to ensure that the increased fluorescence was due to Ca^{2+} influx through T-type Ca^{2+} channels. The left panel in **Fig. 4-1b** shows the frame scan immediately prior to depolarization with Z994 in the recording chamber. In the presence of Z944, the same depolarizing step that resulted in an increased fluorescence signal previously failed to produce a discernible change in intracellular Ca^{2+} (right panel, **Fig. 4-1b**) and blocked the T-type current as well (data not shown).

To quantify fluorescence signals, we measured pixel values within a given region of interest (ROI) drawn onto the dendrite and soma of cells (excluding the nucleus). These values were subtracted from an ROI drawn onto the background of the frame to achieve a true fluorescence signal that was corrected for changes in background. The dimensions of the drawn ROI were kept identical between frames acquired during a single experiment. We performed the above analysis for every frame in both control conditions and after Z944 application. Frames held at –100 mV prior to depolarization were set as "baseline" and values obtained after depolarization were set as "measured". To calculate $\Delta F/F$, we subtracted measured values from baseline values and divided the answer by baseline values ([measured – baseline]/baseline). Peak $\Delta F/F$ after depolarization was higher in the dendrite (dotted line) than soma (solid line) and the fluorescence increase in both areas was completely blocked by Z944 (**Fig. 4-1c**).

4.2.2 Somatic and dendritic Ca^{2+} transients associated with T-type currents are blocked by Z944 in CA3 PCs

The sequence of experiments described in section **4.2.1** was repeated in five CA3 PCs from five different slices obtained from four animals. The time courses of Fluo-4 fluorescence signals

before and after depolarization from soma and proximal dendrites is shown in **Fig. 4-2a** and Fig. **4-2b**, respectively. Somatic fluorescence signals of CA3 PCs (**Fig. 4-2a**) were smaller in magnitude than dendritic signals (**Fig. 4-2b**) and this trend was consistent across all cells tested. The peak fluorescence signal observed after depolarization to –30 mV (denoted by vertical dotted black line in Fig. 4-2a and b) was averaged across neurons in order to make comparisons between spatial locations and recording conditions (i.e. before and after addition of Z944 to the recording chamber). Under control conditions, ΔF/F in the soma of CA3 PCs was 0.639 ± 0.146 and 1.233 ± 0.283 in dendrites (n=5; paired *t*-test; $p = 0.0285$; **Fig. 4-2c**). After Z944 application, ΔF/F in the soma of CA3 PCs decreased to 0.034 ± 0.020 (n=5; paired *t*-test; $p = 0.0147$; **Fig. 4-2c**) and -0.006 ± 0.064 in dendrites (n=5; paired *t*-test; $p = 0.0222$; **Fig. 4-2c**).

4.2.3 Somatic and dendritic Ca^{2+} transients associated with T-type currents are blocked by Z944 in CA1 PCs

Having ascertained the Z944-sensitivity of Ca^{2+} transients associated with T-type currents in CA3 PCs, we examined the spatial distribution of T-type Ca^{2+} channels in CA1 PCs. Data acquisition and analysis for this section are identical to that described in sections **4.2.2** and **4.2.3**. A representative two-photon image of a CA1 PC patched with 400 μM Fluo-4 is shown in the left panel of **Fig. 4-3a**. A single 300 msec depolarizing step to –30 mV elicited a T-type Ca^{2+} current (data not shown) and associated increase in Fluo-4 fluorescence (right panel, **Fig. 4-3a**). Repeating this experiment in the presence of 2 μM Z944 blocked the T-type Ca^{2+} current and prevented the associated fluorescence increase (**Fig. 4-3b**) that was observed in the same cell prior to Z944 application. Similar to CA3 PCs, ΔF/F in the proximal dendrites of CA1 PCs was higher in response to T-type Ca^{2+} current activation when compared to the signal observed in

somatic regions. Under control conditions, average peak ΔF/F in the soma was 0.437 ± 0.046 and 0.724 ± 0.109 in dendrites (n=4; paired *t*-test; $p = 0.0297$; **Fig. 4-3c**). After Z944 application, ΔF/F in somatic and dendritic regions decreased to 0.034 ± 0.005 (n=4; paired *t*-test; $p = 0.004$; **Fig. 4-3c**) and -0.036 ± 0.026 (n=4; paired *t*-test; $p = 0.0045$; **Fig. 4-3c**), respectively.

4.2.4 Two-photon line scan imaging of T-type Ca^{2+} transients in hippocampal PCs

The data presented in sections **4.2.1 – 4.2.3** indicates that T-type Ca^{2+} channels are expressed on both the soma and dendrites of hippocampal PCs. However, the temporal resolution of frame scan imaging used to acquire that data was poor. In order to obtain a better understanding of the spatial distribution of T-type Ca^{2+} channels in hippocampal PCs, we combined current clamp recordings with line scan imaging of distal and proximal regions of basal and apical dendrites. For these experiments, we used a potassium methanesulfonate internal solution to avoid dye quenching by gluconate and supplemented it with 400 μM Fluo-4 to detect changes in intracellular Ca^{2+} and 50 μM Alexa Fluor 594 to image the morphology of the patched cell.

After obtaining access in the whole cell configuration, we waited 10-15 minutes to allow Alexa 594 to fill cellular processes prior to beginning experiments. **Fig. 4-4a** shows a monochrome two-photon stack of a representative CA3 PC loaded with Alexa-594 and Fluo-4. The red line on the image depicts the location of a line scan that was done in combination with current injection at the soma. The imaging software allowed us to draw a line of a given length in any location on the cell. Once prompted, the laser repeatedly scans the length of the line for a time frame chosen by the experimenter and the length of the line determines the duration of a single scan. We ensured that the length of the drawn line for all line scans was identical such that the laser

traversed that line from start to end in an identical manner (1.54 msec) from one scan to another. By doing this, the temporal resolution of our imaging remained constant between experiments. This allowed us to obtain a baseline fluorescence measurement of sufficient duration to allow for comparisons after a LTS was elicited via somatic current injection.

The line drawn on the apical dendrite of the CA3 PC in **Fig. 4-4a** resulted in a scan duration of 1.54 msec. Setting the software to obtain 6000 scans resulted in a total duration of 9.24 seconds. The typical readout from line scans obtained in this manner is shown in the top panel of **Fig. 4-4b**. The red vertical dotted line depicts the occurrence of a single 1 s depolarizing step of 50 pA that elicited a LTS (data not shown). The green bar running down the centre of the scan is where the Fluo-4 signal in the dendritic portion of the cell was captured and the edges of the line outside the cell remain dark green, almost black, in this image. Obtaining pixel information from the entire scan allows for the computation of $\Delta F/F$ values as a function of time (bottom panel; **Fig. 4-4b**). Thus, line scan imaging of various regions of a cell greatly improves temporal resolution when compared to frame scans that provide more spatial information.

4.2.5 Line scan imaging of LTS-associated Ca^{2+} transients in hippocampal PCs

Using the imaging method described in section **4.2.4** we examined the spatial distribution of T-type Ca^{2+} channels in hippocampal PCs. For each cell, we performed one line scan in the soma, two in the apical dendrites and another two in the basal dendrites. For each dendritic arborization (apical and basal), line scans were done in proximal (< 50 μm) and distal (> 50 μm) regions. **Fig. 4-5a** shows a two-photon stack of a CA3 PC loaded with Alexa-594 and Fluo-4. Coloured lines

on different portions of the cell depict the location of line scans. Red lines show the location of line scans done in the apical arborization – the solid line depicts the location of the proximal scan, while the dotted line denotes the location of the distal scan. Similarly, green lines show the location of line scans done in the basal arborization – the solid line depicts the location of proximal scan, while the dotted line indicates location of the distal scan. Beyond the criteria of distance from soma, the location of a given scan was chosen randomly such that primary dendrites were not preferred over secondary ones (or vice versa) and both were interleaved between cells to ensure that a diverse sampling of dendrites was obtained for the final analysis. Time-lapsed pixel information was used to obtain ΔF/F values as described in sections **4.2.1**. and **4.2.4**. ΔF/F values were then averaged in 30.8 msec time bins to obtain a smooth time course of Fluo-4 fluorescence signals.

Fig. 4-5b shows the time course of line scans depicted in **Fig. 4-5a** and both are colour-matched for easier interpretation of data. The black vertical dotted line depicts the timing of a 1 s single depolarization step of 50 pA that elicited a LTS. Peak fluorescence in the soma (purple line) was similar to that observed in proximal regions of apical (solid red line) and basal arborizations (solid green line). Proximodistal decrement of the signal occurred for both the apical (dotted red line) and basal arborization (dotted green line); however, in this cell decrement was larger for the apical arborization. Both the LTS and ensuing increase in Fluo-4 signals were blocked by 2 μm Z944 (data not shown). **Fig. 4-5c** shows a two-photon stack of a CA1 PC loaded with Alexa-594 and Fluo-4. Coloured lines on different portions of the cell depict the location of line scans as described for **Figs. 4-5a and b**. Overall, Ca^{2+} influx from LTS in CA1 PC was of lower magnitude than that observed in CA3 PC and proximodistal decrement of the signals in dendrites

was more precipitous in CA1 PC as well. Similar to CA3 PC, both LTS and the associated Ca^{2+} influx were blocked by 2 μm Z944 (data not shown).

4.2.6 CA3 PCs exhibit larger LTS-associated Ca^{2+} transients compared to CA1 PCs

Line scans done on different regions of CA3 PCs were averaged across six cells to obtain a summary of the time course of Ca^{2+} transients associated with LTS (**Fig. 4-6a**). Peak fluorescence measured from the soma (purple line) was comparable to the signals observed in proximal regions of apical (solid red line) and basal (solid green line) dendrites. Proximodistal decrement of the Fluo-4 signal was nearly 40% for both apical (dotted red line) and basal arborizations (dotted green line) of CA3 PCs. In comparison, Ca^{2+} influx associated with LTS was lower in CA1 PCs (**Fig. 4-6b**). Peak fluorescence measured from the soma, averaged across five CA1 PCs, was 70% lower than the peak somatic fluorescence observed in CA3 PCs. Similarly, LTS-associated fluorescence signal in proximal regions of the apical and basal arborizations was less than 70% of the values observed in proximal dendrites of CA3 PCs. LTS-associated Ca^{2+} influx in the distal dendrites of CA1 PCs increased by less than 10% reflecting greater decrement of the fluorescence signal in distal dendrites of CA1 PCs in comparison with CA3 PCs.

Plotting the relationship between peak Ca^{2+} fluorescence obtained from individual dendrites in (**Figs. 2-6a and b**) and distance from the soma shows that proximodistal decrement of dendritic Ca^{2+} signals is more pronounced in CA1 PCs than CA3 PCs (**Fig. 4-6c**). The intercept of the CA3 (black) regression line (slope -0.010 ± 0.004 μm^{-1} (±SD); $p = 0.0187$) is 1.453. The

intercept of the CA1 (blue) regression line (slope -0.004 ± 0.001 μm^{-1} (±SD); p = 0.0.0261) is 0.505.

4.2.7 Somatic stimulation evokes T-type Ca^{2+} transients in dendrites

In order to quantify the Ca^{2+} influx associated with LTS as a function of time; we computed area under the curve for each dendritic and somatic line scan of CA3 and CA1 PCs. Averaged across cells, area under the curve, and therefore, Ca^{2+} influx per unit of time was higher in all regions of PCs in CA3 when compared to CA1 (**Fig. 4-7**). Ca^{2+} influx from an evoked LTS was higher in proximal dendrites of the CA3 apical arborization (371.71 ± 28.56) when compared to CA1 PCs (218.52 ± 22.30); however, this trend was not statistically significant (n=6; unpaired *t*-test; p = 0.2586; **Fig 4-7a**). Spatial decrement of Ca^{2+} transients was more pronounced in distal apical dendrites of CA1 PCs (31.07 ± 21.02; n=5) than CA3 PCs (242.88 ± 27.90; n=6; unpaired *t*-test; p = 0.0349; **Fig. 4-7a**). LTS-associated Ca^{2+} influx in proximal regions of basal dendrites degraded less in CA3 PCs (429.74 ± 32.74; n=6) than CA1 PCs (81.12 ± 38.04; n=5; unpaired *t*-test; p = 0.0248; Fig. **4-7b**). This was also the case for distal regions of the basal arborization in CA3 PCs (215.84 ± 29.22; n=6) when compared to CA1 PCs (65.13 ± 36.04; n=5; Mann-Whitney test; p = 0.0317; **Fig. 4-7b**). Area under the curve in somatic regions of CA3 PCs (421.96 ± 22.92; n=6) was also significantly higher than CA1 PCs (124.72 ± 33.56; n=5; unpaired *t*-test; p = 0.0247; **Fig. 4-7c**).

4.3 Discussion

Our Ca^{2+} imaging data correlates well with the electrophysiological data presented in Chapter 3. Using line scan imaging, we find that Ca^{2+} influx in the soma, apical and distal dendrites of CA3 PCs is temporally correlated to the onset of LTS evoked with current injection at the soma. Somatic and dendritic LTS-associated Ca^{2+} transients were blocked by Z944 indicating that T-type Ca^{2+} channels are exclusive mediators of the Ca^{2+} influx that results from LTS propagation. Comparisons between CA3 and CA1 reveal that T-type channels in the somatic membrane are likely expressed at a higher density in CA3 PCs because the amplitude of Ca^{2+} transients is significantly larger in PCs of CA3 than CA1. We also found that the amplitude of Ca^{2+} transients decreased with distance from the soma in the apical and basal arbors of both CA1 and CA3 PCs. Such proximodistal decrement of Ca^{2+} transients was especially severe in CA1 PCs – amplitude of Ca^{2+} transients in distal regions of the apical dendrite (>50 μm) was on average less than 80% of that observed in proximal regions. Although the signal decremented distally to a lesser degree in basal dendrites of CA1 PCs, the amplitude was relatively small in basal dendrites as a whole. In contrast, Ca^{2+} transients in proximal regions of both basal and apical dendrites were roughly equal in magnitude to signals observed in the soma of CA3 PCs. Proximodistal decrement occurred in dendrites of CA3 PCs as well – amplitude of Ca^{2+} transients in distal regions of apical and basal dendrites was half of that observed in proximal domains.

This data can be interpreted in two ways: 1) that reduced amplitude of LTS-associated Ca^{2+} signals in the soma of CA1 PCs and sharp proximodistal decrement compared to CA3 PCs reflect reduced density and/or distribution of T-type channels in CA1 PCs; 2) that passive and active properties of CA3 and CA1 dendrites, in addition to their morphology, differ substantially,

such that LTS propagate to varying lengths between the two regions. Either or both of these possibilities could reduce space clamp efficiency resulting in the distorted T-type current kinetics observed in CA3 PCs. Inability to control transmembrane voltage across the entire length of the dendritic tree obscures the voltage response to synaptic activation detected at the soma. Reduction in amplitude and delay in time course of voltage signals are both a direct consequence of space clamp errors, and such attenuation is especially severe for faster conductances that are characteristic of T-type channels. Space clamp errors manifest in two interdependent ways: 1) synaptic events from dendrites (as close as 90 μm from the soma) attenuate significantly towards the soma; and 2) somatic voltage clamp is unable to control the membrane potential of dendrites resulting in voltage escape that activates dendritic voltage-dependent conductances even after the command potential has been terminated (Williams and Mitchell 2008).

The Ca^{2+} imaging data show that at distal dendritic locations (>50 μm from the soma), substantial Ca^{2+} influx occurs in response to LTS initiation, reflecting the activation of T-type channels at distances that are moderately far from the soma. Considering that our imaging experiments were done primarily in large parent dendrites, voltage escape is expected is to be more severe in the smaller dendrites of PCs that have a higher distribution of LVA channels. The higher amplitude and lesser proximodistal decrement of LTS-associated Ca^{2+} transients in CA3 compared to CA1 reflect the higher distribution of T-type channels in CA3 PCs and provide a convincing explanation for the slower kinetics of T-type currents observed in PCs of the CA3 region. Heterogeneous distribution of ion channels between CA1 and CA3 PCs has been reported previously. For example, the magnitude of I_h current, mediated by HCN channels, is significantly

smaller in CA3 than CA1 PCs, suggesting differential distribution in the two cell types (Santoro *et al.* 2000).

In addition to active properties, the morphology of dendrites, including branch density and total dendritic length, have a substantial impact on neuronal physiology. Although PCs in CA3 have structurally similar pyramid-shaped soma as PCs in CA1, the dendritic morphology of CA3 PCs differs from their CA1 neighbours. CA3 neurons have a short apical trunk as the apical dendritic tree bifurcates close to the soma in stratum lucidum and branches into two or more secondary trunks that extend into stratum lacunosum-moleculare (Henze *et al.* 1996). In contrast, CA1 apical dendrites bifurcate in stratum radiatum or travel through to stratum lacunosum-moleculare and bifurcate in this region (Bannister and Larkman 1995). Further, the apical and basal dendritic arbors of CA3 PCs have a larger range than CA1 PCs (Spruston and McBain 2009). The three-dimensional geometry of CA3 PCs consists of two cones for the apical arbor and a single cone for basal arbor, whereas, apical and basal arbors of CA1 PCs each occupy a single conical volume (Henze *et al.* 1996). Neuronal models that account for dendritic morphology of CA3 PCs show that brief changes in membrane potential are attenuated dramatically, and control of dendritic conductances, even at moderate distances from the soma, is nearly impossible (Major *et al.* 1994, Spruston and McBain 2009). The short primary apical dendrite of CA3 PCs has largely impeded the study of dendritic VGCCs in these neurons, and our data attest to the constraints that morphological features of CA3 PCs impose on voltage-gated conductances.

Figure 4-1 Somatic and dendritic Ca^{2+} transients are blocked by Z944 in CA3 PCs.

(**a**) Two-photon image of a patch-clamped CA3 PC loaded with 400 μM Fluo-4. Under control conditions (left panel), the cell is held at –100 mV. Depolarization to –30 mV elicited a T-type current and the associated increase in Ca^{2+} fluorescence (right panel). Scale bar, 5 μm. (**b**) Image of the same cell as (a) in the presence of 2 μM Z944 (left panel) held at –100 mV and depolarized to –30 mV (right panel). (**c**) Time course of the Ca^{2+} fluorescence signal measured from ROI in the soma (solid line) and dendrite (dotted line) of the cell in (a) and (b) under control conditions (top) and after Z944 application (bottom). Dotted line represents the beginning of a depolarizing step to –30 mV from a holding potential of –100 mV.

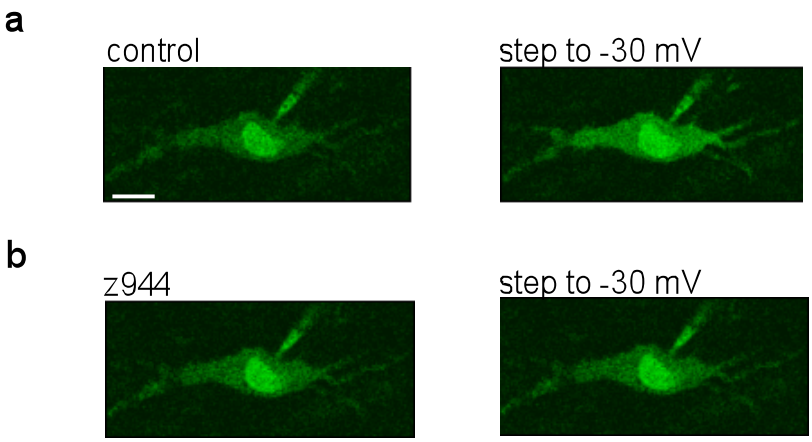
a
control
step to -30 mV
b
z944
step to -30 mV

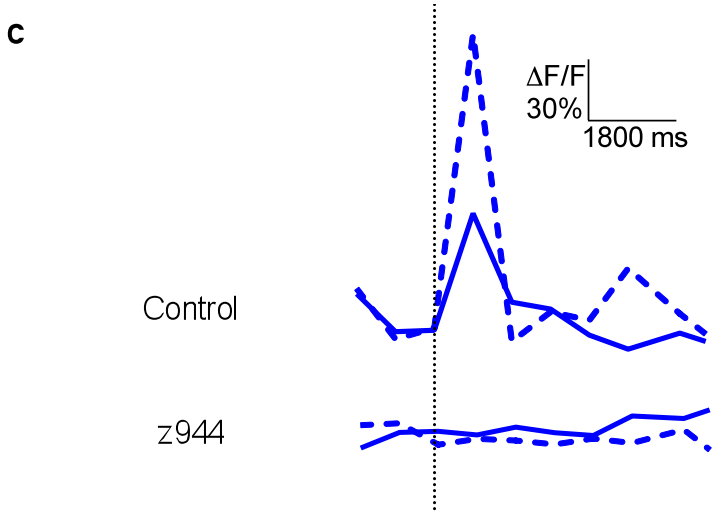
c
ΔF/F
30%
1800 ms
Control
z944

Figure 4-2 Variable somatic and dendritic Ca^{2+} transients in CA3 PCs.

(**a**) Time course of the Ca^{2+} fluorescence signal measured from ROIs in the soma of five different CA3 PCs. (**b**) Time course of Ca^{2+} signal measured from ROIs in the dendrites of the same five cells in (a). Dendrite and soma of the same cell are colour-matched. Dotted lines in both (a) and (b) represent the beginning of a depolarizing step to –30 mV from a holding potential of –100 mV. (**c**) Z944 blocked the T-type current associated Ca^{2+} increase in the soma (n=5; paired *t*-test; $p = 0.0147$) and dendrites (n=5; paired *t*-test; $p = 0.0222$). Ca^{2+} fluorescence in dendrites was higher than somatic signals (n=5; paired *t*-test; $p = 0.0285$).

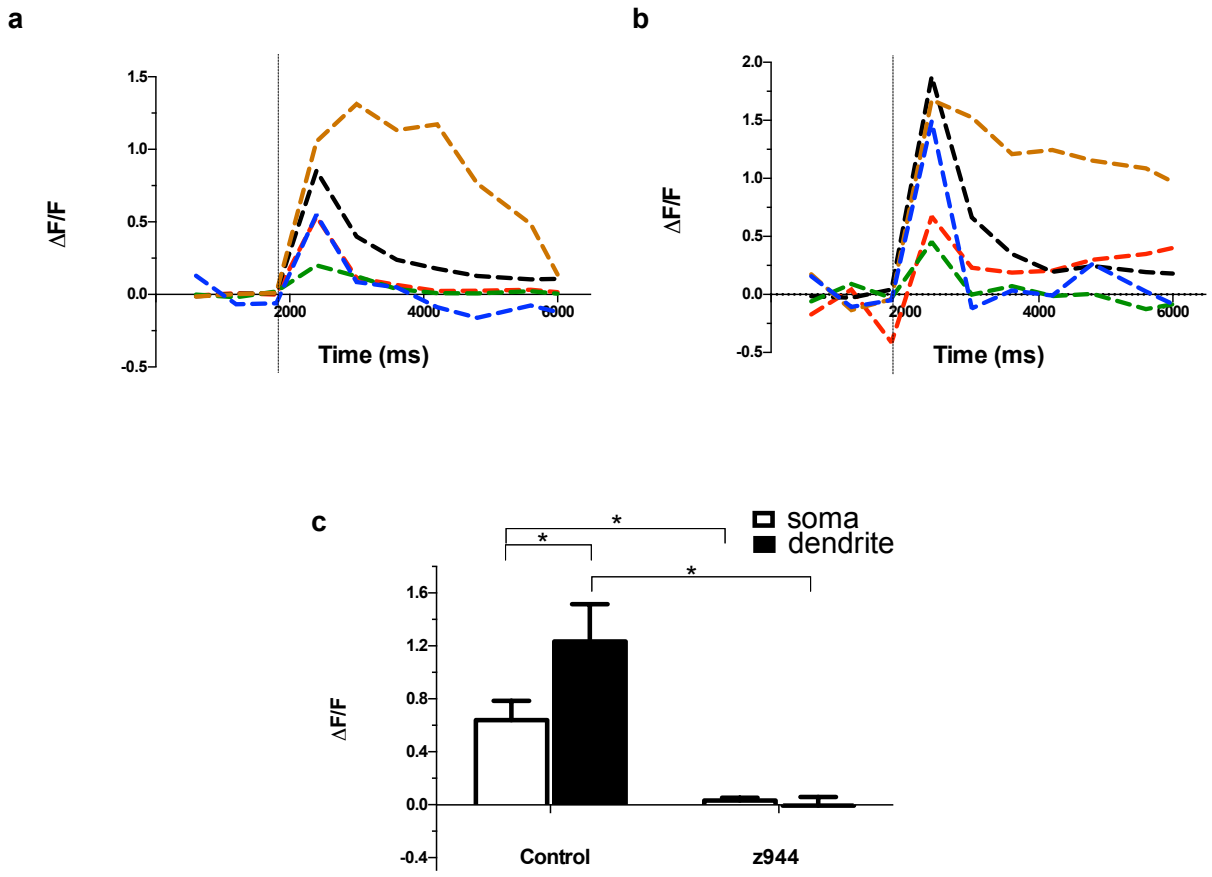
a
b
c
ΔF/F
Time (ms)
soma
dendrite
Control
z944
*
*
*

Figure 4-3 Somatic and dendritic Ca^{2+} transients are blocked by Z944 in CA1 PCs.

(**a**) Two-photon image of a patch-clamped CA1 PC loaded with 400 μM Fluo-4. Under control conditions (left panel), the cell is held at –100 mV. Depolarization to –30 mV elicited a T-type current and the associated increase in Ca^{2+} fluorescence (right panel). Scale bar, 5 μm. (**b**) Image of the same cell as (a) in the presence of 2 μM Z944 (left panel) held at –100 mV and depolarized to –30 mV (right panel). (**c**) Z944 blocked the T-type current associated Ca^{2+} increase in the soma (n=6; paired *t*-test; $p = 0.0040$) and dendrites (n=6; paired *t*-test; $p = 0.0045$). Ca^{2+} fluorescence in dendrites was higher than somatic signals (n=6; paired *t*-test; $p = 0.0297$).

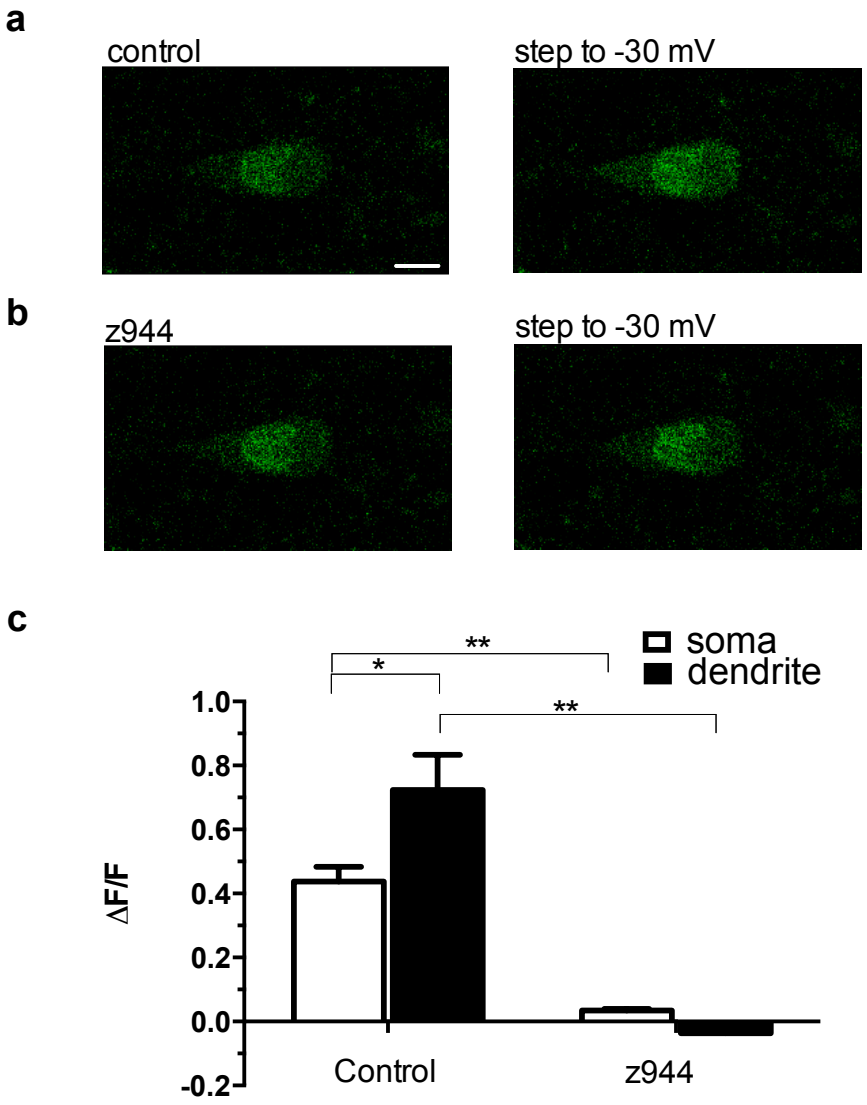
a
control
step to -30 mV
b
z944
step to -30 mV
c
soma
dendrite
**
*
**
1.0
0.8
0.6
0.4
0.2
0.0
-0.2
ΔF/F
Control
z944

Figure 4-4 Two-photon line scan imaging of Ca^{2+} transients in hippocampal PCs.

(**a**) Two-photon z-stack of patch-clamped CA3PC loaded with 50 µM Alexa-594 and 400 µM Fluo-4 showing a sample line scan (red line) done across the proximal apical dendrite. The time required for the laser to traverse the line from one end to the other is 1.54 msec and this duration was kept consistent across line scans and cells. Scale bar, 20 µm. (**b**) Top: Readout from the line scan done in (a) showing the increase in Ca^{2+} fluorescence after a LTS was evoked via somatic current injection of 50 pA for 1 second (denoted by dotted red line). Scale bar, 3 µm. Bottom: Time course of the Ca^{2+} signal obtained from top panel with relative fluorescence on the x-axis and time on the y-axis. Scale bar, 500 msec.

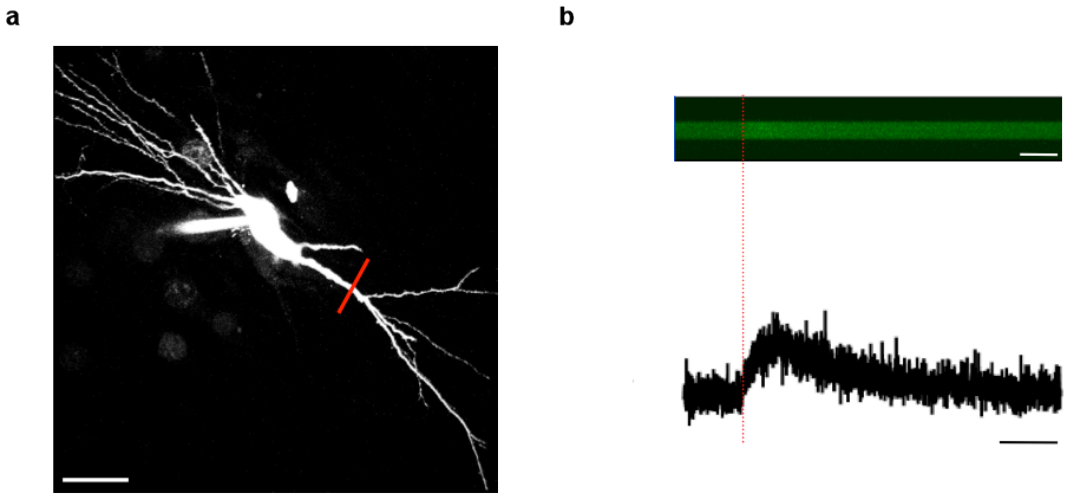

Figure 4-5 Line scan imaging of LTS-associated Ca^{2+} transients in hippocampal PCs.

(**a**) Two-photon z-stack of patch-clamped CA3 PC loaded with 50 μM Alexa-594 and 400 μM Fluo-4. Coloured lines on the image denote location of line scans. Solid lines depict locations of somatic (purple), proximal apical (red) and, and proximal basal (green) line scans. Dotted lines depict locations of distal apical (red) and distal basal (green) line scans. Scale bar, 20 μm. (**b**) Time course of Ca^{2+} fluorescence signal measured from line scans depicted in (a). Dotted black line denotes the occurrence of a LTS evoked by current injection of 50 pA for 1 msec. (**c**) Two-photon z-stack of a patch-clamped CA1 PC loaded with 50 μM Alexa-594 and 400 μM Fluo-4. Lines depict position of line scans similar to (a). Scale bar, 20 μm. (**d**) Time course of Ca^{2+} fluorescence signal measured from line scans depicted in (a). Dotted line denotes the occurrence of a LTS evoked by 1 second depolarizing step of 50 pA. Scale bars in (b) apply to (d) as well.

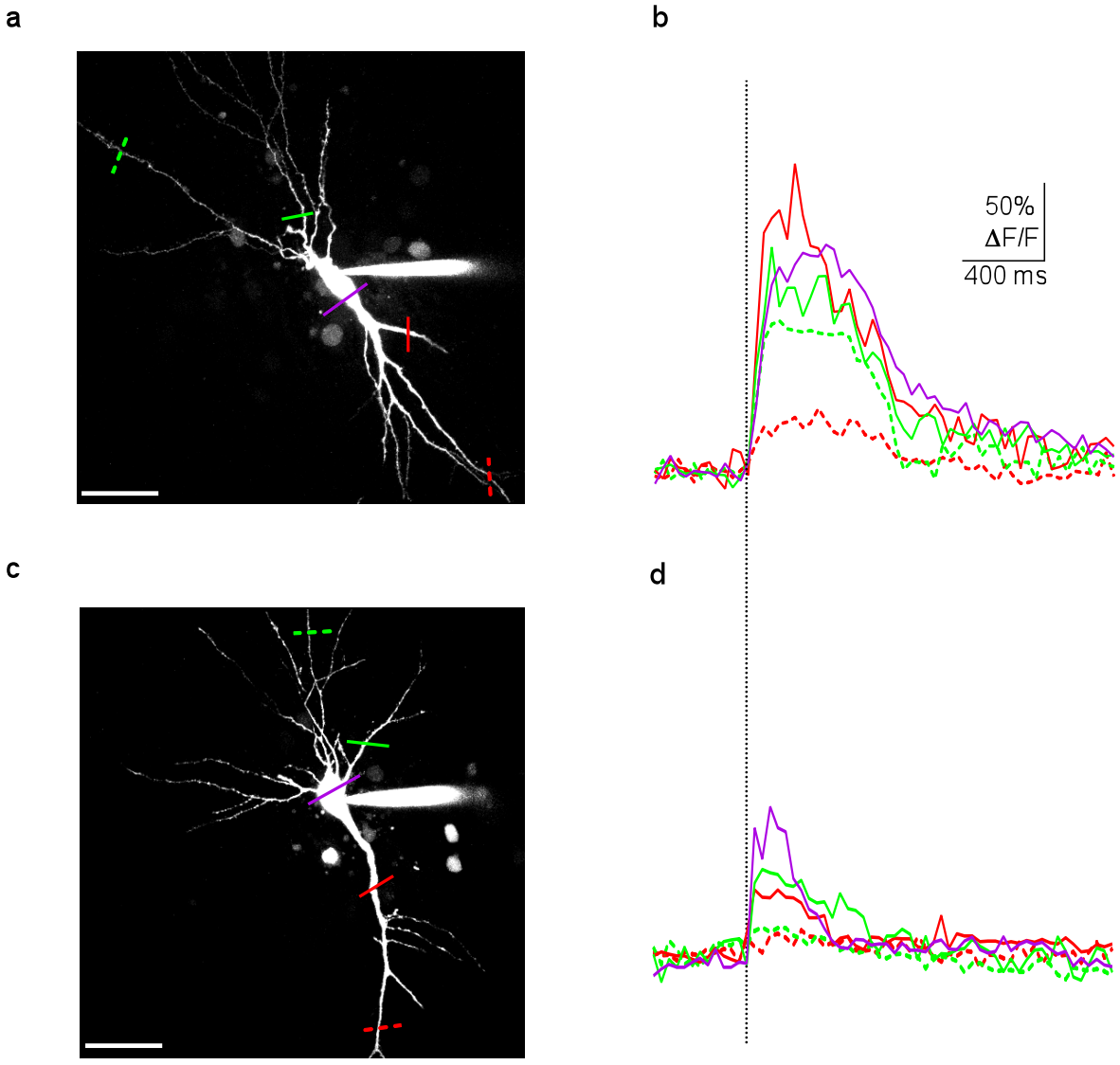
a
b
50%
ΔF/F
400 ms
c
d

Figure 4-6 CA3 PCs display larger LTS-associated Ca^{2+} transients compared to CA1 PCs. (**a**) Time course of the Ca^{2+} fluorescence signal measured from somatic (purple), apical dendritic (red), and basal dendritic (green) line scans in CA3 PCs (n=6). Dotted red and green line scans were done on distal locations of apical and basal dendrites, respectively. Dotted black line denotes the occurrence of a LTS evoked by a 1-s current step of 50 pA. (**b**) Time course of the Ca^{2+} fluorescence signal measured from somatic and dendritic line scans in CA1 PCs (n=5). Different coloured lines depict locations of line scans as detailed in (a). (**c**) Relationship between Ca^{2+} transient amplitude and distance from the soma. The intercept of black regression line (slope -0.010 ± 0.004 μm^{-1} (±SD); p = 0.0187) is 1.453. The intercept of the blue regression line (slope -0.004 ± 0.001 μm^{-1} (±SD); p = 0.0.0261) is 0.505.

a

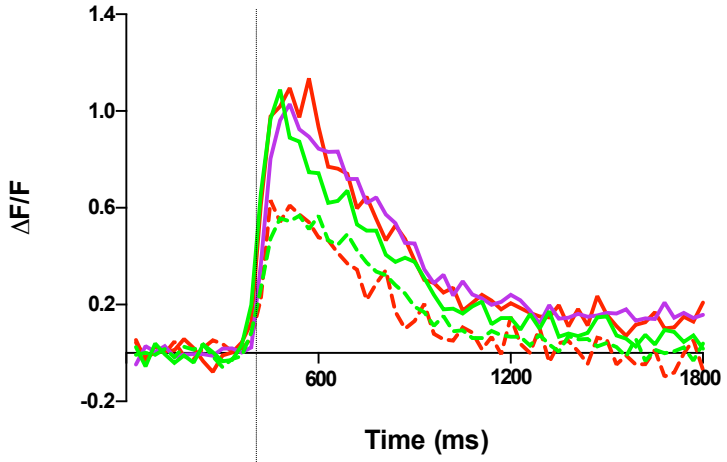
1.4
1.0
0.6
0.2
-0.2
ΔF/F
600
1200
1800
Time (ms)

b

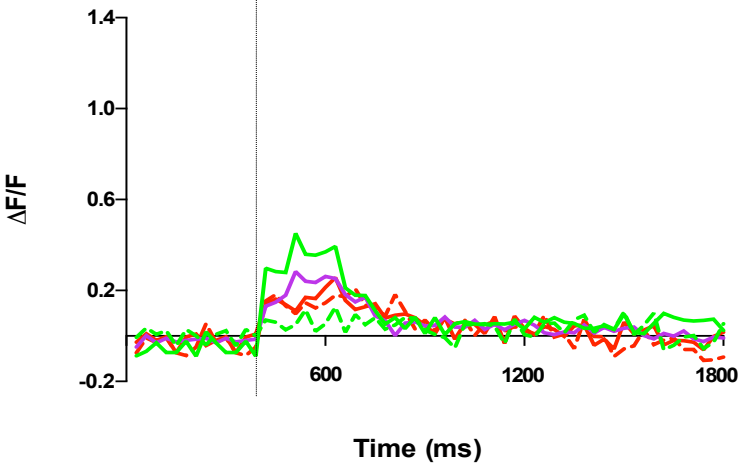
1.4
1.0
0.6
0.2
-0.2
ΔF/F
600
1200
1800
Time (ms)

c

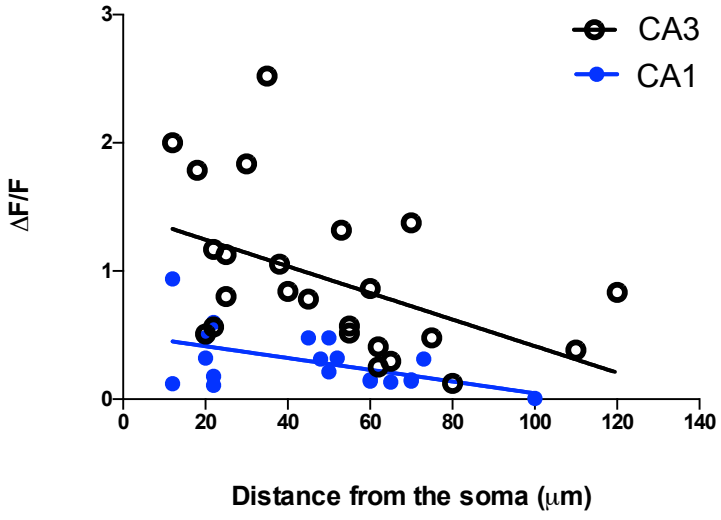
CA3
CA1
3
2
1
0
ΔF/F
0
20
40
60
80
100
120
140
Distance from the soma (μm)

Figure 4-7 Proximo-distal decrement of LTS-associated Ca^{2+} signals in hippocampal PCs. (**a-c**) Average area under the curve of Ca^{2+} transients measured from line scans of CA3 and CA1 PC soma and dendrites. (**a**) Spatial decrement of Ca^{2+} transients was more pronounced in distal apical dendrites of CA1 PCs (n=5) than CA3 PCs (n=6) (unpaired *t*-test; p=0.0349). This was also the case for (**b**) proximal basal dendrites (CA1 PCs n=5; CA3 PCs n=6; unpaired *t*-test; p = 0.0387), distal basal dendrites (n=5; CA1 PCs; n=6, CA3 PCs; Mann-Whitney test; p = 0.0317), and (**c**) soma (CA1 PCs – n=5; CA3 PCs n=6; unpaired *t*-test; p = 0.0247).

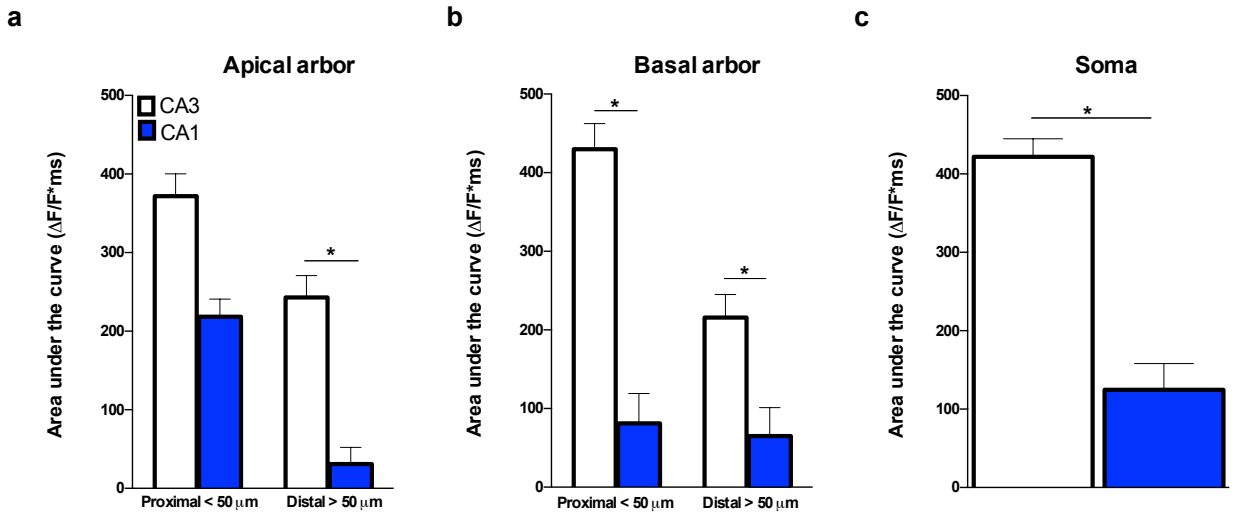

Chapter 5: Regulation of LTS by K^+ channels and GPCRs in CA3 PCs

5.1 Overview

The data outlined in Chapter 3 shows that A-type K^+ channels significantly restrict LTS propagation and without A-type channel blockade, current injection of any magnitude fails to elicit subthreshold depolarization, let alone LTS. This suggests that T-type and A-type K^+ channels would have to be in close proximity in order for the latter to significantly restrict T-type-mediated signal propagation. Such coupling has been shown between $K_v4.2$ and $Ca_v3.3$ channels in cerebellar stellate cells (Anderson *et al.* 2010). The signaling complex formed by these two channels imparts Ca^{2+} dependence on $K_v4.2$ channels and dynamically regulates the firing pattern of stellate cells. A similar association between T-type channels and Ca^{2+}-activated K^+ channels has been reported in medial vestibular neurons, where Ca^{2+} entry through T-type channels over a wide range of membrane voltages activates and enables K^+ channels to contribute to action potential repolarization (Rehak *et al.* 2013). In this Chapter we investigate the influence of a variety of K^+ channels on LTS amplitude, threshold, and decay kinetics.

T-type Ca^{2+} channels are also subject to regulation by GPCRs in part because phosphorylation of specific residues in cytoplasmic linker regions alters gating properties of these channels (Welsby *et al.* 2003). Co-expression of muscarinic receptors and T-type channels shows that M1 activation has an inhibitory effect on $Ca_v3.3$ currents and a moderate stimulating effect on $Ca_v3.1/3.2$ current amplitudes (Hildebrand *et al.* 2007). In a separate study, Pemberton *et al.* showed that M2 and M5 receptor activation stimulates T-type currents and that this is correlated

with increases in intracellular cAMP levels (Pemberton *et al.* 2000). In contrast, M1 activation had no effect on T-type channel activity despite elevation of cAMP levels, suggesting that T-type channel regulation depends on cross-talk between various intracellular pathways and resting phosphorylation levels in a given cell type (Pemberton *et al.* 2000). Because regulation of VGCCs in neurons is also dependent on the activity of other voltage-dependent conductances, it is difficult to draw parallels between expression systems and native preparations. Therefore, in this Chapter, we will also test the effects of muscarinic activation on LTS propagation.

Unlike muscarinic receptors, there is consensus regarding the potentiating effects of mGluR activation on T-type channel activity. $mGluR_1$ potentiation of $Ca_v3.1$ currents in cerebellar Purkinje cells occurs through a G protein- and tyrosine-phosphatase-dependent pathway (Hildebrand *et al.* 2009). Combined $mGluR_1$ activation and depolarization also increases inactivation of A-type K^+ channels in Purkinje cell dendrites and enables initiation of Ca^{2+} spikes at distal sites (Otsu *et al.* 2014). We will determine whether activation of mGluRs in CA3 PCs promotes LTS propagation through direct effects on channel gating or via inactivation of repolarizing conductances.

5.2 Results

5.2.1 M-current blockade increases LTS amplitude in CA3 PCs

We tested the effects of M-current blockade on LTS threshold and amplitude in CA3 PCs. M-currents are mediated by the K_v7 (KCNQ) family of voltage-gated potassium channels (Shah *et al.* 2013) and are defined as muscarinic-sensitive non-inactivating potassium currents that are open at rest and have an increased likelihood for activation when neurons are depolarized toward the threshold for action potential firing (Delmas and Brown 2005). Sustained activation of M-currents leads to hyperpolarization of membrane potential back to rest, thereby reducing neuronal excitability. The current is suppressed by muscarinic receptor activation resulting in increased neuronal excitability upon cholinergic input (Delmas and Brown 2005).

To test the effects of M-current suppression on LTS properties, we used linopirdine (15 μM), a specific blocker of K_v7 channels (Lamas *et al.* 1997). We elicited LTS in CA3 PCs by somatic current injection in 10 pA increments under control conditions and then added linopirdine to the perfusate (**Fig. 5-1a**). Linopirdine increased LTS amplitude but had no impact on the threshold for activation. To ascertain that LTS amplitude increased due to reduced potassium channel conductance after linopridine application and not activation of a secondary conductance, we added Z944 in the aCSF. Application of Z944 resulted in a linear voltage response to somatic current injection and absence of any LTS (**Fig. 5-1a**). Linopirdine significantly increased LTS amplitude from 53.13 ± 2.69 mV to 72.57 ± 4.01 mV (n=4; paired *t*-test; $p = 0.0218$) but did not change the activation threshold significantly (control – 57.5 ± 12.5 pA; linopirdine – 65.0 ± 11.9 n=4; paired *t*-test; $p = 0.2152$; **Fig. 5-1b**). The lack of any subthreshold depolarization after Z944

application shows that the effect of linopirdine on LTS amplitude was the direct consequence of a reduction in resting potassium channel conductance that led to a longer length constant, and not due to opening of a secondary conductance.

5.2.2 BK channel blockade does not affect LTS properties in CA3 PCs

Large conductance Ca^{2+}- and voltage-activated potassium (BK) channels are activated in response to Ca^{2+} influx during action potential firing (Bentzen *et al.* 2014). They contribute to spike repolarization by returning the membrane potential back to rest and limiting further Ca^{2+} entry. To determine whether LTS afterhyperpolarization is mediated by BK channels, we first tested the effects of BK inhibition by using the scorpion venom toxin, iberiotoxin that blocks most BK channels (Bentzen *et al.* 2014). Using somatic current injection, we evoked LTS in patch-clamped CA3 PCs under baseline conditions and then added iberiotoxin (100 nM) to the bath solution (top, **Fig. 5-2a**). Adding iberiotoxin had no effect on LTS afterhyperpolarization, amplitude (control – 50.06 ± 6.32 mV; iberiotoxin – 53.38 ± 6.97 mV; n=4; paired *t*-test; p = 0.3300), or threshold (control – 62.5 ± 10.3 pA; iberiotoxin – 60.0 ± 11.0 pA; n=4; paired *t*-test; p = 0.3910; bottom, **Fig. 5-2a**).

Although most BK channels are sensitive to iberiotoxin, a few subtypes display toxin resistance that is mediated by the accessory β subunit family. Specifically, β4-containing BK channels have a negatively shifted voltage activation range, slower activation kinetics, and iberiotoxin-resistivity (Wang *et al.* 2014). To test the modulatory influence of β4-containing BK conductance on LTS properties, we used paxilline, a potent blocker of β4-containing BK channels (Sanchez and McManus 1996). Top panel of **Fig. 5-2b** shows representative voltage

responses of a CA3 PC to somatic current injection before and after addition of paxilline (10 μM) to the perfusate. Treating slices with paxilline had no effect on LTS afterhyperpolarization, amplitude (control – 56.41 ± 1.19 mV; paxilline – 50.80 ± 2.54 mV; n=4; paired *t*-test; p = 0.0545), or threshold (control – 60.0 ± 8.2 pA; paxilline – 60.1 ± 6.9 pA; n=4; paired *t*-test; p > 0.9999; bottom, **Fig. 5-2b**).

5.2.3 Suppression of SK conductance does not affect LTS properties in CA3 PCs

Small conductance Ca^{2+}-activated potassium (SK) channels have a small single channel conductance in the order of 10 pS (Adelman *et al.* 2012). Similar to BK channels, SK channels regulate action potential firing frequency by controlling spike afterhyperpolarization in neurons (Adelman *et al.* 2012). To test the modulatory capacity of SK conductance on T-type channel function, we recorded LTS from CA3 PCs in current clamp mode via somatic current injection before and after application of 100 nM apamin, a potent and highly selective inhibitor of SK channels (van der Staay *et al.* 1999), onto slices. Representative voltage responses of a patched CA3 PC to current injection before and after apamin treatment are shown in the top panel of **Fig. 5-3a**. Apamin did not affect LTS threshold (control – 50.1 ± 9.0 pA; apamin – 54.3 ± 8.9 pA; n=5; paired *t*-test; p = 0.1778), or amplitude (control – 57.84 ± 3.38 mV; apamin – 56.60 ± 3.45 mV; n=5; paired *t*-test; p = 0.4483; bottom, **Fig. 5-3b**).

5.2.4 Properties of LTS remain unchanged after GIRK channel inhibition

G protein-coupled inwardly-rectifying potassium channels (GIRKs) are a family of inward-rectifier potassium channels that open via a signal-transduction mechanism that is initiated with ligand-stimulated GPCR activation (Luscher and Slesinger 2010). In dendrites and spines of

CA3 PCs, GIRKs are found in tight association with $GABA_B$ receptors allowing them to regulate the time course of voltage responses mediated by glutamate receptors (Makara and Magee 2013). To interrogate the regulation of T-type conductance by GIRK channels, we used the GIRK channel inhibitor, tertiapin-Q (0.5 μM) (Jin and Lu 1999). Examples of LTS evoked by somatic current injection in CA3 PCs before and after tertiapin-Q application are shown in **Fig. 5-4a**. Perfusion of tertiapin-Q onto slices did not affect LTS threshold (control – 33.75 ± 5.54 pA; tertiapin-Q – 38.75 ± 3.15 pA; n=4; paired *t*-test; $p = 0.1817$), or amplitude (control – 58.86 ± 1.41 mV; tertiapin-Q – 58.13 ± 1.44 mV; n=4; paired *t*-test; $p = 0.2826$; **Fig. 5-4b**).

5.2.5 Cholinergic stimulation potentiates LTS in CA3 PCs

Modulation of specific subtypes of T-type Ca^{2+} channels by GPCRs has been shown in HEK cells (Hildebrand *et al.* 2007) and various brain areas including Purkinje cells in the cerebellum (Hildebrand *et al.* 2009) and inhibitory neurons in the thalamus (Pigeat *et al.* 2015). In Chapter 4, we showed that T-type Ca^{2+} channels are expressed in the dendrites of CA3 PCs and in order to study their functional interactions with muscarinic receptors, we tested the effects of muscarinic activation on LTS amplitude and threshold. We elicited LTS in CA3 PCs by somatic current injection and then used 40 μM carbachol to activate muscarinic receptors (top panel, **Fig. 5-5a**). We found that carbachol enhanced LTS amplitude but did not affect the threshold for LTS activation. We then applied Z944 to determine the contribution of T-type conductance to the potentiated LTS. We reasoned that if carbachol was activating Ca^{2+} conductance of non-T-type origin (e.g. R-type), then a component of the spike should remain after Z944 application. Instead, we found that Z944 abolished LTS completely and the small subthreshold depolarization that remained was likely due to a time-dependent incomplete block of T-type channels (bottom panel,

Fig 5-5a). Averaged data pooled across slices showed that carbachol significantly increased LTS amplitude from 42.71 ± 4.64 mV to 55.11 ± 7.53 mV (n=4; paired *t*-test; $p = 0.0228$; **Fig. 5-5b**) and perfusing 1 μM atropine – a competitive antagonist for mAChRs, onto slices before and during carbachol application prevented the potentiation observed with carbachol (atropine – 45.92 ± 6.90 mV; carbachol – 49.8 ± 6.5 mV; n=4; paired *t*-test; $p = 0.2917$; **Fig. 5-5b**). Carbachol did not affect LTS threshold under control conditions (control – 47.5 ± 7.5 pA; carbachol – 50.0 ± 7.1 pA; n=4; paired *t*-test; $p = 0.3910$; **Fig. 5-5c**) or atropine-treated conditions (atropine – 51.3 ± 7.2 pA; carbachol – 48.3 ± 8.6 pA; n=4; paired *t*-test; $p = 0.2223$; **Fig. 5-5c**).

5.2.6 M-current inhibition underlies muscarinic enhancement of LTS amplitude

To elucidate the mechanism underlying muscarinic-mediated LTS amplitude potentiation, we first tested the role of M-channels based on the data presented in section **5.2.1**. A direct and immediate consequence of muscarinic activation is blockade of M-channels (Delmas and Brown 2005), and given the LTS potentiation after M-current inhibition reported earlier, we perfused 15 μM linopirdine onto slices before testing the effects of carbachol on LTS amplitude and threshold. As expected, linopirdine enhanced LTS amplitude; however, sequential perfusion of carbachol in the presence of linopirdine failed to have an additive effect on LTS amplitude beyond what had already occurred after linopirdine application (**Fig. 5-6a**). Linopirdine increased LTS amplitude under control conditions from 52.13 ± 3.69 mV to 75.57 ± 6.01 mV (n=4; repeated measures one-way ANOVA with Tukey's post-hoc; $p = 0.0315$; **Fig. 5-6b**) and although LTS amplitude remained at this enhanced level (73.28 ± 6.11 mV) after carbachol application (n=4; repeated measures one-way ANOVA with Tukey's post-hoc; $p = 0.0309$; **Fig.**

5-6b), there was no significant change in LTS amplitude between cells that were sequentially treated with linopirdine and carbachol (n=4; repeated measures one-way ANOVA with Tukey's post-hoc; $p = 0.6758$; **Fig. 5-6b**). Carbachol application did not affect LTS threshold when compared to control conditions (control – 53.3 ± 12.0 pA; carbachol – 56.12 ± 12.20 pA; n=4; repeated measures one-way ANOVA; $p = 0.2192$; **Fig. 5-6b**) or linopirdine-treated conditions (linopirdine – 55.8 ± 8.6 pA; n=4; repeated measures one-way ANOVA; $p = 0.2192$; **Fig. 5-6b**). Further, there was no difference in LTS threshold between linopirdine and carbachol treatments (n=4; repeated measures one-way ANOVA; $p = 0.2192$; **Fig. 5-6b**).

5.2.7 $mGluR_1$ activation inhibits LTS in CA3 PCs

Enhancement of T-type Ca^{2+} currents in response to mGluR activation has been shown in primary dendrites of mitral cells (Johnston and Delaney 2010) and spines of Purkinje cells in the cerebellum (Otsu *et al.* 2014). Given this precedence, we tested the effects of mGluR activation on LTS properties in CA3 PCs. Addition of 50 μM *t*-ACPD, a selective agonist for mGluRs that is active at both group I and group II mGluRs (Knopfel *et al.* 1995), completely abolished LTS in CA3 PCs (**Fig. 5-7a**). To determine the specific mGluR subtype(s) mediating this inhibition, we first investigated the contribution of group I mGluRs. The group I receptors include $mGluR_1$ and $mGluR_5$. Group I mGluRs are G_q coupled receptors and are primarily found in the postsynaptic density (Pin and Duvoisin 1995). Perfusion of 50 μM (*S*)-3,5-DHPG, a $mGluR_1$ specific agonist (Schoepp *et al.* 1994), resulted in a phenotype that was identical to *t*-ACPD – a linear voltage response to somatic current injection that previously elicited LTS with activation threshold of 20-40 pA (**Fig. 5-7b**). In contrast, application of 100 μM (*RS*)-CHPG, a selective $mGluR_5$ agonist (Doherty *et al.* 1997), had no effect on LTS properties (**Fig. 5-7c**).

5.2.8 LTS in CA3 PCs are not modulated by group II or III mGluRs

We also tested the effects of group II and group III mGluR activation on LTS properties in CA3 PCs. Both group II and group III families of mGluRs are G_i/G_o-coupled and are found primarily in presynaptic terminals (Pin and Duvoisin 1995). Although the data presented in Chapter 4 shows that T-type Ca^{2+} channels are expressed on the dendrites of CA3 PCs, we tested the effects of group II and III mGluR activation on LTS because their expression is not well studied in CA3 region of the hippocampus. Activation of group II mGluRs with 10 μM (2*R*,4*R*)-APDC, a highly selective and potent group II mGluR agonist (Schoepp *et al.* 1999), had no effect on LTS properties (**Fig. 5-8a**). We found similar results after adding 10 μM L-AP4, a selective group III mGluR agonist (Bushell *et al.* 1995) (**Fig. 5-8b**).

Pooling data across cells showed that adding *t*-ACPD and DHPG to current clamped cells with a respective LTS threshold of 46.0 ± 3.1 pA and 50.0 ± 7.1 pA resulted in a linear voltage response to somatic current injection, such that no amount of current injection could elicit a LTS (**Fig. 5-8c**). LTS threshold remained unchanged after adding CHPG to the bath solution (control – 66.0 ± 3.1 pA; CHPG – 67.0 ± 3.1 pA; n=4; paired *t*-test; $p > 0.9999$; **Fig. 5-8c**). Respective activation of group II and group III mGluRs with (2*R*,4*R*)-APDC (control – 55.0 ± 9.3 pA; (2*R*,4*R*)-APDC – 62.5 ± 11.1 pA; n=4; paired *t*-test; $p = 0.2152$; **Fig. 5-8c**) and L-AP4 (control – 55.0 ± 3.2 pA; L-AP4 – 57.5 ± 4.8 pA; n=4; paired *t*-test; $p = 0.3910$; **Fig. 5-8c**) also failed to elicit a change in LTS threshold. CHPG, (2*R*,4*R*)-APDC, and L-AP4 did not cause a significant change in LTS amplitude (data not shown).

5.2.9 $mGluR_1$-mediated inhibition of LTS in CA3 PCs is PLC- and PKC-dependent

To further ascertain the role of $mGluR_1$ in suppressing T-type function, we current clamped slices incubated with 10 μM LY456236, a selective $mGluR_1$ antagonist (Shannon *et al.* 2005), and found that adding 50 μM *t*-ACPD to the bath solution did not inhibit LTS (**Fig. 5-9a**). The lack of effect by activation of a broad family of mGluRs with *t*-ACPD in the presence of a selective antagonist of $mGluR_1$ shows that inhibition of LTS by metabotropic glutamate receptors is mediated specifically by $mGluR_1$. To investigate the underlying transduction mechanisms leading to LTS inhibition by $mGluR_1$, we first considered phosphoinositide phospholipase C (PLC) as a potential candidate. $mGluR_1$ are coupled to G_q proteins (Pin and Duvoisin 1995) that activate PLC – a phosphodiesterase that participates in lipid metabolism and signaling (Cattaneo *et al.* 2014). We incubated slices with 1 μM U73122, an inhibitor of PLC (Bleasdale *et al.* 1990), and then current clamped CA3 PCs from these slices. Addition of DHPG to U72133-treated slices failed to have an effect as LTS properties remained unchanged after blockade of PLC (**Fig. 5-9b**).

The catalytic mechanism performed by PLC results in the generation of diacylglycerol (DAG) and inositol triphosphate (IP_3) from hydrolysis of phosphatidylinositol (PIP_2) (Cattaneo *et al.* 2014). A common target of DAG is the protein kinase C family of protein kinase enzymes that in turn phosphorylate ion channels to regulate their function (Sun and Alkon 2014). We incubated slices in 5 μM chelerythrine chloride, a broad spectrum PKC inhibitor (Herbert *et al.* 1990) and then recorded LTS from these slices. As with PLC inhibition, we found that application of DHPG onto chelerythrine chloride-treated slices failed to have an effect on LTS properties (**Fig. 5-8c**).

5.2.10 $mGluR_1$-mediated inhibition of LTS in CA3 PCs is Ca^{2+}-independent

In order to determine whether inhibition of T-type channels by $mGluR_1$ was dependent on elevation in intracellular Ca^{2+} concentration $[Ca^{2+}]_i$, we replaced EGTA in the patch pipette solution with a cell-impermeant cesium based derivative of BAPTA – a Ca^{2+} chelator with fast kinetics. Adding DHPG onto cells that were patched with a BAPTA-based internal solution did not completely block LTS, but did increase the threshold for LTS activation by nearly 50% (**Fig. 5-10a**). Because $mGluR_1$ activation can also increase resting potassium conductance (Chu and Hablitz 2000), which would have a shunting effect of LTS, we reasoned that the increase in LTS threshold observed with a cesium-based BAPTA internal solution could be due to replacement of cesium with potassium. In order to differentiate between the effects of chelating Ca^{2+} with BAPTA and blocking a subset of potassium channels with cesium, we used a potassium-based derivative of BAPTA in our internal solution. DHPG application on cells patched with the potassium-BAPTA solution resulted in a phenotype that was similar to the cesium-BAPTA condition – an increase in LTS threshold by approximately 50% (**Fig. 5-10b**).

Pooled data showed that there was no difference in LTS threshold for cells that were incubated with $mGluR_1$ selective antagonist LY456236 (70.0 ± 9.1 pA) and then treated with *t*-ACPD (65.8 ± 17.1 pA; n=4; paired *t*-test; $p = 0.7027$; **Fig. 5-10c)** or DHPG (LY456236 – 65.23 ± 6.0 pA; DHPG – 62.5 ± 12.6 pA; n=4; paired *t*-test; $p = 0.8205$; **Fig. 5-10c**). Respective inhibition of PLC and PKC with U73122 (70.0 ± 15.4 pA; DHPG – 74.0 ± 9.3 pA; n=4; paired *t*-test; $p = 0.6483$; **Fig. 5-10c**) and chelerythrine chloride (61.25 ± 9.66 pA; 66.25 ± 7.47 pA; n=4; paired *t*-test; $p = 0.1817$; **Fig. 5-10c**) also prevented the inhibitory effects of DHPG on LTS in CA3 PCs. In contrast, application of DHPG on CA3 PCs patched with an internal solution containing

cesium-BAPTA increased LTS threshold significantly (BAPTA – 55.0 ± 13.4 pA; DHPG – 115.0 ± 10.6 pA; n=4; paired *t*-test; $p = 0.0007$; **Fig. 5-10c**) and this was also the case for cells that were patched with a potassium-BAPTA based internal solution (65.7 ± 12.58 pA; DHPG – 117.0 ± 6.57 pA; n=4; paired *t*-test; $p = 0.0385$; **Fig. 5-10c**).

5.3 Discussion

In this Chapter, we explored the potential for T-type regulation by several types of K^+ channels and GPCRs. We found that LTS properties are significantly altered by inhibition of M-currents mediated by K_v7 channels, while SK, BK, and GIRK channels have no apparent effect on LTS propagation in CA3 PCs. M-current inhibition with linopirdine increased LTS amplitude without changing the threshold for activation or spike afterhyperpolarization. This shows that M-current inhibition directly increases dendritic excitability of CA3 PCs by increasing input resistance and length constant, which serves to increase T-type-mediated depolarization and voltage propagation. M-current inhibition also underlies muscarinic enhancement of LTS in CA3 PCs and this has functional consequences because cholinergic inputs from the medial septal area to CA3 PCs have an important role in synaptic transmission, plasticity and rhythmic network oscillations (Teles-Grilo Ruivo and Mellor 2013). We show that the enhancement of dendritic excitability by muscarinic activation leads to an increase in dendritic Ca^{2+} concentrations and this could facilitate LTP induction in CA3PCs. In CA1 PCs, muscarinic activation enhances NMDA receptor opening by M-current inhibition during LTP induction (Petrovic *et al.* 2012) and it also promotes action potential generation and backpropagation into dendrites (Tsubokawa and Ross

1997). Similar mechanisms in CA3 PCs would greatly enhance dendritic Ca^{2+} levels by activating T-type Ca^{2+} channels and promoting LTS propagation.

Although we failed to observe a direct effect of BK, SK, or GIRK channels on LTS, we did not investigate the effects of T-type channel opening on these conductances, thus we cannot exclude the possibility that T-type channels can modulate dendritic excitability by altering the activity of voltage/Ca^{2+}-activated K^+ channels. For example, modeling data indicates that T-type channels in close proximity are capable of elevating intracellular Ca^{2+} levels to a degree that is sufficient to activate BK channels and the combined effect of T-type channel inhibition in this case results in an increased rate of repolarization/firing and reduced spike afterhyperpolarization (Rehak *et al.* 2013). Similarly, because K_v4 family of channels is expressed in a complex with K^+ channel interacting proteins (KChIPs) and KChIPs contain Ca^{2+}-binding domains, K_v4 channels can also be modulated by T-type Ca^{2+} channels (Anderson *et al.* 2010). Ca^{2+} influx through T-type channels induces a depolarizing shift in the voltage dependence of K_v4 channels inactivation and results in increased cerebellar stellate cell excitability during periods of repetitive stimulation (Anderson *et al.* 2013). This association between T-type and K_v4 channel activity is important for the rapid increase in firing rate gain of cerebellar stellate cells in response to physiologically relevant stimuli (Anderson *et al.* 2013). Therefore, the lack of an effect on LTS by BK, SK, or GIRK channels does not necessarily mean that T-type channels cannot modify K^+ channel activity and CA3 PC excitability indirectly.

A surprising finding from this Chapter is the inhibition of LTS by mGlu1 receptors in CA3 PCs. This result was unexpected because most studies report a potentiation of T-type activity by

mGluRs (Hildebrand *et al.* 2009, Johnston and Delaney 2010, Otsu *et al.* 2014). Anatomical distribution of mGluRs in the hippocampus shows that $mGluR_1$ is highly expressed in postsynaptic regions of CA3 PCs, while a dense distribution of $mGluR_5$ is found in dendritic processes of the dentate gyrus molecular layer (Cosgrove *et al.* 2011). In contrast with group I mGluRs, group II and III mGluRs are expressed primarily presynaptically in mossy fiber boutons (Cosgrove *et al.* 2011). Consistent with this anatomical data, we found that $mGluR_1$ activation was sufficient for LTS inhibition and activation of $mGluR_5$ or group II/III mGluRs had no effect on LTS initiation or propagation.

We found that LTS inhibition by $mGluR_1$ was dependent on PLC and PKC, but independent of an elevation in intracellular Ca^{2+} levels, implicating the role of a Ca^{2+}-independent PKC isoform. Inclusion of BAPTA in the patch pipette failed to rescue $mGuR_1$-mediated inhibition and by using a cesium-based internal we also showed that LTS inhibition is not due to activation of a K^+ conductance by $mGlu_1$ receptors. In fact, stimulation of $mGluR_1$ inhibits a Ca^{2+}-activated K^+ conductance that mediates spike afterhyperpolarization in CA3 PCs (Young *et al.* 2004). $mGluR_1$ activation blocks spike afterhyperpolarization through a G-protein-dependent mechanism (Guerineau *et al.* 1994); thus, although $mGlu_1$ receptors increase CA3 PC excitability, their activation of downstream kinases inhibits T-type channel activity. Inhibition of T-type channel activity by PKC has been reported previously. Rangel *et al.* showed that $Ca_v3.2$ channels are inhibited by neurokinin 1 receptors through a voltage-independent pathway that includes $G\alpha_{q/11}$ and PKC (Rangel *et al.* 2010). Similarly, in dorsal root ganglion cells, M3 muscarinic receptors block T-type channels through a chelerhythrine-sensitive PKC and G-protein-dependent pathway (Zhang *et al.* 2011). Actions of kinases on T-type channel activity have been localized to a series

of serine and threonine residues in a highly conserved domain II-III linker region – modulation of these residues is especially strong in $Ca_v3.2$ channels (Wolfe *et al.* 2002, Zhang *et al.* 2013). Phosphorylation of residues in the II-III linker region can inhibit channel activity likely via altering the control of channel gating (Welsby *et al.* 2003).

In conclusion, we have shown that $mGluR_1$ activation potently and rapidly inhibits LTS in CA3 PCs. Transient activation of these receptors by glutamate is predicted to dramatically reduce membrane excitability and dendritic Ca^{2+} concentrations. Long-term pre-synaptic plasticity changes at the mossy fiber-CA3 interneuron synapse involve inhibition of P/Q Ca^{2+} channels by group II mGluRs ($mGluR_7$) in mossy fiber boutons (Pelkey *et al.* 2006). Postsynaptic $mGlu_1$ receptors also regulate synaptic communication and determine the output of CA3 PCs by altering intrinsic cell excitability and tuning the timing of inputs – LTP of interneurons in stratum lacunosum-moleculare by $mGluR_1$ is well documented (Galvan *et al.* 2011). Our data provide an additional mechanism for $mGluR_1$-mediated long-term alteration in CA3 PC excitability that is independent of K^+ conductances.

Figure 5-1 LTS in CA3 PCs is potentiated by the M-current blocker linopirdine.

(**a**) Representative trace of an evoked LTS in a current-clamped CA3 PC held at –75 mV and depolarized by current injection of 10 pA increments. LTS amplitude is increased by addition of 15 μM linopirdine. LTS is sensitive to Z944 after potentiation by linopirdine. (**b**) Linopirdine increased mean LTS amplitude (n=5; paired *t*-test; $p = 0.0218$) but did not affect LTS threshold (n=4; paired *t*-test; $p = 0.2152$).

a

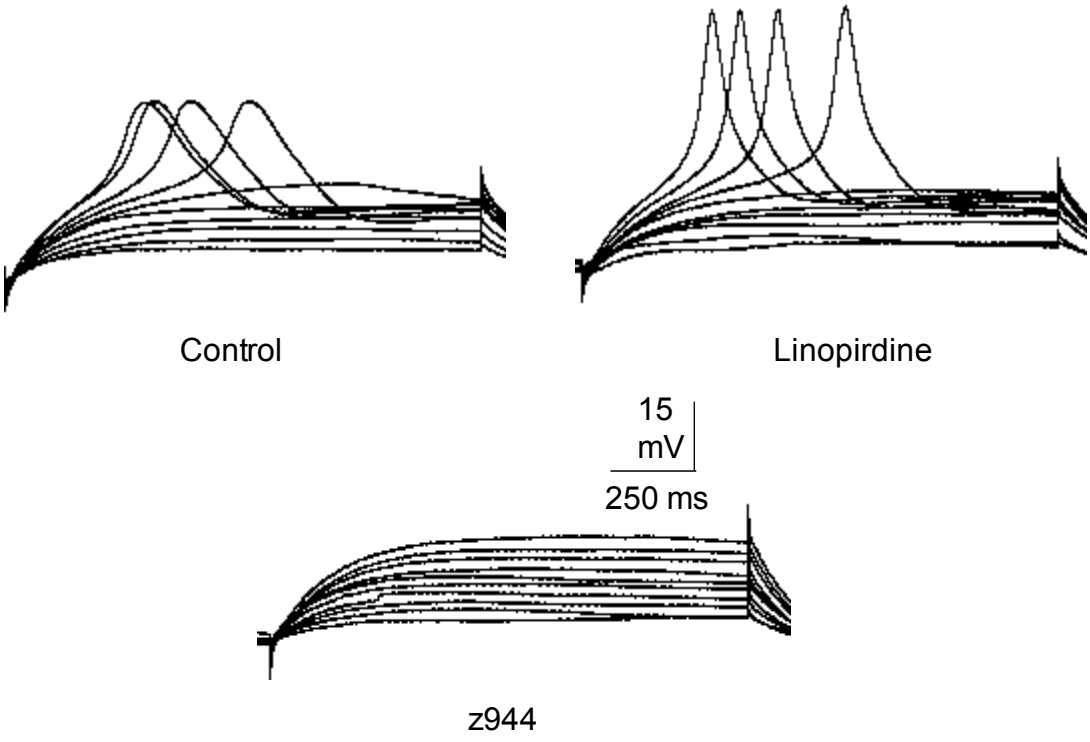
Control
Linopirdine
15
mV
250 ms
z944

b

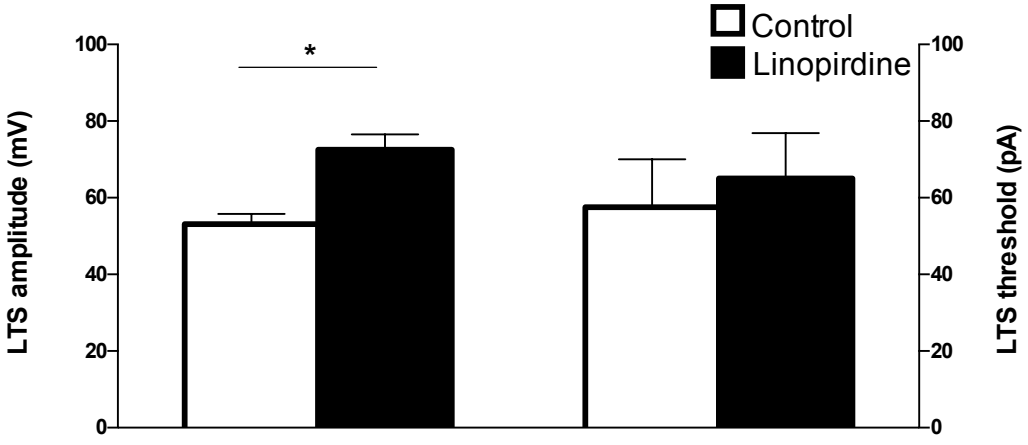
Control
Linopirdine
*
LTS amplitude (mV)
LTS threshold (pA)
100
80
60
40
20
0

Figure 5-2 BK channel blockade has no effect on LTS in CA3 PCs.

(**a**) Representative traces of evoked LTS in current-clamped CA3 PC held at –75 mV and depolarized by current injection of 10 pA increments before and after treatment with 10 μM paxilline. Addition of BK channel blocker paxilline did not impact LTS threshold (n=4; paired *t*-test; $p > 0.999$) or amplitude (n=4; paired *t*-test; $p = 0.0545$). (**b**) Representative traces of evoked LTS in current-clamped CA3 PC held at -75 mV and depolarized by somatic current injection of 10 pA increments before and after treatment with 100 nM iberiotoxin. Addition of iberiotoxin did not change LTS threshold (n=4; paired *t*-test; $p > 0.3910$) or amplitude (n=4; paired *t*-test; $p = 0.3300$).

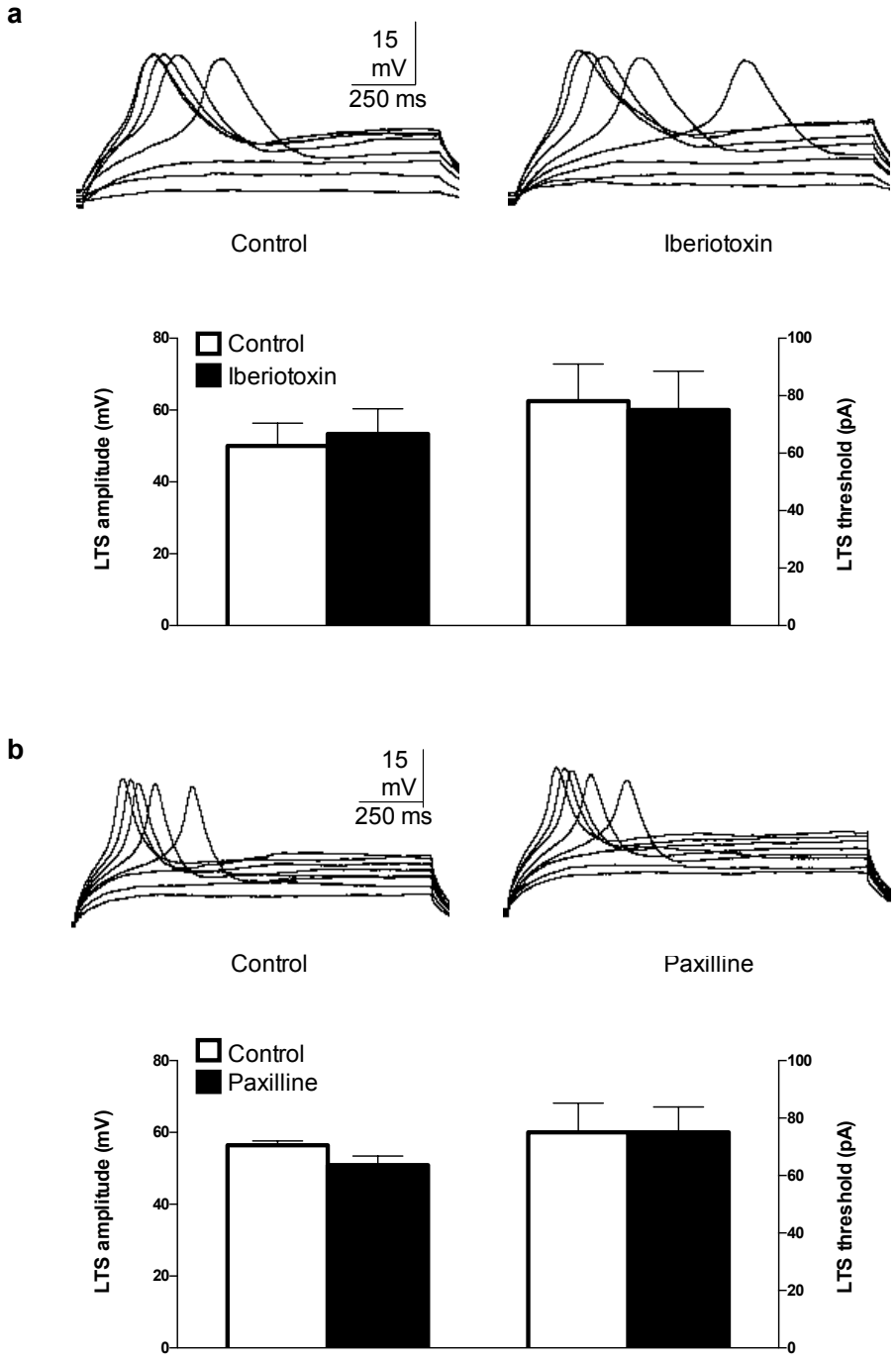
a
15
mV
250 ms
Control
Iberiotoxin
Control
Iberiotoxin
LTS amplitude (mV)
LTS threshold (pA)
0
20
40
60
80
0
20
40
60
80
100
b
15
mV
250 ms
Control
Paxilline
Control
Paxilline
LTS amplitude (mV)
LTS threshold (pA)
0
20
40
60
80
0
20
40
60
80
100

Figure 5-3 SK channel blockade has no effect on LTS in CA3 PCs.

(**a**) Representative trace of a LTS evoked in a current-clamped CA3 PC by somatic current injection before and after 100 nM apamin application. (**b**) Addition of SK channel blocker apamin did not impact LTS threshold (n=5; paired *t*-test; $p = 0.1778$) or amplitude (n=5; paired *t*-test; $p = 0.4483$).

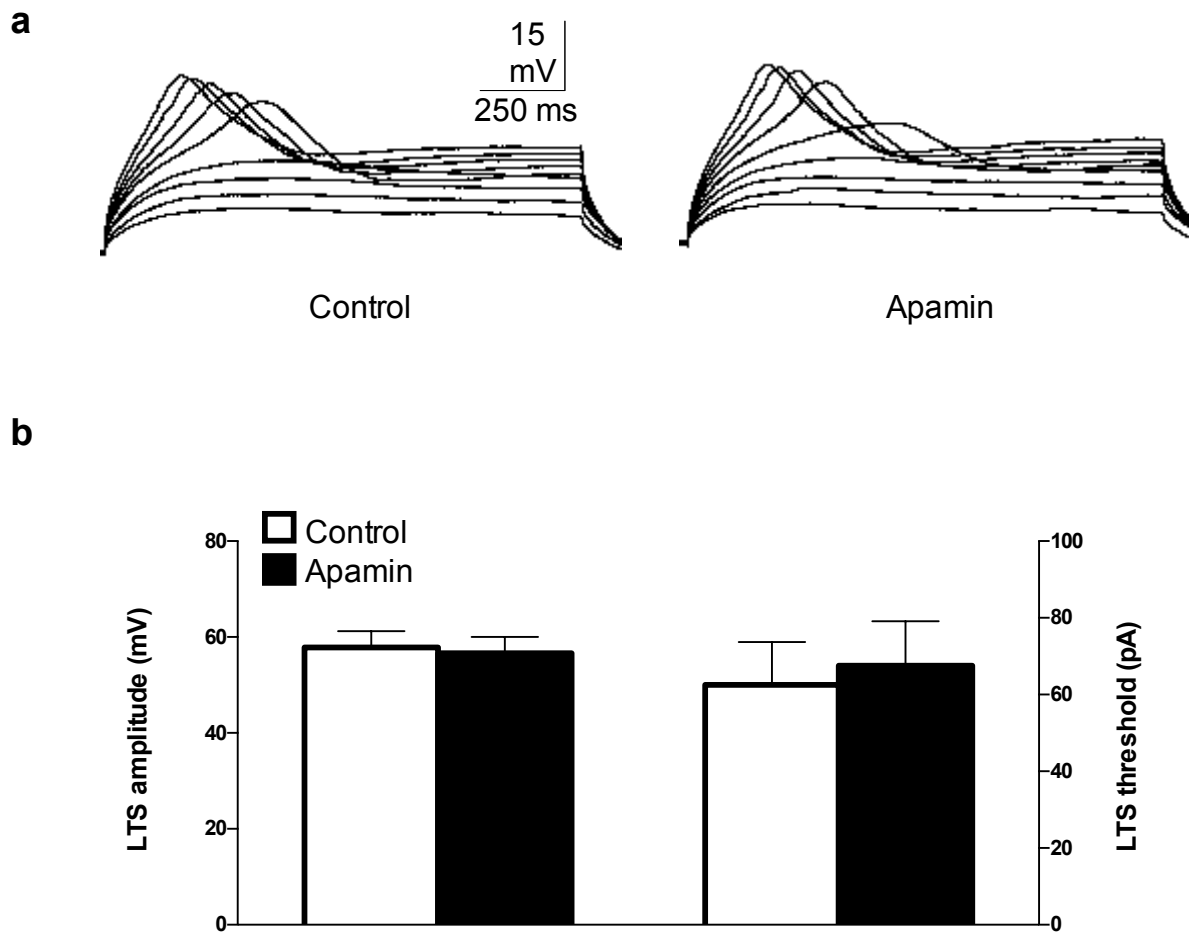

Figure 5-4 GIRK channel blockade has no effect on LTS in CA3 PCs.

(**a**) Representative traces of a LTS evoked in a current-clamped CA3 PC by somatic current injection before and after 0.5 μM tertiapin-Q application. (**b**) Addition of GIRK channel blocker tertiapin-Q did not impact LTS threshold (n=4; paired *t*-test; $p = 0.1817$) or amplitude (n=4; paired *t*-test; $p = 0.2826$).

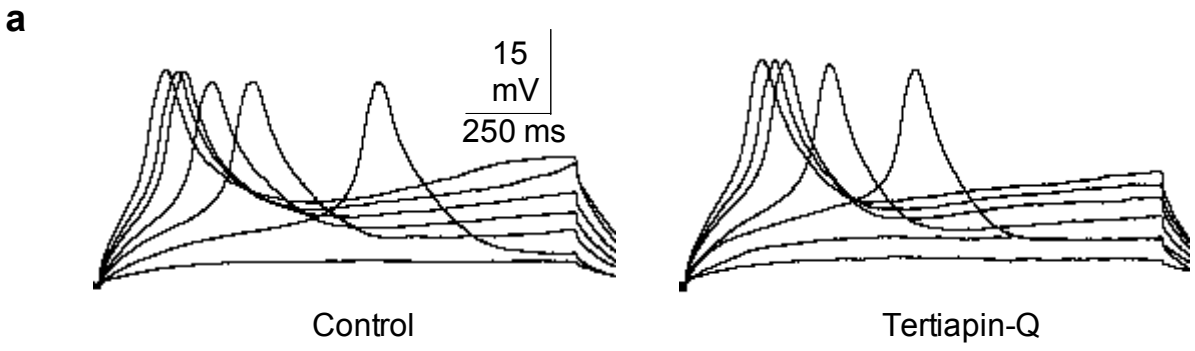

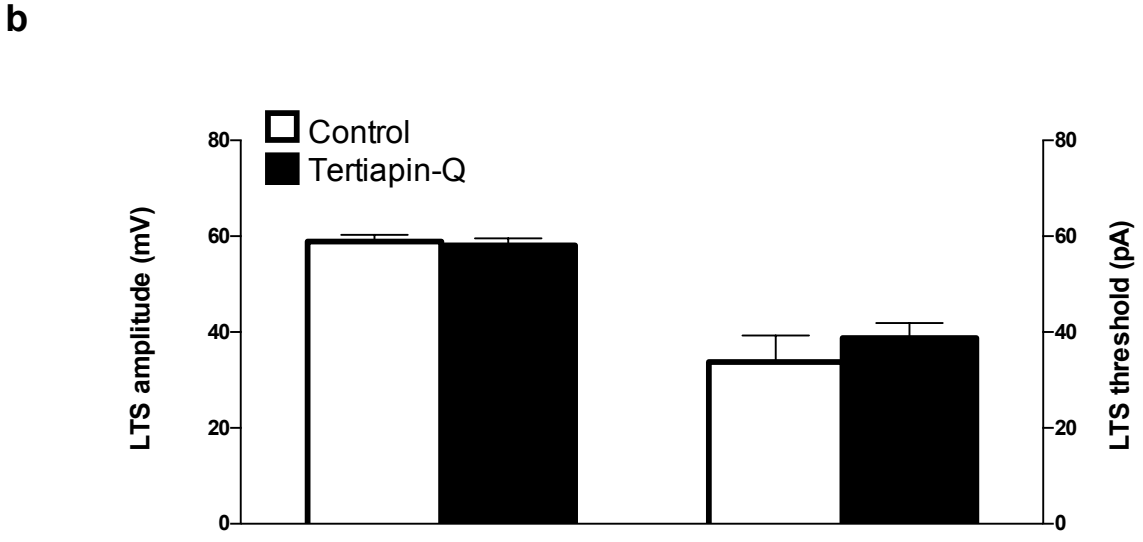

Figure 5-5 mAChR activation increases LTS amplitude in CA3 PCs.

(**a**) Representative trace of an evoked LTS in a current-clamped CA3 PC held at –75 mV and depolarized by current injection of 10 pA increments. LTS amplitude is increased by addition of 40 μM carbachol. LTS is sensitive to Z944 after potentiation by carbachol. (**b**) Addition of carbachol increased LTS amplitude (n=4, paired *t*-test; $p = 0.0228$); however, application of carbachol after treating slices with 2 μM atropine failed to elicit an effect (n=4; paired *t*-test; $p = 0.2917$). (**c**) Carbachol application did not affect LTS threshold under control conditions (n=4; paired *t*-test; $p = 0.3910$) or after incubating slices with atropine (n=4; paired *t*-test; $p = 0.2223$).

a

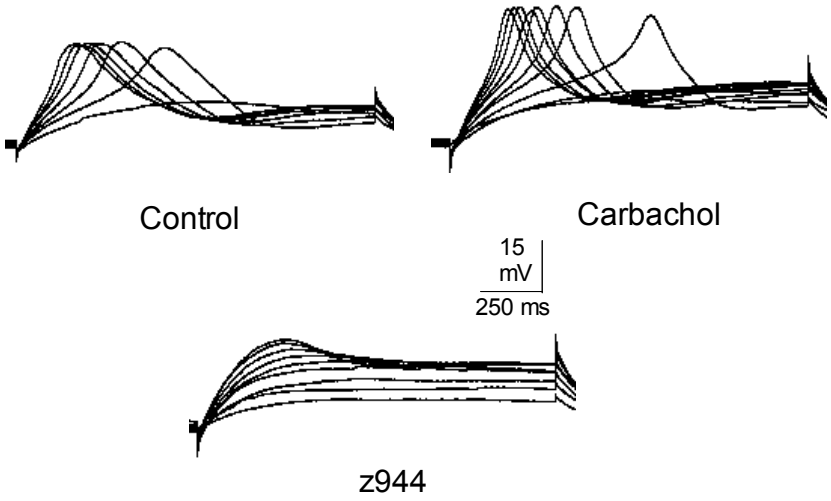
Control
Carbachol
15
mV
250 ms
z944

b

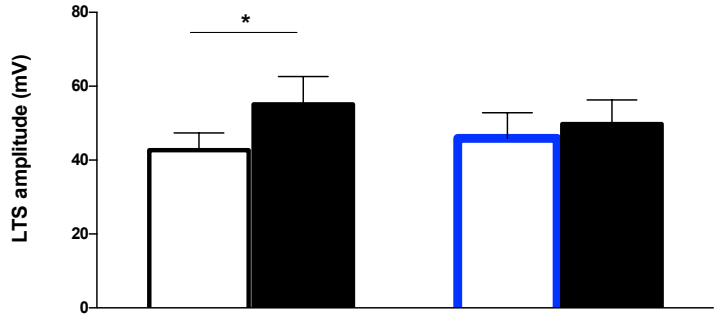
LTS amplitude (mV)
80
60
40
20
0
*

c

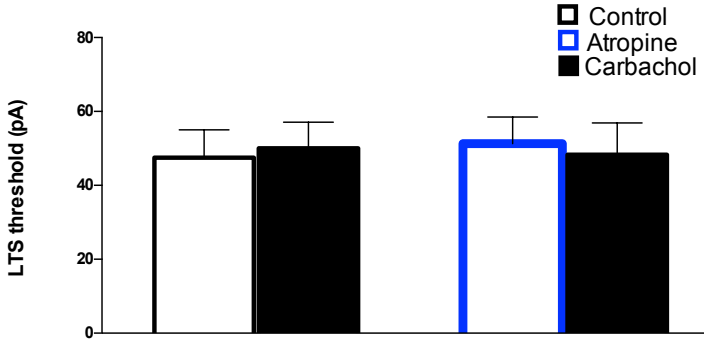
LTS threshold (pA)
80
60
40
20
0
Control
Atropine
Carbachol

Figure 5-6 Potentiation of LTS amplitude by carbachol is mediated via M-current blockade.

(**a**) Representative trace of an evoked LTS in a current-clamped CA3 PC held at –75 mV and depolarized by current injection of 10 pA increments. LTS amplitude is increased by addition of 15 μM linopirdine. LTS is not further potentiated by application of 40 μM carbachol. (**b**) Addition of linopridine increased LTS amplitude (n=4, repeated measures one-way ANOVA; p = 0.0315) and this was also the case when cells under control conditions were compared with carbachol-treated cells (n=4; repeated measures one-way ANOVA; p = 0.0309); however, adding carbachol to linopirdine-treated cells failed to elicit a further potentiation (n=4; repeated measures one-way ANOVA; p = 0.6758). Carbachol application did not affect LTS threshold under control conditions (n=4; repeated measures one-way ANOVA; p = 0.2192) or after adding linopirdine to the aCSF (n=4; repeated measures one-way ANOVA; p = 0.2192).

a

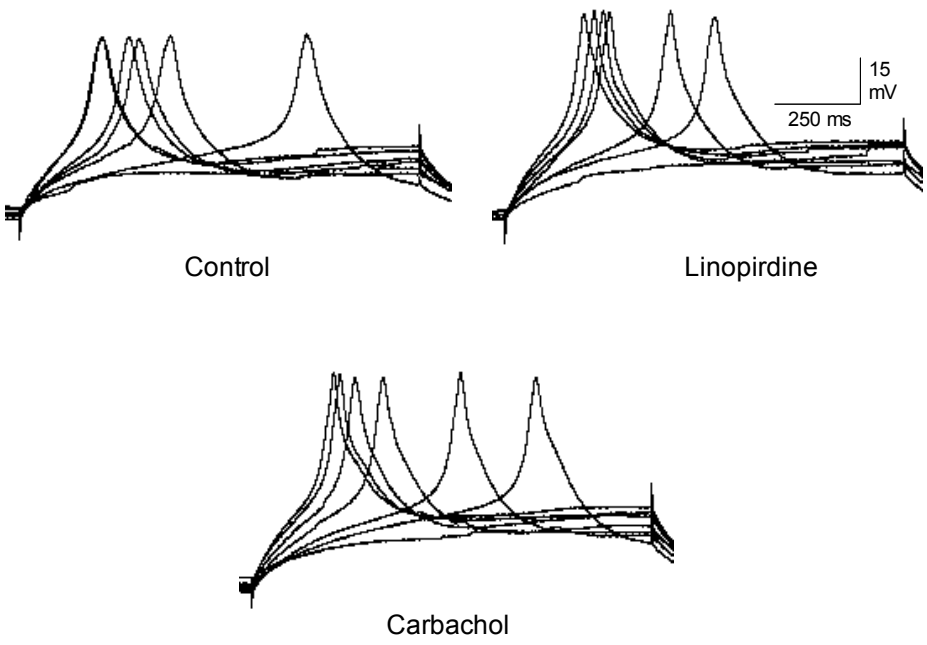
15
mV
250 ms
Control
Linopirdine
Carbachol

b

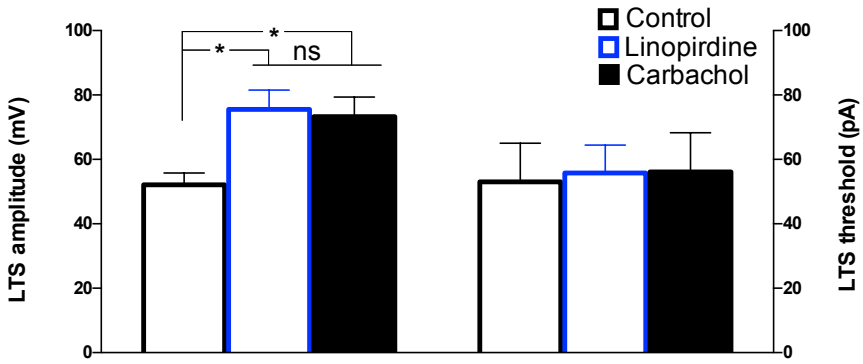
Control
Linopirdine
Carbachol
*
*
ns
LTS amplitude (mV)
LTS threshold (pA)
100
80
60
40
20
0

Figure 5-7 $mGluR_1$ activation leads to inhibition of LTS in CA3 PCs.

(a) Representative traces of a current-clamped CA3 PC held at –75 mV and depolarized by current injection of 10 pA increments before and after application of 50 μM *t*-ACPD. (**b**) Representative traces of a current-clamped CA3 PC held at –75 mV and depolarized by current injection of 10 pA increments under control conditions and after 50 μM DHPG ($mGluR_1$ agonist) application. (**c**) Representative traces of LTS elicited by current injection in a current-clamped CA3 PC before and after application of $mGluR_5$ agonist CHPG (100 μM).

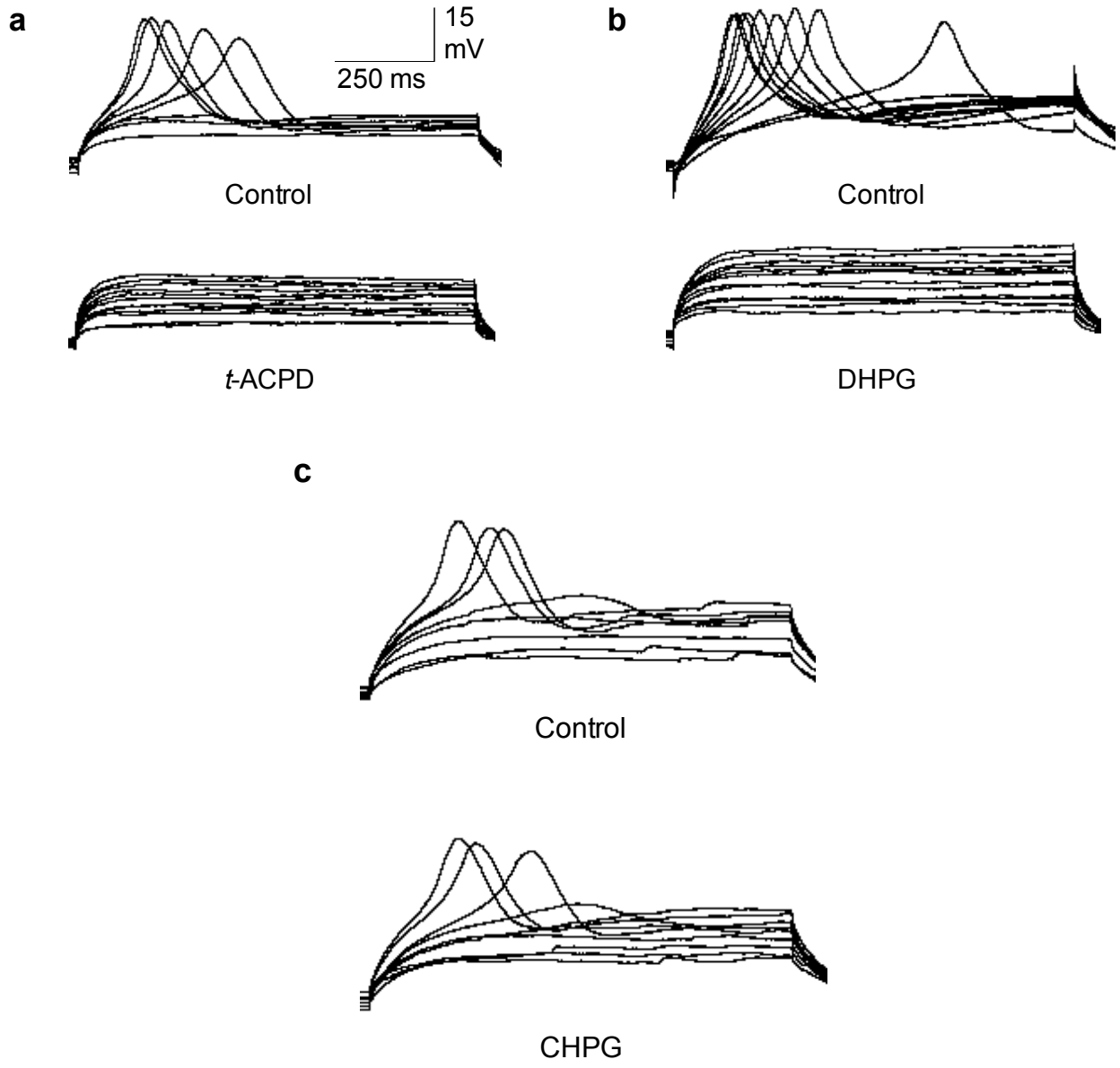
a
15
mV
250 ms
Control
t-ACPD
b
Control
DHPG
c
Control
CHPG

Figure 5-8 $mGluR_1$ activation is sufficient for inhibition of LTS in CA3 PCs.

(a) Representative traces of a current-clamped CA3 PC held at –75 mV and depolarized by current injection of 10 pA increments before and after addition of group II mGluR agonist (2R,4R)-APDC (10 μM). (**b**) Representative traces of a current-clamped CA3 PC depolarized to elicit LTS by somatic current injection of 10 pA increments under control conditions and after application of group III mGluR agonist L-AP4 (10 μM). (**c**) Pooled data showing that $mGluR_1$ activation with *t*-ACPD or DHPG abolishes LTS, while activation of mGluR5, group II mGluRs, and group III mGluRs with CHPG (n=4; paired *t*-test; $p > 0.9999$), (2R,4R)-APDC (n=4; paired *t*-test; $p = 0.2152$), and L-AP4 (n=4; paired *t*-test; $p = 0.3910$), respectively, has no effect on LTS threshold.

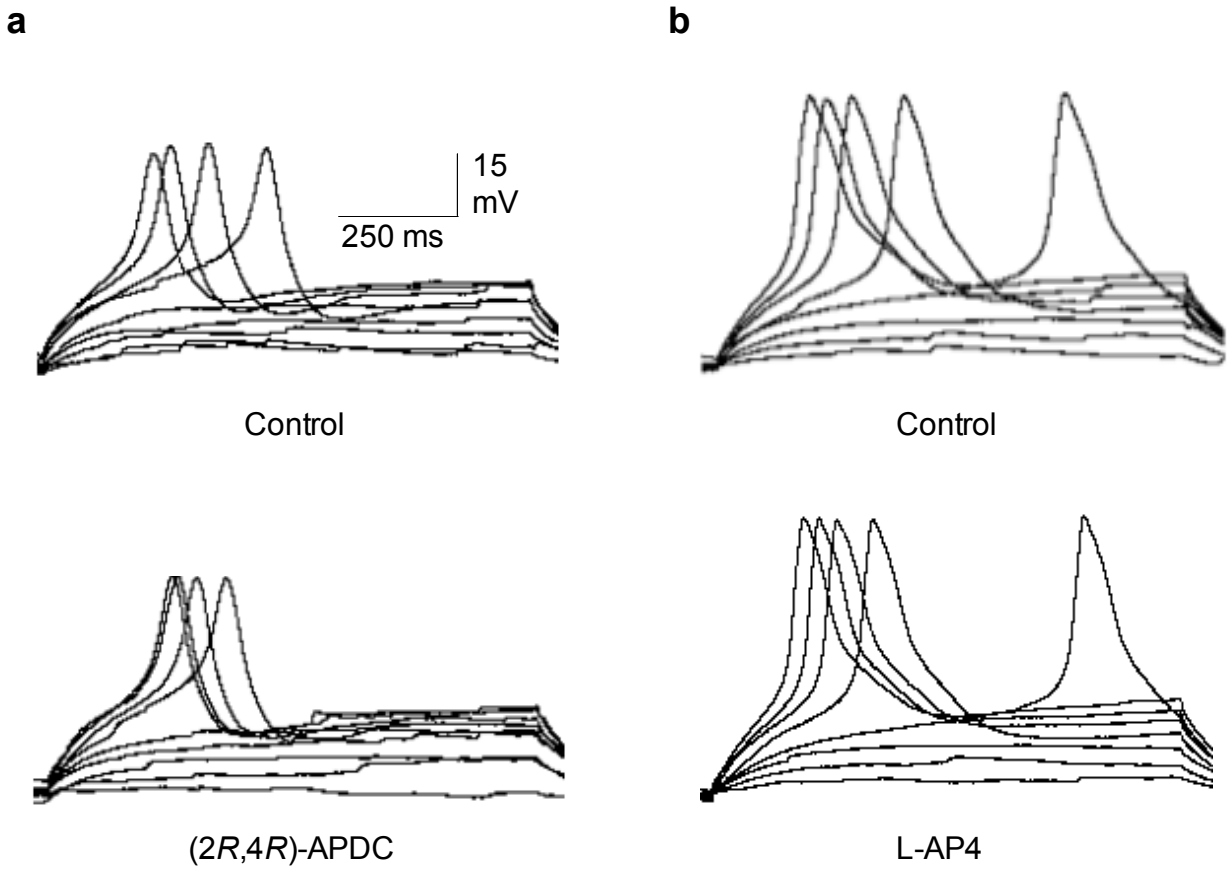
a
b
15
mV
250 ms
Control
Control
(2R,4R)-APDC
L-AP4
c
Control
Treatment
LTS threshold (pA)
80
60
40
20
0
t-ACPD
DHPG
CHPG
(2R,4R)-APDC
L-AP4

Figure 5-9 $mGluR_1$-mediated inhibition of LTS is dependent on PKC activity.

(**a**) Representative trace of a current-clamped CA3 PC that is depolarized by somatic current injection to elicit a LTS in aCSF treated with $mGluR_1$ antagonist LY456236 (10 μM). Application of broad spectrum mGluR agonist *t*-ACPD in the presence of LY456236 does not have an effect on LTS threshold or amplitude. (**b**) Representative trace of LTS elicited in a current-clamped CA3 PC from a hippocampal slice incubated in PLC inhibitor U73122. DHPG fails to inhibit LTS after PLC blockade. (**c**) Representative trace of evoked LTS from a current-clamped CA3PC in aCSF containing PKC inhibitor chelerythrine chloride (5 μM). Taken together, PKC inhibition occludes the effect of DHPG on CA3 PC LTS.

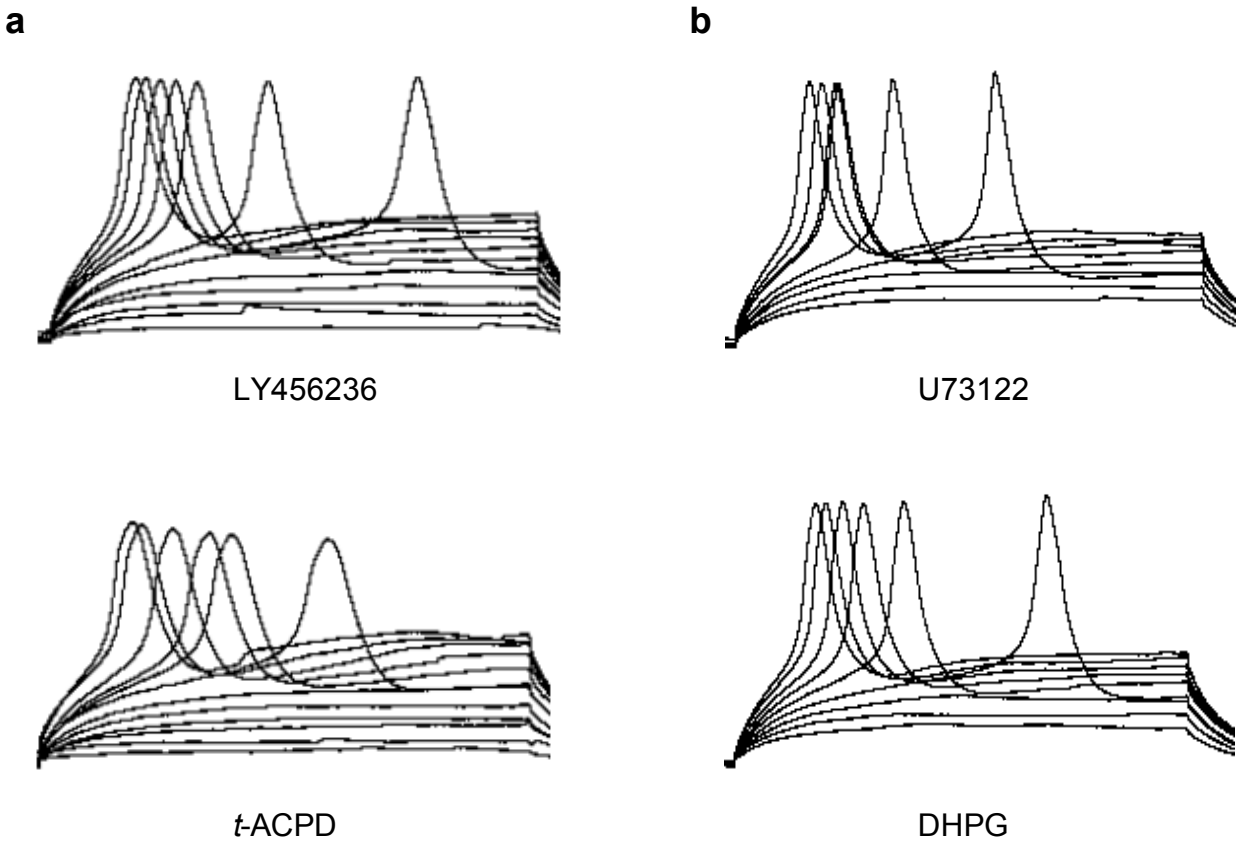
a
b
LY456236
U73122
t-ACPD
DHPG
c
15
mV
250 ms
Chelerythrine chloride
DHPG

Figure 5-10 $mGluR_1$-mediated inhibition of LTS is independent of intracellular Ca^{2+}.

(**a**) Representative trace of a current-clamped CA3PC that was patched with an internal solution containing Cs-BAPTA and depolarized by somatic current injection to elicit a LTS. Application of $mGluR_1$ agonist DHPG increased LTS spike threshold. (**b**) Representative trace of a current-clamped CA3 PC that was patched with an internal solution containing K-BAPTA and depolarized by somatic current injection to elicit a LTS. Application of $mGluR_1$ agonist DHPG increased LTS spike threshold. (**c**) Pooled data showing that blocking $mGlu_1$ receptors with LY456236 occludes the effects of DHPG (n=4; paired *t*-test; $p = 0.8205$) and *t*-ACPD (n=4; paired *t*-test; $p = 0.7027$) on LTS in CA3 PCs. Inhibition of PLC and PKC with U73122 (n=5; paired *t*-test; $p = 0.6483$) and chelerythrine chloride (n=4; paired *t*-test; $p = 0.1817$), respectively, prevents inhibition of LTS by DHPG. DHPG application on CA3PCs patched with internal solution containing Cs-BAPTA (n=4; paired *t*-test; $p = 0.0007$) or K-BAPTA (n=4; paired *t*-test; $p = 0.0385$) increased LTS threshold significantly.

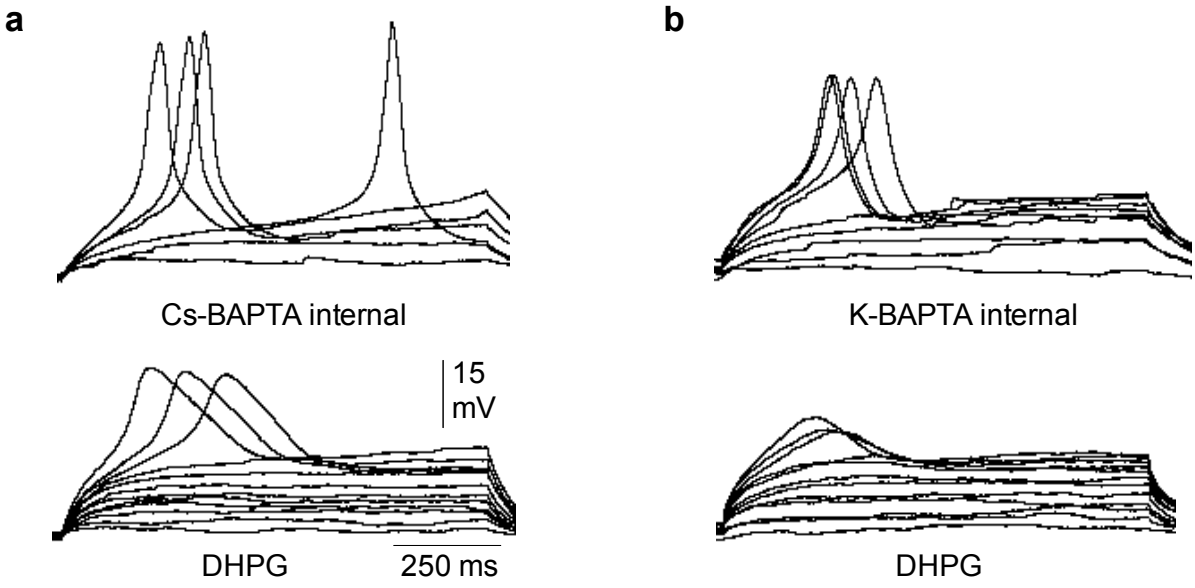
a
b
Cs-BAPTA internal
K-BAPTA internal
15
mV
DHPG
250 ms
DHPG

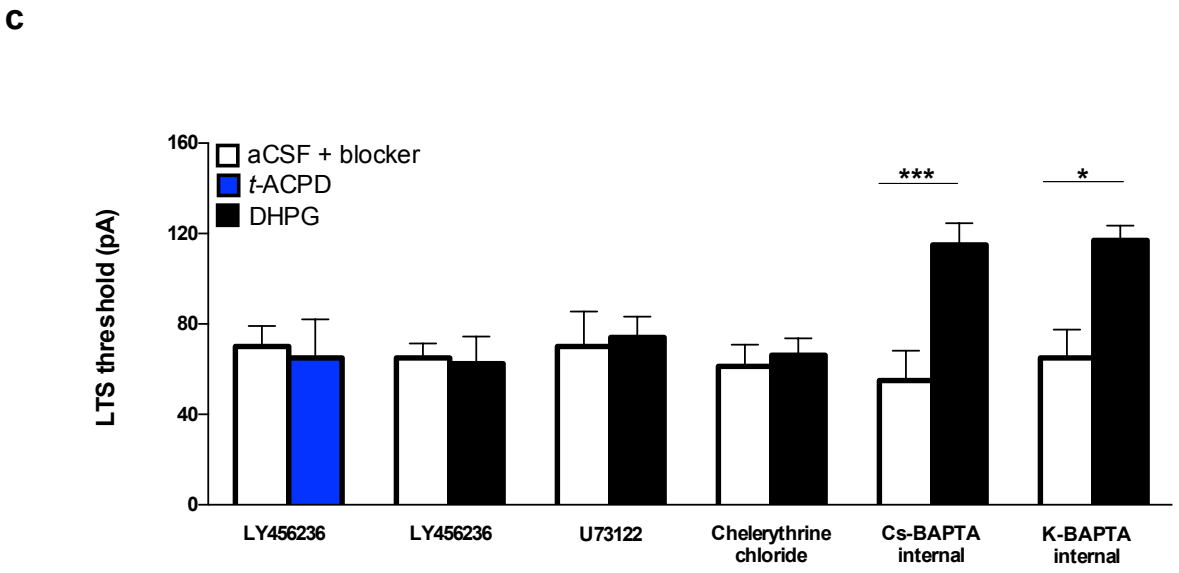
c
LTS threshold (pA)
160
120
80
40
0
aCSF + blocker
t-ACPD
DHPG
***
*
LY456236
LY456236
U73122
Chelerythrine chloride
Cs-BAPTA internal
K-BAPTA internal

Chapter 6: T-type Ca^{2+} channels facilitate synaptic transmission in CA3 PCs

6.1 Overview

Studies of synaptic transmission involving T-type Ca^{2+} channels have focused almost exclusively on their presynaptic role in facilitating neurotransmitter release. The advent of glutamate uncaging and two-photon imaging of dendritic and spine Ca^{2+} transients has given rise to a large body of literature highlighting the role of VGCCs in dendritic depolarization by subthreshold stimuli and backpropagating action potentials. The main theme that emerges from these studies is the compensatory influence of voltage-gated ion conductances on signal attenuation from distal synaptic sites. Dendritic excitability achieved through expression of voltage-gated ion channels is of critical importance for the integration of spatially and temporally dispersed inputs into patterned output. Modeling studies build on this idea further to show that an active dendritic tree amplifies dynamic range of neurons and this enhancement could be the main function of active dendritic conductances (Gollo *et al.* 2009).

Integration of synaptic inputs is especially problematic for CA3 PCs because of the stratified nature of intrinsic and extrinsic connections that populate their dendritic tree. Increased filtering of more distal synapses, due to intrinsic resistance and capacitance properties of dendrites, would mean that proximal inputs, namely mossy fibers have exclusive control of CA3 PC excitability. Arguing against this, it is has been known for some time that distance-dependent filtering is compensated by heterogeneous distribution of voltage-gated ion channels in a distance-from-soma-dependent manner. Despite this, the study of dendritic voltage-gated Ca^{2+} channels and

their contribution, if any, to dendritic depolarization in CA3 PCs has lagged behind that of CA1 PCs. In Chapters 3-5 we showed electrophysiological and Ca^{2+} imaging data indicating that T-type Ca^{2+} channels are expressed on dendrites of CA3 PCs and their interaction with voltage-gated conductances and GPCRs has a functional impact on dendritic excitability. In this Chapter, we aim to determine whether T-type Ca^{2+} channels have a boosting effect on synaptic potentials evoked by subthreshold stimulation of distal inputs.

6.2 Results

6.2.1 Neurotransmitter release is necessary for evoking EPSPs in CA3 PCs

The data presented in Chapter 4 indicates that T-type Ca^{2+} channels are expressed on the soma and dendrites of CA3 PCs. In order to study their potential involvement in synaptic transmission, we recorded subthreshold EPSPs by stimulating inputs in stratum radiatum/lacunosum-moleculare and recording from whole-cell current clamped CA3 PCs in acute slices of rat hippocampus (left, **Fig. 6-1a**). A CA3 PC that was patched and loaded with Alexa-594 is shown in the inset of **Fig. 6-1a**. Cells used for stimulation experiments were restricted to the region of CA3 shown and the dotted line depicts the location where the stimulation electrode was placed. Picrotoxin (10 μM) and QX314 (1 mM) were included in the patch pipette to block $GABA_A$ receptors and voltage-gated Na^+ channels, respectively. This approach allowed for unperturbed background neuronal activity and action potential propagation to take place, while impeding the contribution of voltage-gated Na^+ channels to EPSP generation. In the aCSF, we added 1 mM 4AP to block A-type K^+ channels and 500 μM L-cysteine to remove any tonic blockade of T-type Ca^{2+} channels by heavy metals.

Examples of subthreshold EPSPs, evoked by graded stimulation of 3, 4, and 5V, recorded in CA3 PCs are shown in the right panel of **Fig. 6-1a**. The graded nature of the EPSP response to increasing stimulus voltage along with the temporal delay between the stimulus artifact and EPSP onset indicates that synaptic potentials were evoked by neurotransmitter release and not direct stimulation of CA3 PC dendrites. In order to verify this, we measured the effects of HVA Ca^{2+} channel blockade by recording EPSPs every 30 s in response to 5V stimulation, before and after wash-in of 60 μM cadmium chloride. Cadmium reduced peak EPSP amplitude progressively and after 10 minutes of application, EPSPs were nearly completely diminished (**Fig. 6-1b**). The representative average EPSP recorded during the 6 min immediately prior to cadmium application is shown in the top left panel of **Fig. 6-1b**. The average was obtained from individual EPSPs recorded during time points shown in the gray region marked (a) in the scatter plot below. Similarly, the representative average EPSP recorded during the last 6 min of cadmium application is shown in the top right panel of **Fig. 6-1b**. This average was obtained from individual EPSPs recorded during the time points shown in the gray region marked (b) in the scatter plot below.

EPSPs from time points shown in the gray shaded regions of **Fig. 6-1b** are graphed in **Fig. 6-1c**. EPSPs recorded immediately prior to cadmium application (5.89 ± 0.43 mV) significantly differed from those recorded 10 min after cadmium application (0.41 ± 0.06 mV; n=4 cells; paired *t*-test; $p < 0.0001$; **Fig. 6-1c**). We also measured the sensitivity of evoked EPSPs to voltage-gated Na^{+} channels by repeating the experiment detailed above using TTX. As with cadmium, TTX reduced peak amplitude progressively and after 10 minutes of perfusion, EPSPs

could not be evoked by stimulation (n=4; **Fig. 6-1d**). Representative averaged EPSPs from time points immediately prior to and at the end of TTX application are marked (a) and (b) respectively, above the scatter plot. EPSPs recorded immediately prior to TTX application (19.52 ± 1.59 mV) significantly differed from those recorded 10 min after TTX application (0.71 ± 0.30 mV; n=4 cells; paired *t*-test; $p < 0.0001$; **Fig. 6-1e**).

6.2.2 T-type Ca^{2+} channels enhance EPSP amplitudes in PCs of CA3 but not CA1

In order to study the role of T-type Ca^{2+} channels in CA3 synaptic transmission, we recorded EPSPs every 30 s in response to 5V stimulation before and after wash-in of 2 μM Z944. Time course of EPSP amplitude in CA3 PCs is shown in **Fig. 6-2a**. Representative averaged EPSPs from time points shown in gray are displayed above the scatter blot. Inhibition of T-type channels by Z944 reduced EPSP amplitude by approximately 50%. Peak amplitude of individual EPSPs from time points shown in the gray shaded regions of **Fig. 6-2a** are graphed in **Fig. 6-2b**. EPSPs recorded at the commencement of the experiment (control (a) – 13.45 ± 1.02 mV) did not differ significantly from those recorded immediately prior to Z944 application (control (b) – 13.68 ± 0.93 mV; n=4 cells; repeated measures one-way ANOVA with Tukey's post-hoc; $p = 0.9788$; **Fig. 6-2b**). Peak EPSP amplitude recorded during the first 6 min of experimental period (control (a)) significantly differed from those recorded during the last 5 min of z944 application (z944 – 4.51 ± 0.53 mV; n=4 cells; repeated measures one-way ANOVA with Tukey's post-hoc; $p < 0.0001$; **Fig. 6-2b**). This was also the case when EPSPs recorded at the end of Z944 application were compared with those recorded immediately prior to drug perfusion (control (b); n=4 cells; repeated measures one-way ANOVA with Tukey's post-hoc; $p < 0.0001$; **Fig. 6-2b**).

Previous studies have shown the boosting effect of R-type Ca^{2+} channel blockade on EPSP amplitude in CA1 PCs (Wang *et al.* 2014). Given that our two-photon imaging data showed expression of T-type channels in the proximal dendrites and soma of CA1 PCs, we repeated the above time course experiments in CA1 PCs. We recorded subthreshold EPSPs, evoked by stimulating Schaffer collateral axons in stratum radiatum, from whole-cell current clamped CA1 PCs. To measure the effects of T-type channels, we recorded EPSPs every 30 s before and after application of Z944.

Averaged peak EPSPs recorded during time points shown in grey areas are shown above the scatter plot as described previously (**Fig. 6-2c**). Wash-in of Z944 had no significant effect on peak EPSP amplitude. Comparison between individual EPSPs from control periods (5.52 ± 0.41 mV) and after Z944 treatment (5.11 ± 0.45 mV) showed lack of an effect on synaptic transmission in CA1 PCs after blockade of T-type channels (n=5 cells; paired *t*-test; $p = 0.3827$; **Fig. 6-2d**).

6.3 Discussion

In this Chapter, we investigated the potential for EPSP amplification by T-type Ca^{2+} channel activity. We found that blocking T-type channels with Z944 reduced EPSP amplitude in CA3 PCs but not CA1 PCs. There is a possibility that the diminishing effect of Z944 is mediated by its inhibition of R-type channels; however, R-type blockade in CA1 PCs potentiates EPSP amplitude (Wang *et al*., 2014) and the lack of this effect in CA1PCs reflects the insensitivity of R-type channels to Z944. The diminishing effect of Z944 could also occur from blockade of pre- and/or postsynaptic channels. By using a high concentration of cadmium chloride, we show that

neurotransmitter release at distal synapses in area CA3 is facilitated entirely by HVA Ca^{2+} channels. If release could be supported by T-type expression in terminals, stimulation would elicit an EPSP, albeit of small magnitude, after cadmium application. Because we failed to see this result, we conclude that reduction in EPSP amplitude after Z944 application occurs via inhibition of T-type channels in dendrites of CA3 PCs.

The lack of Z944 effect on EPSP amplitude in CA1 PCs is not surprising given the high expression of dendritic R-type channels in area CA1. Enhancement of R-type currents by muscarinic receptors in CA1 PCs elicits Ca^{2+} spikes and repetitive firing activity (Tai *et al.* 2006). R-type channels also modulate synaptic responses of CA1 PCs to Schaffer collateral stimulation. By activating A-type K^+ channels, R-type channels reduce dendritic membrane excitability, such that blockade of the latter conductance causes a significant enhancement of EPSP amplitude (Wang *et al.* 2014). Further, activity-dependent depression of Ca^{2+} transients in spines of CA1 PCs occurs through an R-type, but not T-type-dependent pathway (Yasuda *et al.* 2003). Our electrophysiological data on LTS (Chapter 3) indicates that T-type channels are expressed in CA1 PCs; however, the Ca^{2+} imaging data presented in Chapter 4 suggests that their expression is limited to the soma and proximal regions of dendrites.

Our data cannot be extrapolated to account for dendritic depolarization at other, more proximal, sites in the dendritic tree because we did not test the effects of Z944 on EPSP amplitude evoked by stimulation of mossy fiber inputs. Mossy fiber-CA3 synapse is a large "detonator" synapse and release of neurotransmitter from mossy fiber terminals results in giant mini EPSPs, reflecting the dramatic ability of dentate granule cells to drive spiking activity in CA3 PCs (Henze *et al.*

2002). Reid *et al*. report that spontaneous release from mossy fibers under resting conditions blocks a nickel-dependent Ca^{2+} conductance in CA3 PCs implying that the need for LVA channels to boost subthreshold inputs is diminished at synapses that are relatively close to the soma (Reid *et al.* 2008).

Our finding that T-type Ca^{2+} channels boost EPSP amplitude in CA3 PCs suggests that signaling cascades that alter their activity will have a significant impact on synaptic transmission. We have shown that muscarinic activation enhances LTS propagation through M-current blockade. The combined action of muscarinic activation and synaptic depolarization could cause a further elevation in dendritic Ca^{2+} levels through T-type channels. Such activity-dependent Ca^{2+} signaling through coupling between T-type Ca^{2+} channels and mGluRs has been reported in cerebellar Purkinje cells (Hildebrand *et al.* 2009). In contrast, activation of mGluRs is expected to have the opposite effect in CA3 PCs. By inhibiting T-type channel activity, mGluRs will decrease dendritic excitability although the overall consequence of mGluR activation on synaptic depolarization in CA3 PCs will ultimately depend on the concerted inhibition of T-type Ca^{2+} channels and activation of K^+ channels. Downstream actions of T-type channel opening and Ca^{2+} influx on voltage/Ca^{2+}-activated K^+ channels (Cai *et al.* 2004) and Ca^{2+} activated chloride channels (Huang *et al.* 2012) can add further complexity to the control of synaptic signals by voltage-gated conductances in dendrites.

Figure 6-1 Synaptically evoked EPSPs in CA3 PCs are dependent on action potential propagation.

(**a**) Left: low-magnification image of an acute hippocampal slice showing the general region of area CA3 where PCs were targeted for experimentation. Scale bar, 300 μm. CA3 PC was patched and loaded with 50 μM Alexa-594. Dashed line depicts placement of the stimulation electrode that was used to elicit EPSPs in clamped CA3 PCs. Inset shows a confocal stack of the apical and basal arborizations of the same neuron Scale bar, 30 μm. Right: representative traces showing responses of a CA3 PC to graded stimulation of 3, 4, and 5V. (**b**) Time course of EPSP amplitude (mean ± SEM) for baseline and during perfusion of cadmium as indicated by horizontal line above. Inset shows the average of 12 EPSPs taken from indicated shaded time points in control conditions and after application of cadmium. Scale bars, 5 mV and 25 msec. (**c**) Scatter plot of EPSP peak amplitude in control conditions and after cadmium application from individual cells in (b). Cadmium reduced the amplitude of EPSPs when compared to control conditions (n=4 cells; paired *t*-test; $p < 0.0001$). (**d**) Time course of EPSP amplitude (mean ± SEM) for baseline and during perfusion of TTX as indicated by line above. Inset shows the average of 12 EPSPs taken from indicated shaded time points in control conditions and after application of TTX. Scale bars, 10 mV and 25 msec. (**e**) Scatter plot of EPSP peak amplitude in control conditions and after TTX application from individual cells in (d). TTX reduced the amplitude of EPSPs when compared to control conditions (n=4 cells; paired *t*-test; $p < 0.0001$).

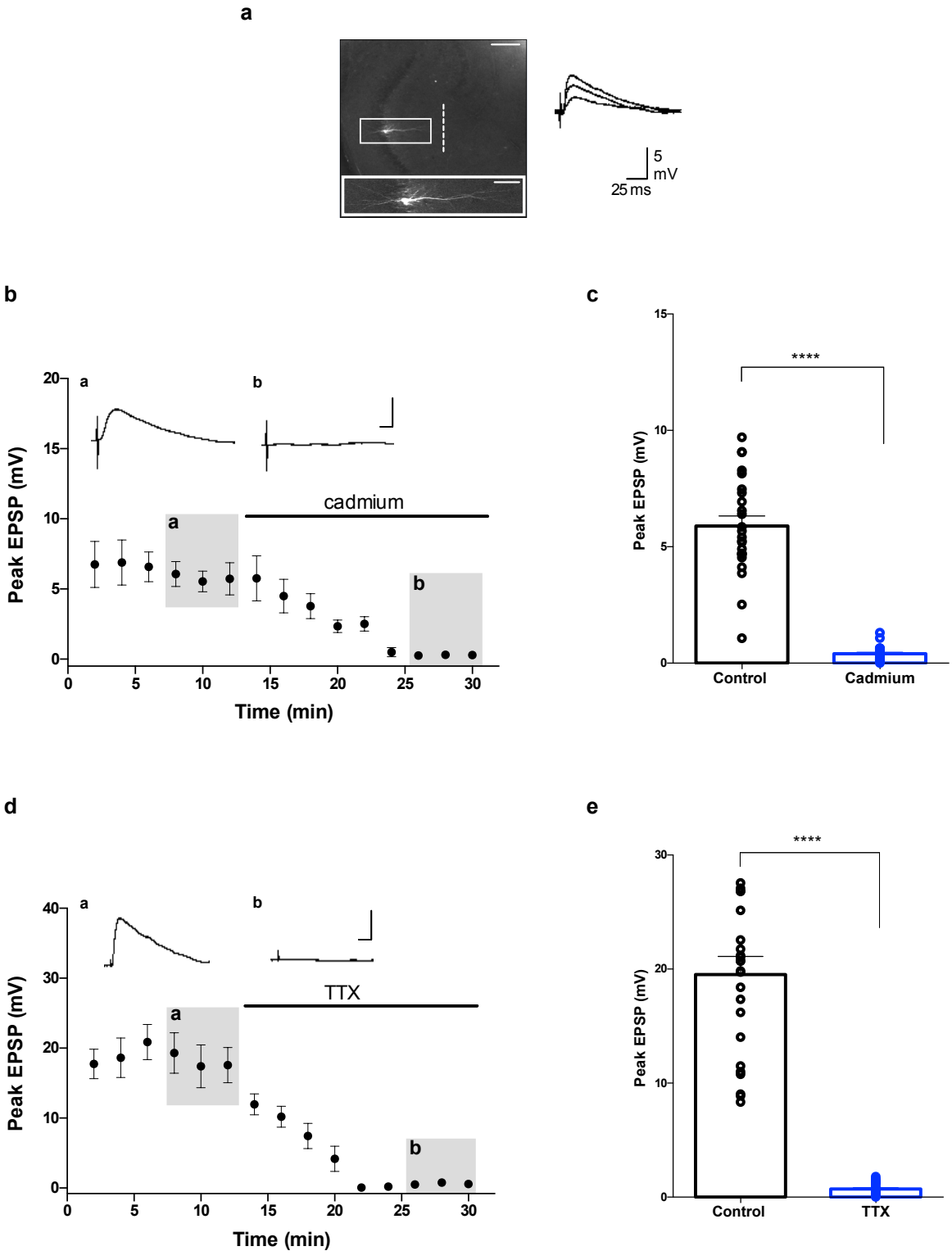
a
5
mV
25 ms
b
Peak EPSP (mV)
cadmium
a
b
Time (min)
c
****
Peak EPSP (mV)
Control
Cadmium
d
Peak EPSP (mV)
TTX
a
b
Time (min)
e
****
Peak EPSP (mV)
Control
TTX

Figure 6-2 Z944 decreases EPSPs in CA3 PCs but not in CA1 PCs.

(**a**) Time course of EPSP amplitude (mean ± SEM) in CA3 PCs for baseline and during perfusion of Z944 as indicated by horizontal line above. Inset shows the average of 12 EPSPs taken from indicated shaded time points in control conditions and after application of Z944. Scale bars, 5 mV and 25 msec. (**b**) Scatter plot of EPSP peak amplitude in control conditions and after Z944 application from individual cells in (a). Z944 reduced the amplitude of EPSPs when compared to control conditions (n=4 cells; repeated measures one-way ANOVA; $p < 0.0001$). (**c**) Time course of EPSP amplitude (mean ± SEM) in CA1 PCs for baseline and during perfusion of Z944 as indicated by horizontal line above. Inset shows the average of 12 EPSPs taken from indicated shaded time points in control conditions and after application of Z944. Scale bars, 5 mV and 25 msec. (**d**) Scatter plot of EPSP peak amplitude in control conditions and after Z944 application from individual cells in (c). Z944 had no effect on EPSP amplitude when compared to control conditions (n=4 cells; paired *t*-test; $p = 0.3827$).

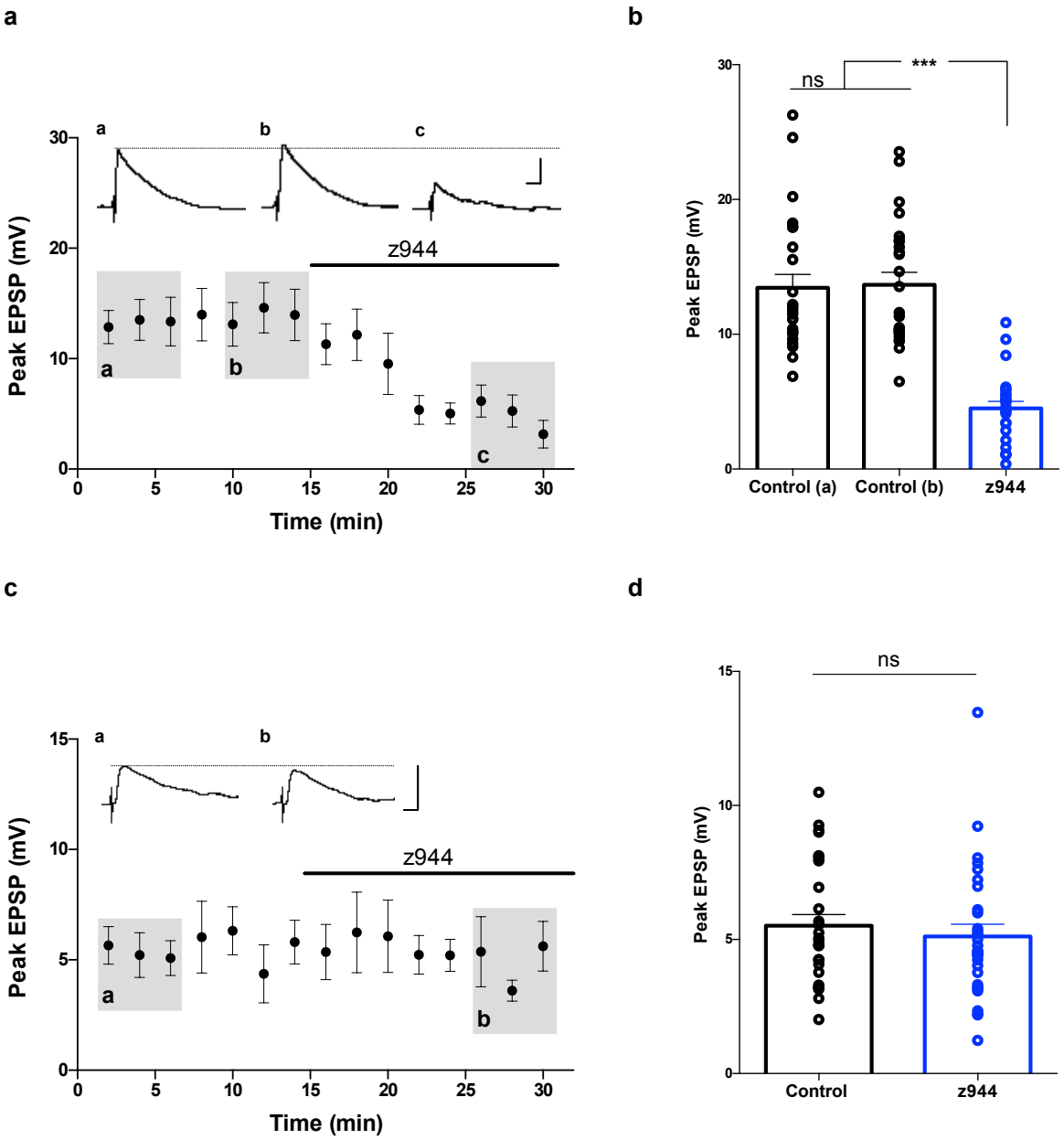
a
b
c
d
Peak EPSP (mV)
Time (min)
z944
ns
***
Control (a)
Control (b)
Control
z944

Chapter 7: Conclusions and future directions

7.1 Research significance

As discussed in **3.1**, LTS have not been reported in CA3 PCs despite observations that T-type channels contribute to Ca^{2+} currents in this region. Our study shows that T-type-mediated depolarization is under the strong repolarizing influence of A-type K^+ channels. Dendritic K^+ channels have distinct control over backpropagating action potentials, the kinetics of excitatory postsynaptic potentials, and the extent of dendritic membrane excitability (Johnston *et al.* 2000). Our data adds to the repertoire of functions that K^+ channels exert control over in dendrites of PCs. The LTS experiments detailed in this thesis were performed under conditions wherein A-type K^+ channels were blocked because this was a necessity for LTS expression and examination of LTS amplitude and threshold. There are various physiological conditions under which A-type K^+ channel activity is downregulated in dendrites and this can significantly increase membrane excitability through T-type channel activity in CA3 PCs.

Activation of either PKA or PKC in distal dendrites of CA1 PCs results in a depolarizing shift in the activation curve of transient K^+ channels and this leads to an increase in the amplitude of backpropagating action potentials (Hoffman and Johnston 1998). Potentiation of backpropagating action potentials by neuromodulators (e.g. beta-adrenergic, muscarinic acetylcholine, and dopaminergic receptors) is also dependent on A-type K^+ channel gating modification by PKA and PKC (Hoffman and Johnston 1999). In a seminal paper Magee and Johnston showed that backpropagating action potentials are crucial for LTP induction that occurs by pairing of EPSPs with postsynaptic action potentials (Magee and Johnston 1997).

Computational studies show that K^+ channel conductance can be reduced by precisely timed EPSPs such that the amplitude of subsequent backpropagating action potentials is increased leading to LTP induction through VGCC-mediated depolarization that removes Mg^{2+} block of NMDA receptors (Migliore *et al.* 1999). For example, depolarization induced by a synaptic input (4 nS, 100 Hz) 250 μm away from the soma can inactivate transient K^+ channel conductance resulting in increased amplitude of the paired backpropagating action potential (Migliore *et al.* 1999). Further, activation of distal inputs (4-8 nS, 400 μm from the soma) delivered 2-8 msec before an action potential can significantly increase the amplitude of backpropagating action potentials through inactivation of transient K^+ channels (Migliore *et al.* 1999). Similar modifications of A-type K^+ channel gating properties by neuromodulators or synaptic inputs should reveal the contribution of T-type channels to synaptic plasticity in CA3 PCs.

In addition to A-type K^+ channels, our data show that LTS amplitude is strongly influenced by the M-current such that blockade of M-current caused an increase in LTS amplitude without having an impact on LTS threshold. M-currents significantly influence membrane excitability and neuronal output because they are the only persist currents in the voltage range for action potential initiation. A sustained M current conductance acts as a break for recurrent neuronal firing, and as a result M-current inhibition causes severe hyperexcitability that is further exacerbated by kinetics of T-type channels that underlie burst firing. The KCNQ gene family encodes K^+ channels that mediate M-currents and KCNQ channelopathies underlie specific forms of epilepsy (Jentsch 2000). Consistent with this, anticonvulsants such as retigabine activate KCNQ channels by shifting their voltage dependence of activation to more negative potentials (Jentsch 2000). In CA3 PCs, M current blockade will have a profound influence on

membrane excitability because of their indirect influence on T-type channel activity. In a recent study, Qi *et al*. showed that mice with partial deficiency of Sentrin-specific protease 2 (SENP2) develop spontaneous seizures and that this mutation directly diminishes M-currents in CA3 PCs leading to neuronal hyperexcitability (Qi *et al.* 2014). The data presented in Chapter 5 support the notion that the ensuing influence of M-current inhibition on T-type channel activity would further contribute to hyperexcitability and seizure phenotype in these mice.

We also found that M-current inhibition underlies the enhancement of LTS by muscarinic receptors. The functional consequences of this finding cannot be understated because M-current inhibition via M1 receptors directly facilitates LTP and hippocampus-dependent cognitive function. M-current inhibition does not directly promote NMDA receptor opening during LTP induction at Schaffer collateral synapses but rather through enhancement of depolarization during and after bursts of action potentials that facilitates NMDA receptor opening (Petrovic *et al.* 2012). A similar scenario in CA3 PCs would amplify this depolarization and cause a significant Ca^{2+} influx through activation of T-type channels in dendrites. Ca^{2+} elevation could directly underlie LTP and/or membrane depolarization achieved through T-type activation and promote NMDA receptor opening, thereby facilitating LTP. The dense cholinergic innervation of CA3 PCs by the medial septal area is already documented in detail (Buzsaki 2002) and our data suggest that enhancement of LTS by muscarinic stimulation has the potential to contribute to synaptic plasticity.

In contrast to muscarinic stimulation, we found that $mGluR_1$ activation, which can occur as a result of synaptically released glutamate, potently inhibits T-type Ca^{2+} channels in CA3 PCs and

that this downregulation is independent of K^+ channels and intracellular Ca^{2+} levels. This is in stark contrast to the effects of group I mGluR activation in CA1 PCs where DHPG application increases CA1 PC excitability by upregulating R-type Ca^{2+} channels through a PLC/intracellular Ca^{2+}-dependent pathway (Park *et al.* 2010). This upregulation shifts the post-spike afterhyperpolarization (AHP) to an afterdepolarization (ADP) that lasts greater than 200 msec (Park *et al.* 2010). A similar blockade of AHP and induction of ADP after activation of group I mGluRs is also observed in CA3 PCs. Our findings show that T-type Ca^{2+} channels do not underlie this ADP because $mGluR_1$ activation potently blocks these channels. The ADP in CA3 PCs could be mediated by mGluR activation of R-type Ca^{2+} channels/nonselective cation currents and/or downregulation of Ca^{2+}-activated K^+ currents (Young *et al.* 2004). The interaction between these two opposing factors, namely the profile of currents that underlie an ADP and reduced excitability via T-type inhibition, is required for determining the overall influence of mGluR activation on CA3 PC excitability.

Of further note, the data presented in **6.2** suggest that T-type Ca^{2+} channels increase the amplitude of EPSPs elicited by subthreshold stimulation of inputs to CA3 PCs. Because T-type channel activity is regulated by mAChRs and K_v7 channels, conditions that perturb their activity will have a significant impact on T-type mediated dendritic depolarization. For example, the combined activation of muscarinic receptors, subsequent inhibition of M-current, and subthreshold synaptic activation could cause sufficient depolarization to elicit a dendritic LTS spike. As pointed out earlier, T-type channel contributions to dendritic excitability were studied under conditions of A-type K^+ channel blockade. The role of dendritic A-type K^+ conductance in shaping the amplitude, duration, and compartmentalization of synaptic potentials has been

elucidated and it appears that these channels confine synaptic depolarization to single dendritic branches, thereby regulating synaptic integration (Cai *et al.* 2004). Based on these observations, it has been suggested that the dendritic compartmentalization achieved by A-type K^+ channel activity allows specific dendrites to function as "quasi-independent binary signaling units" (Wei *et al.* 2001, Cai *et al.* 2004). This likely explains the significant amplification of synaptic potentials by T-type Ca^{2+} channels that we observed in CA3 PCs. As discussed earlier, various physiological conditions can cause temporary and persistent inactivation of A-type K^+ channels. Timing of synaptic inputs is expected to affect transient A-type K^+ conductance (Migliore *et al.* 1999) and this is also the manipulation that will have the most profound impact on T-type-mediated amplification of synaptic potentials because these channels are densely expressed on dendrites of CA3 PCs. Although the distinct roles of A-type K^+ channels in dendritic integration are already known, it remains to be determined whether their interaction with T-type Ca^{2+} channels contributes to this phenomenon in CA3 PCs.

7.2 Future directions

7.2.1 Physiological mechanisms of A-type K^+ current inhibition in CA3 PCs

Our data show that at least *in vitro*, detection of LTS at the soma is not possible without pharmacological blockade of A-type K^+ channels. Various properties of the dendritic membrane, including A-type K^+ channel density and phosphorylation state, will likely ultimately determine LTS kinetics. As such, a next step towards understanding the functional role of T-type channels in CA3 neuronal physiology is determining the conditions under which a LTS can propagate to the soma without pharmacological intervention. This could be achieved by examining the effects

of various neuromodulators that are known to downregulate A-type K^+ channel activity on LTS in CA3 PCs. A few candidate neurotransmitter systems include the beta-adrenergic, muscarinic, and dopaminergic receptors (Hoffman and Johnston 1999). Although muscarinic stimulation potentiated LTS amplitude in CA3 PCs, we failed to observe a somatic LTS with muscarinic stimulation in the absence of A-type K^+ channel blockade. This implies that the level of A-type K^+ channel inhibition required to unlock LTS is not achieved with muscarinic stimulation, and/or that muscarinic receptors in CA3 PCs have no effect on A-type K^+ channel kinetics. Modulation of dendritic action potentials by beta-adrenergic and cholinergic stimulation has been reported in CA1 PCs; however, in this study recordings were made from dendrites that were on average 200 μm away from the soma (Hoffman and Johnston 1999). Given this technical difference between that reported in the literature and our experiments, it is possible that carbachol application results in dendritic LTS in CA3 PCs and a dense distribution of A-type K^+ channels in the proximal somatodendritic compartment sets a high threshold for somatic Ca^{2+} spikes, thereby restricting their expression to dendrites. In order to confirm this, future experiments utilizing dendritic recordings are required to test the neuromodulation of A-type K^+ conductance and its ensuing influence on LTS initiation and propagation in CA3 PCs.

A-type K^+ channel kinetics can also be altered with precisely timed synaptic activation. Combined experimental and computational approaches show that supralinear increases in action potential amplitude occur when a somatic action potential is paired with synaptic activation in the distal dendrite, representing the importance of coincident pre- and post-synaptic activity (Magee and Johnston 1997, Migliore *et al.* 1999). The underlying mechanism for this potentiation is due to inactivation of A-type K^+ conductance by the synaptic input (Migliore *et*

al. 1999). 4AP-dependent K^+ conductance is also involved in setting the timing constraints that are a requirement for Hebbian modification of synaptic strength (Migliore *et al.* 1999). This propensity of A-type K^+ channels is due to their fast inactivation kinetics – the optimal condition for potentiation of backpropagating action potentials is when pre- and postsynaptic pairing occurs within a time window of 2-5 msec (Migliore *et al.* 1999). Thus, it is suggested that activation of VGCCs or NMDA receptors, through amplification of backpropagating action potentials, is a determining factor for whether relative timing of inputs leads to LTP or LTD (Johnston *et al.* 2003). The possibility of: 1) precisely timed synaptic activation leading to LTS initiation; and 2) involvement of T-type Ca^{2+} channels in amplifying backpropagating action potentials needs to be explored in future experiments.

7.2.2 Role of LTS in mAChR-facilitated LTP induction in CA3 PCs

M1 subtype of mAChRs are ubiquitously expressed in all subregions of the hippocampus (Levey *et al.* 1995) and cholinergic signaling via M1 receptors underlies learning, working memory, and synaptic plasticity (Anagnostaras *et al.* 2003, Shinoe *et al.* 2005). Specific activation of M1 mAChRs facilitates LTP induction and improves cognitive performance in animal models (Boddeke *et al.* 1992), whereas, loss of cholinergic activity results in cognitive impairment that can be pathological, for example, in the case of Schizophrenia and Alzheimer's disease (Dean *et al.* 2003). Muscarinic receptors modulate glutamatergic synaptic transmission by boosting synaptic potentials and Ca^{2+} influx in dendritic spines of CA1 PCs (Giessel and Sabatini 2010). Facilitation of LTP at the Schaffer collateral synapse in CA1 PCs has also been studied extensively and several lines of evidence indicate that M1 receptors facilitate LTP by enhancing synaptic NMDAR opening through direct modulation of ionic conductances, and therefore,

dendritic excitability (Buchanan *et al.* 2010). Specifically, M1 receptor activation causes an increase in input resistance and membrane time constant through inactivation of K_v7 channels and this subserves depolarization during and after spiking activity (Petrovic *et al.* 2012).

The data presented in **5.2.5** indicates that muscarinic activation facilitates LTS amplitude in CA3 PCs and this enhancement is mediated through the inhibition of K_v7 channels. Thus, T-type Ca^{2+} channels could play a role in the enhancement of ADP amplitude and reduced attenuation of backpropagating action potentials that is observed after muscarinic activation (Tsubokawa and Ross 1997). This could be achieved by examining ADP and backpropagating action potential amplitude after muscarinic stimulation with or without T-type channel blockade. In addition, the contribution of T-type Ca^{2+} channels to synaptic plasticity can be studied by inducing LTP in CA3 PCs using a theta burst pairing protocol (Buchanan *et al.* 2010) and determining whether blockade of T-type channels has an impact on LTP facilitation by M1 receptors.

7.2.3 Boosting of local synaptic potentials and Ca^{2+} influx by T-type Ca^{2+} channels in dendritic spines of CA3 PCs

The data presented in **6.2.2** indicate that T-type Ca^{2+} channels enhance the amplitude of synaptic potentials evoked by stimulation of distal synapses in CA3 PCs. This contribution of T-type Ca^{2+} channels to dendritic depolarization was observed in the presence of A-type K^+ channel blocker 4AP. A-type K^+ channels restrict depolarizing events to single dendritic compartments and prevent regenerative events such as LTS and plateau potentials from propagating to neighbouring dendrites (Cai *et al.* 2004). A-type K^+ channel expression at or near branch points is especially important for restricting depolarization to the stimulated dendrite such that the threshold for VGCC activation in adjacent dendrites is never exceeded by voltage escape from the dendrite of

origin (Cai *et al.* 2004). Given this limiting effect of A-type K^+ channels on dendritic depolarization, it is currently unclear whether T-type Ca^{2+} channels are capable of boosting synaptic potentials alongside preserved A-type K^+ channel activity. Even if T-type-mediated dendritic depolarization fails to propagate to the soma in the absence of 4AP, Ca^{2+} influx through T-type channels might be sufficient to induce local changes within spines in CA3 PCs.

In order to study boosting of synaptic potentials and dendritic spine Ca^{2+} influx in the absence of 4AP, future experiments will require the use of glutamate uncaging combined with Ca^{2+} imaging. Uncaging glutamate at specific spines using two-photon laser scanning microscopy, with or without T-type channels blockers, will reveal the extent of T-type channel contribution to dendritic depolarization in CA3 PCs. Using this approach will also shed light on whether T-type Ca^{2+} signaling contributes to synaptic integration in CA3 PCs. Dendritic Ca^{2+} spikes are an integral component of supralinear integration in region CA3 (Makara and Magee 2013) and it remains to be known whether T-type Ca^{2+} channels can contribute to this phenomenon. Further, as discussed in **7.2.1**, physiological mechanisms that modulate A-type K^+ channel activity and/or expression are expected to have profound effects on T-type channel-dependent synaptic depolarization and Ca^{2+} signaling.

References

Abrahamsson, T., L. Cathala, K. Matsui, R. Shigemoto and D. A. Digregorio (2012). "Thin dendrites of cerebellar interneurons confer sublinear synaptic integration and a gradient of short-term plasticity." Neuron **73**(6): 1159-1172.

Adams, M. E., R. A. Myers, J. S. Imperial and B. M. Olivera (1993). "Toxityping rat brain calcium channels with omega-toxins from spider and cone snail venoms." Biochemistry **32**(47): 12566-12570.

Adelman, J. P., J. Maylie and P. Sah (2012). "Small-conductance Ca2+-activated K+ channels: form and function." Annu Rev Physiol **74**: 245-269.

Alvina, K., G. Ellis-Davies and K. Khodakhah (2009). "T-type calcium channels mediate rebound firing in intact deep cerebellar neurons." Neuroscience **158**(2): 635-641.

Amaral, D. G. and J. A. Dent (1981). "Development of the mossy fibers of the dentate gyrus: I. A light and electron microscopic study of the mossy fibers and their expansions." J Comp Neurol **195**(1): 51-86.

Amaral, D. G., N. Ishizuka and B. Claiborne (1990). "Neurons, numbers and the hippocampal network." Prog Brain Res **83**: 1-11.

Amaral, D. G., H. E. Scharfman and P. Lavenex (2007). "The dentate gyrus: fundamental neuroanatomical organization (dentate gyrus for dummies)." Prog Brain Res **163**: 3-22.

Anagnostaras, S. G., G. G. Murphy, S. E. Hamilton, S. L. Mitchell, N. P. Rahnama, N. M. Nathanson and A. J. Silva (2003). "Selective cognitive dysfunction in acetylcholine M1 muscarinic receptor mutant mice." Nat Neurosci **6**(1): 51-58.

Andersen, P., T. V. Bliss and K. K. Skrede (1971). "Lamellar organization of hippocampal pathways." Exp Brain Res **13**(2): 222-238.

Anderson, D., J. D. Engbers, N. C. Heath, T. M. Bartoletti, W. H. Mehaffey, G. W. Zamponi and R. W. Turner (2013). "The Cav3-Kv4 complex acts as a calcium sensor to maintain inhibitory charge transfer during extracellular calcium fluctuations." J Neurosci **33**(18): 7811-7824.

Anderson, D., W. H. Mehaffey, M. Iftinca, R. Rehak, J. D. Engbers, S. Hameed, G. W. Zamponi and R. W. Turner (2010). "Regulation of neuronal activity by Cav3-Kv4 channel signaling complexes." Nat Neurosci **13**(3): 333-337.

Angelo, K. and T. W. Margrie (2011). "Population diversity and function of hyperpolarization-activated current in olfactory bulb mitral cells." Sci Rep **1**: 50.

Avery, R. B. and D. Johnston (1996). "Multiple channel types contribute to the low-voltage-activated calcium current in hippocampal CA3 pyramidal neurons." J Neurosci **16**(18): 5567-5582.

Bannister, N. J. and A. U. Larkman (1995). "Dendritic morphology of CA1 pyramidal neurones from the rat hippocampus: I. Branching patterns." J Comp Neurol **360**(1): 150-160.

Barnes, C. A., B. L. McNaughton, S. J. Mizumori, B. W. Leonard and L. H. Lin (1990). "Comparison of spatial and temporal characteristics of neuronal activity in sequential stages of hippocampal processing." Prog Brain Res **83**: 287-300.

Bast, T. (2007). "Toward an integrative perspective on hippocampal function: from the rapid encoding of experience to adaptive behavior." Rev Neurosci **18**(3-4): 253-281.

Bazzazi, H., M. Ben Johny, P. J. Adams, T. W. Soong and D. T. Yue (2013). "Continuously tunable Ca(2+) regulation of RNA-edited CaV1.3 channels." Cell Rep **5**(2): 367-377.

Beenhakker, M. P. and J. R. Huguenard (2009). "Neurons that fire together also conspire together: is normal sleep circuitry hijacked to generate epilepsy?" Neuron **62**(5): 612-632.

Bentzen, B. H., S. P. Olesen, L. C. Ronn and M. Grunnet (2014). "BK channel activators and their therapeutic perspectives." Front Physiol **5**: 389.

Bichet, D., V. Cornet, S. Geib, E. Carlier, S. Volsen, T. Hoshi, Y. Mori and M. De Waard (2000). "The I-II loop of the Ca2+ channel alpha1 subunit contains an endoplasmic reticulum retention signal antagonized by the beta subunit." Neuron **25**(1): 177-190.

Bleasdale, J. E., N. R. Thakur, R. S. Gremban, G. L. Bundy, F. A. Fitzpatrick, R. J. Smith and S. Bunting (1990). "Selective inhibition of receptor-coupled phospholipase C-dependent processes in human platelets and polymorphonuclear neutrophils." J Pharmacol Exp Ther **255**(2): 756-768.

Bloodgood, B. L. and B. L. Sabatini (2007). "Ca(2+) signaling in dendritic spines." Curr Opin Neurobiol **17**(3): 345-351.

Bloodgood, B. L. and B. L. Sabatini (2007). "Nonlinear regulation of unitary synaptic signals by CaV(2.3) voltage-sensitive calcium channels located in dendritic spines." Neuron **53**(2): 249-260.

Bloodgood, B. L. and B. L. Sabatini (2008). "Regulation of synaptic signalling by postsynaptic, non-glutamate receptor ion channels." J Physiol **586**(6): 1475-1480.

Boddeke, E. W., A. Enz and G. Shapiro (1992). "SDZ ENS 163, a selective muscarinic M1 receptor agonist, facilitates the induction of long-term potentiation in rat hippocampal slices." Eur J Pharmacol **222**(1): 21-25.

Bossu, J. L. and A. Feltz (1986). "Inactivation of the low-threshold transient calcium current in rat sensory neurones: evidence for a dual process." J Physiol **376**: 341-357.

Bragin, A., G. Jando, Z. Nadasdy, J. Hetke, K. Wise and G. Buzsaki (1995). "Gamma (40-100 Hz) oscillation in the hippocampus of the behaving rat." J Neurosci **15**(1 Pt 1): 47-60.

Braun, A. P. and H. Schulman (1995). "The multifunctional calcium/calmodulin-dependent protein kinase: from form to function." Annu Rev Physiol **57**: 417-445.

Buchanan, K. A., M. M. Petrovic, S. E. Chamberlain, N. V. Marrion and J. R. Mellor (2010). "Facilitation of long-term potentiation by muscarinic M(1) receptors is mediated by inhibition of SK channels." Neuron **68**(5): 948-963.

Bushell, T. J., D. E. Jane, H. W. Tse, J. C. Watkins, C. H. Davies, J. Garthwaite and G. L. Collingridge (1995). "Antagonism of the synaptic depressant actions of L-AP4 in the lateral perforant path by MAP4." Neuropharmacology **34**(2): 239-241.

Buzsaki, G. (2002). "Theta oscillations in the hippocampus." Neuron **33**(3): 325-340.

Cai, X., C. W. Liang, S. Muralidharan, J. P. Kao, C. M. Tang and S. M. Thompson (2004). "Unique roles of SK and Kv4.2 potassium channels in dendritic integration." Neuron **44**(2): 351-364.

Cain, S. M. and T. P. Snutch (2011). "Voltage-gated calcium channels and disease." Biofactors **37**(3): 197-205.

Cain, S. M. and T. P. Snutch (2013). "T-type calcium channels in burst-firing, network synchrony, and epilepsy." Biochim Biophys Acta **1828**(7): 1572-1578.

Canti, C., M. Nieto-Rostro, I. Foucault, F. Heblich, J. Wratten, M. W. Richards, J. Hendrich, L. Douglas, K. M. Page, A. Davies and A. C. Dolphin (2005). "The metal-ion-dependent adhesion site in the Von Willebrand factor-A domain of alpha2delta subunits is key to trafficking voltage-gated Ca2+ channels." Proc Natl Acad Sci U S A **102**(32): 11230-11235.

Carbone, E., C. Calorio and D. H. Vandael (2014). "T-type channel-mediated neurotransmitter release." Pflugers Arch **466**(4): 677-687.

Cattaneo, F., G. Guerra, M. Parisi, M. De Marinis, D. Tafuri, M. Cinelli and R. Ammendola (2014). "Cell-surface receptors transactivation mediated by g protein-coupled receptors." Int J Mol Sci **15**(11): 19700-19728.

Catterall, W. A. (2000). "Structure and regulation of voltage-gated Ca2+ channels." Annu Rev Cell Dev Biol **16**: 521-555.

Catterall, W. A. (2010). "Ion channel voltage sensors: structure, function, and pathophysiology." Neuron **67**(6): 915-928.

Catterall, W. A., E. Perez-Reyes, T. P. Snutch and J. Striessnig (2005). "International Union of Pharmacology. XLVIII. Nomenclature and structure-function relationships of voltage-gated calcium channels." Pharmacol Rev **57**(4): 411-425.

Chawla, M. K., J. F. Guzowski, V. Ramirez-Amaya, P. Lipa, K. L. Hoffman, L. K. Marriott, P. F. Worley, B. L. McNaughton and C. A. Barnes (2005). "Sparse, environmentally selective expression of Arc RNA in the upper blade of the rodent fascia dentata by brief spatial experience." Hippocampus **15**(5): 579-586.

Chemin, J., A. Mezghrani, I. Bidaud, S. Dupasquier, F. Marger, C. Barrere, J. Nargeot and P. Lory (2007). "Temperature-dependent modulation of CaV3 T-type calcium channels by protein kinases C and A in mammalian cells." J Biol Chem **282**(45): 32710-32718.

Chemin, J., A. Monteil, E. Perez-Reyes, E. Bourinet, J. Nargeot and P. Lory (2002). "Specific contribution of human T-type calcium channel isotypes (alpha(1G), alpha(1H) and alpha(1I)) to neuronal excitability." J Physiol **540**(Pt 1): 3-14.

Cherubini, E. and R. Miles (2015). "The CA3 region of the hippocampus: how is it? What is it for? How does it do it?" Front Cell Neurosci **9**: 19.

Chiovini, B., G. F. Turi, G. Katona, A. Kaszas, D. Palfi, P. Maak, G. Szalay, M. F. Szabo, G. Szabo, Z. Szadai, S. Kali and B. Rozsa (2014). "Dendritic spikes induce ripples in parvalbumin interneurons during hippocampal sharp waves." Neuron **82**(4): 908-924.

Christie, B. R. and W. C. Abraham (1992). "Priming of associative long-term depression in the dentate gyrus by theta frequency synaptic activity." Neuron **9**(1): 79-84.

Christie, B. R., L. S. Eliot, K. Ito, H. Miyakawa and D. Johnston (1995). "Different Ca2+ channels in soma and dendrites of hippocampal pyramidal neurons mediate spike-induced Ca2+ influx." J Neurophysiol **73**(6): 2553-2557.

Chu, Z. and J. J. Hablitz (2000). "Quisqualate induces an inward current via mGluR activation in neocortical pyramidal neurons." Brain Res **879**(1-2): 88-92.

Claiborne, B. J., D. G. Amaral and W. M. Cowan (1986). "A light and electron microscopic analysis of the mossy fibers of the rat dentate gyrus." J Comp Neurol **246**(4): 435-458.

Clapham, D. E. (2007). "Calcium signaling." Cell **131**(6): 1047-1058.

Conn, P. J. and J. P. Pin (1997). "Pharmacology and functions of metabotropic glutamate receptors." Annu Rev Pharmacol Toxicol **37**: 205-237.

Contreras, D. (2006). "The role of T-channels in the generation of thalamocortical rhythms." CNS Neurol Disord Drug Targets **5**(6): 571-585.

Cosgrove, K. E., E. J. Galvan, G. Barrionuevo and S. D. Meriney (2011). "mGluRs modulate strength and timing of excitatory transmission in hippocampal area CA3." Mol Neurobiol **44**(1): 93-101.

Coulon, P., D. Herr, T. Kanyshkova, P. Meuth, T. Budde and H. C. Pape (2009). "Burst discharges in neurons of the thalamic reticular nucleus are shaped by calcium-induced calcium release." Cell Calcium **46**(5-6): 333-346.

Crunelli, V., D. W. Cope and S. W. Hughes (2006). "Thalamic T-type Ca2+ channels and NREM sleep." Cell Calcium **40**(2): 175-190.

Crunelli, V. and S. W. Hughes (2010). "The slow (<1 Hz) rhythm of non-REM sleep: a dialogue between three cardinal oscillators." Nat Neurosci **13**(1): 9-17.

Crunelli, V., T. I. Toth, D. W. Cope, K. Blethyn and S. W. Hughes (2005). "The 'window' T-type calcium current in brain dynamics of different behavioural states." J Physiol **562**(Pt 1): 121-129.

Cueni, L., M. Canepari, R. Lujan, Y. Emmenegger, M. Watanabe, C. T. Bond, P. Franken, J. P. Adelman and A. Luthi (2008). "T-type Ca2+ channels, SK2 channels and SERCAs gate sleep-related oscillations in thalamic dendrites." Nat Neurosci **11**(6): 683-692.

David, L. S., E. Garcia, S. M. Cain, E. Thau, J. R. Tyson and T. P. Snutch (2010). "Splice-variant changes of the Ca(V)3.2 T-type calcium channel mediate voltage-dependent facilitation and associate with cardiac hypertrophy and development." Channels (Austin) **4**(5): 375-389.

Davies, A., I. Kadurin, A. Alvarez-Laviada, L. Douglas, M. Nieto-Rostro, C. S. Bauer, W. S. Pratt and A. C. Dolphin (2010). "The alpha2delta subunits of voltage-gated calcium channels form GPI-anchored proteins, a posttranslational modification essential for function." Proc Natl Acad Sci U S A **107**(4): 1654-1659.

Dean, B., F. P. Bymaster and E. Scarr (2003). "Muscarinic receptors in schizophrenia." Curr Mol Med **3**(5): 419-426.

Delmas, P. and D. A. Brown (2005). "Pathways modulating neural KCNQ/M (Kv7) potassium channels." Nat Rev Neurosci **6**(11): 850-862.

DePuy, S. D., J. Yao, C. Hu, W. McIntire, I. Bidaud, P. Lory, F. Rastinejad, C. Gonzalez, J. C. Garrison and P. Q. Barrett (2006). "The molecular basis for T-type Ca2+ channel inhibition by G protein beta2gamma2 subunits." Proc Natl Acad Sci U S A **103**(39): 14590-14595.

Deshmukh, S. S. and J. J. Knierim (2011). "Representation of non-spatial and spatial information in the lateral entorhinal cortex." Front Behav Neurosci **5**: 69.

Doherty, A. J., M. J. Palmer, J. M. Henley, G. L. Collingridge and D. E. Jane (1997). "(RS)-2-chloro-5-hydroxyphenylglycine (CHPG) activates mGlu5, but no mGlu1, receptors expressed in CHO cells and potentiates NMDA responses in the hippocampus." Neuropharmacology **36**(2): 265-267.

Dolphin, A. C. (2013). "The alpha2delta subunits of voltage-gated calcium channels." Biochim Biophys Acta **1828**(7): 1541-1549.

Egger, V., K. Svoboda and Z. F. Mainen (2003). "Mechanisms of lateral inhibition in the olfactory bulb: efficiency and modulation of spike-evoked calcium influx into granule cells." J Neurosci **23**(20): 7551-7558.

Ekstein, D., F. Benninger, M. Daninos, J. Pitsch, K. M. van Loo, A. J. Becker and Y. Yaari (2012). "Zinc induces long-term upregulation of T-type calcium current in hippocampal neurons in vivo." J Physiol **590**(Pt 22): 5895-5905.

Ellinor, P. T., J. Yang, W. A. Sather, J. F. Zhang and R. W. Tsien (1995). "Ca2+ channel selectivity at a single locus for high-affinity Ca2+ interactions." Neuron **15**(5): 1121-1132.

Engbers, J. D., D. Anderson, H. Asmara, R. Rehak, W. H. Mehaffey, S. Hameed, B. E. McKay, M. Kruskic, G. W. Zamponi and R. W. Turner (2012). "Intermediate conductance calcium-activated potassium channels modulate summation of parallel fiber input in cerebellar Purkinje cells." Proc Natl Acad Sci U S A **109**(7): 2601-2606.

Engel, D. and P. Jonas (2005). "Presynaptic action potential amplification by voltage-gated Na+ channels in hippocampal mossy fiber boutons." Neuron **45**(3): 405-417.

Eroglu, C., N. J. Allen, M. W. Susman, N. A. O'Rourke, C. Y. Park, E. Ozkan, C. Chakraborty, S. B. Mulinyawe, D. S. Annis, A. D. Huberman, E. M. Green, J. Lawler, R. Dolmetsch, K. C. Garcia, S. J. Smith, Z. D. Luo, A. Rosenthal, D. F. Mosher and B. A. Barres (2009). "Gabapentin receptor alpha2delta-1 is a neuronal thrombospondin receptor responsible for excitatory CNS synaptogenesis." Cell **139**(2): 380-392.

Fermini, B. and R. D. Nathan (1991). "Removal of sialic acid alters both T- and L-type calcium currents in cardiac myocytes." Am J Physiol **260**(3 Pt 2): H735-743.

Fischer, Y., B. H. Gahwiler and S. M. Thompson (1999). "Activation of intrinsic hippocampal theta oscillations by acetylcholine in rat septo-hippocampal cocultures." J Physiol **519 Pt 2**: 405-413.

Fisher, R. and D. Johnston (1990). "Differential modulation of single voltage-gated calcium channels by cholinergic and adrenergic agonists in adult hippocampal neurons." J Neurophysiol **64**(4): 1291-1302.

Fox, S. E., S. Wolfson and J. B. Ranck, Jr. (1986). "Hippocampal theta rhythm and the firing of neurons in walking and urethane anesthetized rats." Exp Brain Res **62**(3): 495-508.

Fraser, D. D. and B. A. MacVicar (1991). "Low-threshold transient calcium current in rat hippocampal lacunosum-moleculare interneurons: kinetics and modulation by neurotransmitters." J Neurosci **11**(9): 2812-2820.

Frazier, C. J., J. R. Serrano, E. G. George, X. Yu, A. Viswanathan, E. Perez-Reyes and S. W. Jones (2001). "Gating kinetics of the alpha1I T-type calcium channel." J Gen Physiol **118**(5): 457-470.

Galvan, E. J., K. E. Cosgrove and G. Barrionuevo (2011). "Multiple forms of long-term synaptic plasticity at hippocampal mossy fiber synapses on interneurons." Neuropharmacology **60**(5): 740-747.

Gasparini, S., M. Migliore and J. C. Magee (2004). "On the initiation and propagation of dendritic spikes in CA1 pyramidal neurons." J Neurosci **24**(49): 11046-11056.

Giessel, A. J. and B. L. Sabatini (2010). "M1 muscarinic receptors boost synaptic potentials and calcium influx in dendritic spines by inhibiting postsynaptic SK channels." Neuron **68**(5): 936-947.

Gillessen, T. and C. Alzheimer (1997). "Amplification of EPSPs by low Ni(2+)- and amiloride-sensitive Ca2+ channels in apical dendrites of rat CA1 pyramidal neurons." J Neurophysiol **77**(3): 1639-1643.

Gilmore, A. J., M. Heblinski, A. Reynolds, M. Kassiou and M. Connor (2012). "Inhibition of human recombinant T-type calcium channels by N-arachidonoyl 5-HT." Br J Pharmacol **167**(5): 1076-1088.

Gold, A. E. and R. P. Kesner (2005). "The role of the CA3 subregion of the dorsal hippocampus in spatial pattern completion in the rat." Hippocampus **15**(6): 808-814.

Golding, N. L., H. Y. Jung, T. Mickus and N. Spruston (1999). "Dendritic calcium spike initiation and repolarization are controlled by distinct potassium channel subtypes in CA1 pyramidal neurons." J Neurosci **19**(20): 8789-8798.

Golding, N. L. and N. Spruston (1998). "Dendritic sodium spikes are variable triggers of axonal action potentials in hippocampal CA1 pyramidal neurons." Neuron **21**(5): 1189-1200.

Gollo, L. L., O. Kinouchi and M. Copelli (2009). "Active dendrites enhance neuronal dynamic range." PLoS Comput Biol **5**(6): e1000402.

Guerineau, N. C., J. L. Bossu, B. H. Gahwiler and U. Gerber (1995). "Activation of a nonselective cationic conductance by metabotropic glutamatergic and muscarinic agonists in CA3 pyramidal neurons of the rat hippocampus." J Neurosci **15**(6): 4395-4407.

Guerineau, N. C., B. H. Gahwiler and U. Gerber (1994). "Reduction of resting K+ current by metabotropic glutamate and muscarinic receptors in rat CA3 cells: mediation by G-proteins." J Physiol **474**(1): 27-33.

Gupta, A. S., M. A. van der Meer, D. S. Touretzky and A. D. Redish (2012). "Segmentation of spatial experience by hippocampal theta sequences." Nat Neurosci **15**(7): 1032-1039.

Guzowski, J. F., J. J. Knierim and E. I. Moser (2004). "Ensemble dynamics of hippocampal regions CA3 and CA1." Neuron **44**(4): 581-584.

Hagiwara, N., H. Irisawa and M. Kameyama (1988). "Contribution of two types of calcium currents to the pacemaker potentials of rabbit sino-atrial node cells." J Physiol **395**: 233-253.

Hagiwara, S., S. Ozawa and O. Sand (1975). "Voltage clamp analysis of two inward current mechanisms in the egg cell membrane of a starfish." J Gen Physiol **65**(5): 617-644.

Hall, D. D., S. Dai, P. Y. Tseng, Z. Malik, M. Nguyen, L. Matt, K. Schnizler, A. Shephard, D. P. Mohapatra, F. Tsuruta, R. E. Dolmetsch, C. J. Christel, A. Lee, A. Burette, R. J. Weinberg and J. W. Hell (2013). "Competition between alpha-actinin and Ca(2)(+)-calmodulin controls surface retention of the L-type Ca(2)(+) channel Ca(V)1.2." Neuron **78**(3): 483-497.

Hell, J. W., R. E. Westenbroek, C. Warner, M. K. Ahlijanian, W. Prystay, M. M. Gilbert, T. P. Snutch and W. A. Catterall (1993). "Identification and differential subcellular localization of the neuronal class C and class D L-type calcium channel alpha 1 subunits." J Cell Biol **123**(4): 949-962.

Henze, D. A., W. E. Cameron and G. Barrionuevo (1996). "Dendritic morphology and its effects on the amplitude and rise-time of synaptic signals in hippocampal CA3 pyramidal cells." J Comp Neurol **369**(3): 331-344.

Henze, D. A., D. B. McMahon, K. M. Harris and G. Barrionuevo (2002). "Giant miniature EPSCs at the hippocampal mossy fiber to CA3 pyramidal cell synapse are monoquantal." J Neurophysiol **87**(1): 15-29.

Herbert, J. M., J. M. Augereau, J. Gleye and J. P. Maffrand (1990). "Chelerythrine is a potent and specific inhibitor of protein kinase C." Biochem Biophys Res Commun **172**(3): 993-999.

Herrington, J. and C. J. Lingle (1992). "Kinetic and pharmacological properties of low voltage-activated Ca2+ current in rat clonal (GH3) pituitary cells." J Neurophysiol **68**(1): 213-232.

Higley, M. J. and B. L. Sabatini (2008). "Calcium signaling in dendrites and spines: practical and functional considerations." Neuron **59**(6): 902-913.

Hildebrand, M. E., L. S. David, J. Hamid, K. Mulatz, E. Garcia, G. W. Zamponi and T. P. Snutch (2007). "Selective inhibition of Cav3.3 T-type calcium channels by Galphaq/11-coupled muscarinic acetylcholine receptors." J Biol Chem **282**(29): 21043-21055.

Hildebrand, M. E., P. Isope, T. Miyazaki, T. Nakaya, E. Garcia, A. Feltz, T. Schneider, J. Hescheler, M. Kano, K. Sakimura, M. Watanabe, S. Dieudonne and T. P. Snutch (2009). "Functional coupling between mGluR1 and Cav3.1 T-type calcium channels contributes to parallel fiber-induced fast calcium signaling within Purkinje cell dendritic spines." J Neurosci **29**(31): 9668-9682.

Hoffman, D. A. and D. Johnston (1998). "Downregulation of transient K+ channels in dendrites of hippocampal CA1 pyramidal neurons by activation of PKA and PKC." J Neurosci **18**(10): 3521-3528.

Hoffman, D. A. and D. Johnston (1999). "Neuromodulation of dendritic action potentials." J Neurophysiol **81**(1): 408-411.

Hoffman, D. A., J. C. Magee, C. M. Colbert and D. Johnston (1997). "K+ channel regulation of signal propagation in dendrites of hippocampal pyramidal neurons." Nature **387**(6636): 869-875.

Hoppa, M. B., B. Lana, W. Margas, A. C. Dolphin and T. A. Ryan (2012). "alpha2delta expression sets presynaptic calcium channel abundance and release probability." Nature **486**(7401): 122-125.

Hsu, C. L., H. W. Yang, C. T. Yen and M. Y. Min (2012). "A requirement of low-threshold calcium spike for induction of spike-timing-dependent plasticity at corticothalamic synapses on relay neurons in the ventrobasal nucleus of rat thalamus." Chin J Physiol **55**(6): 380-389.

Huang, W. C., S. Xiao, F. Huang, B. D. Harfe, Y. N. Jan and L. Y. Jan (2012). "Calcium-activated chloride channels (CaCCs) regulate action potential and synaptic response in hippocampal neurons." Neuron **74**(1): 179-192.

Huerta, P. T. and J. E. Lisman (1993). "Heightened synaptic plasticity of hippocampal CA1 neurons during a cholinergically induced rhythmic state." Nature **364**(6439): 723-725.

Huerta, P. T. and J. E. Lisman (1995). "Bidirectional synaptic plasticity induced by a single burst during cholinergic theta oscillation in CA1 in vitro." Neuron **15**(5): 1053-1063.

Hughes, S. W., D. W. Cope, K. L. Blethyn and V. Crunelli (2002). "Cellular mechanisms of the slow (<1 Hz) oscillation in thalamocortical neurons in vitro." Neuron **33**(6): 947-958.

Iftinca, M., J. Hamid, L. Chen, D. Varela, R. Tadayonnejad, C. Altier, R. W. Turner and G. W. Zamponi (2007). "Regulation of T-type calcium channels by Rho-associated kinase." Nat Neurosci **10**(7): 854-860.

Jackson, J., B. Amilhon, R. Goutagny, J. B. Bott, F. Manseau, C. Kortleven, S. L. Bressler and S. Williams (2014). "Reversal of theta rhythm flow through intact hippocampal circuits." Nat Neurosci **17**(10): 1362-1370.

Jacus, M. O., V. N. Uebele, J. J. Renger and S. M. Todorovic (2012). "Presynaptic Cav3.2 channels regulate excitatory neurotransmission in nociceptive dorsal horn neurons." J Neurosci **32**(27): 9374-9382.

Jan, L. Y. and Y. N. Jan (1990). "A superfamily of ion channels." Nature **345**(6277): 672.

Jentsch, T. J. (2000). "Neuronal KCNQ potassium channels: physiology and role in disease." Nat Rev Neurosci **1**(1): 21-30.

Jeong, S. W., B. G. Park, J. Y. Park, J. W. Lee and J. H. Lee (2003). "Divalent metals differentially block cloned T-type calcium channels." Neuroreport **14**(11): 1537-1540.

Jin, W. and Z. Lu (1999). "Synthesis of a stable form of tertiapin: a high-affinity inhibitor for inward-rectifier K+ channels." Biochemistry **38**(43): 14286-14293.

Johnston, D., B. R. Christie, A. Frick, R. Gray, D. A. Hoffman, L. K. Schexnayder, S. Watanabe and L. L. Yuan (2003). "Active dendrites, potassium channels and synaptic plasticity." Philos Trans R Soc Lond B Biol Sci **358**(1432): 667-674.

Johnston, D., D. A. Hoffman, J. C. Magee, N. P. Poolos, S. Watanabe, C. M. Colbert and M. Migliore (2000). "Dendritic potassium channels in hippocampal pyramidal neurons." J Physiol **525 Pt 1**: 75-81.

Johnston, J. and K. R. Delaney (2010). "Synaptic activation of T-type Ca2+ channels via mGluR activation in the primary dendrite of mitral cells." J Neurophysiol **103**(5): 2557-2569.

Joksovic, P. M., M. T. Nelson, V. Jevtovic-Todorovic, M. K. Patel, E. Perez-Reyes, K. P. Campbell, C. C. Chen and S. M. Todorovic (2006). "CaV3.2 is the major molecular substrate for redox regulation of T-type Ca2+ channels in the rat and mouse thalamus." J Physiol **574**(Pt 2): 415-430.

Kamondi, A., L. Acsady and G. Buzsaki (1998). "Dendritic spikes are enhanced by cooperative network activity in the intact hippocampus." J Neurosci **18**(10): 3919-3928.

Kamondi, A., L. Acsady, X. J. Wang and G. Buzsaki (1998). "Theta oscillations in somata and dendrites of hippocampal pyramidal cells in vivo: activity-dependent phase-precession of action potentials." Hippocampus **8**(3): 244-261.

Kang, H. W., J. Y. Park, S. W. Jeong, J. A. Kim, H. J. Moon, E. Perez-Reyes and J. H. Lee (2006). "A molecular determinant of nickel inhibition in Cav3.2 T-type calcium channels." J Biol Chem **281**(8): 4823-4830.

Khosravani, H. and G. W. Zamponi (2006). "Voltage-gated calcium channels and idiopathic generalized epilepsies." Physiol Rev **86**(3): 941-966.

Kim, S., S. J. Guzman, H. Hu and P. Jonas (2012). "Active dendrites support efficient initiation of dendritic spikes in hippocampal CA3 pyramidal neurons." Nat Neurosci **15**(4): 600-606.

Klockner, U., J. H. Lee, L. L. Cribbs, A. Daud, J. Hescheler, A. Pereverzev, E. Perez-Reyes and T. Schneider (1999). "Comparison of the Ca2 + currents induced by expression of three cloned alpha1 subunits, alpha1G, alpha1H and alpha1I, of low-voltage-activated T-type Ca2 + channels." Eur J Neurosci **11**(12): 4171-4178.

Knierim, J. J., I. Lee and E. L. Hargreaves (2006). "Hippocampal place cells: parallel input streams, subregional processing, and implications for episodic memory." Hippocampus **16**(9): 755-764.

Knopfel, T., R. Kuhn and H. Allgeier (1995). "Metabotropic glutamate receptors: novel targets for drug development." J Med Chem **38**(9): 1417-1426.

Kocsis, B., A. Bragin and G. Buzsaki (1999). "Interdependence of multiple theta generators in the hippocampus: a partial coherence analysis." J Neurosci **19**(14): 6200-6212.

Konig, P., A. K. Engel and W. Singer (1996). "Integrator or coincidence detector? The role of the cortical neuron revisited." Trends Neurosci **19**(4): 130-137.

Konopacki, J. and H. Golebiewski (1993). "Theta-like activity in hippocampal formation slices: cholinergic-GABAergic interaction." Neuroreport **4**(7): 963-966.

Konopacki, J., M. B. MacIver, B. H. Bland and S. H. Roth (1987). "Carbachol-induced EEG 'theta' activity in hippocampal brain slices." Brain Res **405**(1): 196-198.

Konopacki, J., M. B. Maciver, B. H. Bland and S. H. Roth (1987). "Theta in hippocampal slices: relation to synaptic responses of dentate neurons." Brain Res Bull **18**(1): 25-27.

Kowalczyk, T., R. Bocian and J. Konopacki (2013). "The generation of theta rhythm in hippocampal formation maintained in vitro." Eur J Neurosci **37**(5): 679-699.

Kress, G. J., M. J. Dowling, J. P. Meeks and S. Mennerick (2008). "High threshold, proximal initiation, and slow conduction velocity of action potentials in dentate granule neuron mossy fibers." J Neurophysiol **100**(1): 281-291.

Krueppel, R., S. Remy and H. Beck (2011). "Dendritic integration in hippocampal dentate granule cells." Neuron **71**(3): 512-528.

Kuo, C. C. and S. Yang (2001). "Recovery from inactivation of t-type ca2+ channels in rat thalamic neurons." J Neurosci **21**(6): 1884-1892.

Lamas, J. A., A. A. Selyanko and D. A. Brown (1997). "Effects of a cognition-enhancer, linopirdine (DuP 996), on M-type potassium currents (IK(M)) and some other voltage- and ligand-gated membrane currents in rat sympathetic neurons." Eur J Neurosci **9**(3): 605-616.

Larkum, M. E., J. J. Zhu and B. Sakmann (1999). "A new cellular mechanism for coupling inputs arriving at different cortical layers." Nature **398**(6725): 338-341.

Lassalle, J. M., T. Bataille and H. Halley (2000). "Reversible inactivation of the hippocampal mossy fiber synapses in mice impairs spatial learning, but neither consolidation nor memory retrieval, in the Morris navigation task." Neurobiol Learn Mem **73**(3): 243-257.

Le Duigou, C., J. Simonnet, M. T. Telenczuk, D. Fricker and R. Miles (2014). "Recurrent synapses and circuits in the CA3 region of the hippocampus: an associative network." Front Cell Neurosci **7**: 262.

Lee, I. and R. P. Kesner (2004). "Encoding versus retrieval of spatial memory: double dissociation between the dentate gyrus and the perforant path inputs into CA3 in the dorsal hippocampus." Hippocampus **14**(1): 66-76.

Lee, J. H., J. C. Gomora, L. L. Cribbs and E. Perez-Reyes (1999). "Nickel block of three cloned T-type calcium channels: low concentrations selectively block alpha1H." Biophys J **77**(6): 3034-3042.

Lengyel, M., Z. Szatmary and P. Erdi (2003). "Dynamically detuned oscillations account for the coupled rate and temporal code of place cell firing." Hippocampus **13**(6): 700-714.

Levey, A. I., S. M. Edmunds, V. Koliatsos, R. G. Wiley and C. J. Heilman (1995). "Expression of m1-m4 muscarinic acetylcholine receptor proteins in rat hippocampus and regulation by cholinergic innervation." J Neurosci **15**(5 Pt 2): 4077-4092.

Li, X. G., P. Somogyi, A. Ylinen and G. Buzsaki (1994). "The hippocampal CA3 network: an in vivo intracellular labeling study." J Comp Neurol **339**(2): 181-208.

Li, Y., G. Calfa, T. Inoue, M. D. Amaral and L. Pozzo-Miller (2010). "Activity-dependent release of endogenous BDNF from mossy fibers evokes a TRPC3 current and Ca2+ elevations in CA3 pyramidal neurons." J Neurophysiol **103**(5): 2846-2856.

Lievremont, J. P., G. S. Bird and J. W. Putney, Jr. (2005). "Mechanism of inhibition of TRPC cation channels by 2-aminoethoxydiphenylborane." Mol Pharmacol **68**(3): 758-762.

Lipowsky, R., T. Gillessen and C. Alzheimer (1996). "Dendritic Na+ channels amplify EPSPs in hippocampal CA1 pyramidal cells." J Neurophysiol **76**(4): 2181-2191.

Llinas, R. and Y. Yarom (1981). "Properties and distribution of ionic conductances generating electroresponsiveness of mammalian inferior olivary neurones in vitro." J Physiol **315**: 569-584.

Llinas, R. R., M. Sugimori and B. Cherksey (1989). "Voltage-dependent calcium conductances in mammalian neurons. The P channel." Ann N Y Acad Sci **560**: 103-111.

Losonczy, A. and J. C. Magee (2006). "Integrative properties of radial oblique dendrites in hippocampal CA1 pyramidal neurons." Neuron **50**(2): 291-307.

Losonczy, A., J. K. Makara and J. C. Magee (2008). "Compartmentalized dendritic plasticity and input feature storage in neurons." Nature **452**(7186): 436-441.

Luscher, C. and P. A. Slesinger (2010). "Emerging roles for G protein-gated inwardly rectifying potassium (GIRK) channels in health and disease." Nat Rev Neurosci **11**(5): 301-315.

MacVicar, B. A. and F. W. Tse (1989). "Local neuronal circuitry underlying cholinergic rhythmical slow activity in CA3 area of rat hippocampal slices." J Physiol **417**: 197-212.

Magee, J. C. and M. Carruth (1999). "Dendritic voltage-gated ion channels regulate the action potential firing mode of hippocampal CA1 pyramidal neurons." J Neurophysiol **82**(4): 1895-1901.

Magee, J. C., G. Christofi, H. Miyakawa, B. Christie, N. Lasser-Ross and D. Johnston (1995). "Subthreshold synaptic activation of voltage-gated Ca2+ channels mediates a localized Ca2+ influx into the dendrites of hippocampal pyramidal neurons." J Neurophysiol **74**(3): 1335-1342.

Magee, J. C. and D. Johnston (1995). "Synaptic activation of voltage-gated channels in the dendrites of hippocampal pyramidal neurons." Science **268**(5208): 301-304.

Magee, J. C. and D. Johnston (1997). "A synaptically controlled, associative signal for Hebbian plasticity in hippocampal neurons." Science **275**(5297): 209-213.

Magee, J. C. and D. Johnston (2005). "Plasticity of dendritic function." Curr Opin Neurobiol **15**(3): 334-342.

Major, G., A. U. Larkman, P. Jonas, B. Sakmann and J. J. Jack (1994). "Detailed passive cable models of whole-cell recorded CA3 pyramidal neurons in rat hippocampal slices." J Neurosci **14**(8): 4613-4638.

Makara, J. K., A. Losonczy, Q. Wen and J. C. Magee (2009). "Experience-dependent compartmentalized dendritic plasticity in rat hippocampal CA1 pyramidal neurons." Nat Neurosci **12**(12): 1485-1487.

Makara, J. K. and J. C. Magee (2013). "Variable dendritic integration in hippocampal CA3 pyramidal neurons." Neuron **80**(6): 1438-1450.

Marr, D. (1971). "Simple memory: a theory for archicortex." Philos Trans R Soc Lond B Biol Sci **262**(841): 23-81.

Maurer, A. P. and B. L. McNaughton (2007). "Network and intrinsic cellular mechanisms underlying theta phase precession of hippocampal neurons." Trends Neurosci **30**(7): 325-333.

McCleskey, E. W., A. P. Fox, D. H. Feldman, L. J. Cruz, B. M. Olivera, R. W. Tsien and D. Yoshikami (1987). "Omega-conotoxin: direct and persistent blockade of specific types of calcium channels in neurons but not muscle." Proc Natl Acad Sci U S A **84**(12): 4327-4331.

McHugh, T. J., M. W. Jones, J. J. Quinn, N. Balthasar, R. Coppari, J. K. Elmquist, B. B. Lowell, M. S. Fanselow, M. A. Wilson and S. Tonegawa (2007). "Dentate gyrus NMDA receptors mediate rapid pattern separation in the hippocampal network." Science **317**(5834): 94-99.

McKay, B. E., J. E. McRory, M. L. Molineux, J. Hamid, T. P. Snutch, G. W. Zamponi and R. W. Turner (2006). "Ca(V)3 T-type calcium channel isoforms differentially distribute to somatic and dendritic compartments in rat central neurons." Eur J Neurosci **24**(9): 2581-2594.

Migliore, M., D. A. Hoffman, J. C. Magee and D. Johnston (1999). "Role of an A-type K+ conductance in the back-propagation of action potentials in the dendrites of hippocampal pyramidal neurons." J Comput Neurosci **7**(1): 5-15.

Mintz, I. M., V. J. Venema, K. M. Swiderek, T. D. Lee, B. P. Bean and M. E. Adams (1992). "P-type calcium channels blocked by the spider toxin omega-Aga-IVA." Nature **355**(6363): 827-829.

Mogul, D. J. and A. P. Fox (1991). "Evidence for multiple types of Ca2+ channels in acutely isolated hippocampal CA3 neurones of the guinea-pig." J Physiol **433**: 259-281.

Monyer, H., N. Burnashev, D. J. Laurie, B. Sakmann and P. H. Seeburg (1994). "Developmental and regional expression in the rat brain and functional properties of four NMDA receptors." Neuron **12**(3): 529-540.

Nelson, M. T., P. M. Joksovic, E. Perez-Reyes and S. M. Todorovic (2005). "The endogenous redox agent L-cysteine induces T-type Ca2+ channel-dependent sensitization of a novel subpopulation of rat peripheral nociceptors." J Neurosci **25**(38): 8766-8775.

Nelson, M. T., P. M. Joksovic, P. Su, H. W. Kang, A. Van Deusen, J. P. Baumgart, L. S. David, T. P. Snutch, P. Q. Barrett, J. H. Lee, C. F. Zorumski, E. Perez-Reyes and S. M. Todorovic (2007). "Molecular mechanisms of subtype-specific inhibition of neuronal T-type calcium channels by ascorbate." J Neurosci **27**(46): 12577-12583.

Nelson, M. T., J. Woo, H. W. Kang, I. Vitko, P. Q. Barrett, E. Perez-Reyes, J. H. Lee, H. S. Shin and S. M. Todorovic (2007). "Reducing agents sensitize C-type nociceptors by relieving high-affinity zinc inhibition of T-type calcium channels." J Neurosci **27**(31): 8250-8260.

Nettleton, J. S. and W. J. Spain (2000). "Linear to supralinear summation of AMPA-mediated EPSPs in neocortical pyramidal neurons." J Neurophysiol **83**(6): 3310-3322.

Neunuebel, J. P. and J. J. Knierim (2014). "CA3 retrieves coherent representations from degraded input: direct evidence for CA3 pattern completion and dentate gyrus pattern separation." Neuron **81**(2): 416-427.

Neunuebel, J. P., D. Yoganarasimha, G. Rao and J. J. Knierim (2013). "Conflicts between local and global spatial frameworks dissociate neural representations of the lateral and medial entorhinal cortex." J Neurosci **33**(22): 9246-9258.

Newcomb, R., B. Szoke, A. Palma, G. Wang, X. Chen, W. Hopkins, R. Cong, J. Miller, L. Urge, K. Tarczy-Hornoch, J. A. Loo, D. J. Dooley, L. Nadasdi, R. W. Tsien, J. Lemos and G. Miljanich (1998). "Selective peptide antagonist of the class E calcium channel from the venom of the tarantula Hysterocrates gigas." Biochemistry **37**(44): 15353-15362.

Newman, E. L. and M. E. Hasselmo (2014). "CA3 sees the big picture while dentate gyrus splits hairs." Neuron **81**(2): 226-228.

Nowycky, M. C., A. P. Fox and R. W. Tsien (1985). "Three types of neuronal calcium channel with different calcium agonist sensitivity." Nature **316**(6027): 440-443.

O'Keefe, J. and M. L. Recce (1993). "Phase relationship between hippocampal place units and the EEG theta rhythm." Hippocampus **3**(3): 317-330.

Otsu, Y., P. Marcaggi, A. Feltz, P. Isope, M. Kollo, Z. Nusser, B. Mathieu, M. Kano, M. Tsujita, K. Sakimura and S. Dieudonne (2014). "Activity-dependent gating of calcium spikes by A-type K+ channels controls climbing fiber signaling in Purkinje cell dendrites." Neuron **84**(1): 137-151.

Pan, Z. H., H. J. Hu, P. Perring and R. Andrade (2001). "T-type Ca(2+) channels mediate neurotransmitter release in retinal bipolar cells." Neuron **32**(1): 89-98.

Park, J. Y., H. W. Kang, H. J. Moon, S. U. Huh, S. W. Jeong, N. M. Soldatov and J. H. Lee (2006). "Activation of protein kinase C augments T-type Ca2+ channel activity without changing channel surface density." J Physiol **577**(Pt 2): 513-523.

Park, J. Y., S. Remy, J. Varela, D. C. Cooper, S. Chung, H. W. Kang, J. H. Lee and N. Spruston (2010). "A post-burst after depolarization is mediated by group i metabotropic glutamate receptor-dependent upregulation of Ca(v)2.3 R-type calcium channels in CA1 pyramidal neurons." PLoS Biol **8**(11): e1000534.

Pelkey, K. A., L. Topolnik, J. C. Lacaille and C. J. McBain (2006). "Compartmentalized Ca(2+) channel regulation at divergent mossy-fiber release sites underlies target cell-dependent plasticity." Neuron **52**(3): 497-510.

Pemberton, K. E., L. J. Hill-Eubanks and S. V. Jones (2000). "Modulation of low-threshold T-type calcium channels by the five muscarinic receptor subtypes in NIH 3T3 cells." Pflugers Arch **440**(3): 452-461.

Perez-Reyes, E. (2003). "Molecular physiology of low-voltage-activated t-type calcium channels." Physiol Rev **83**(1): 117-161.

Petrovic, M. M., J. Nowacki, V. Olivo, K. Tsaneva-Atanasova, A. D. Randall and J. R. Mellor (2012). "Inhibition of post-synaptic Kv7/KCNQ/M channels facilitates long-term potentiation in the hippocampus." PLoS One **7**(2): e30402.

Petsche, H., C. Stumpf and G. Gogolak (1962). "[The significance of the rabbit's septum as a relay station between the midbrain and the hippocampus. I. The control of hippocampus arousal activity by the septum cells]." Electroencephalogr Clin Neurophysiol **14**: 202-211.

Pigeat, R., P. Chausson, F. M. Dreyfus, N. Leresche and R. C. Lambert (2015). "Sleep slow wave-related homo and heterosynaptic LTD of intrathalamic GABAAergic synapses: involvement of T-type Ca2+ channels and metabotropic glutamate receptors." J Neurosci **35**(1): 64-73.

Pin, J. P. and R. Duvoisin (1995). "The metabotropic glutamate receptors: structure and functions." Neuropharmacology **34**(1): 1-26.

Qi, Y., J. Wang, V. C. Bomben, D. P. Li, S. R. Chen, H. Sun, Y. Xi, J. G. Reed, J. Cheng, H. L. Pan, J. L. Noebels and E. T. Yeh (2014). "Hyper-SUMOylation of the Kv7 potassium channel diminishes the M-current leading to seizures and sudden death." Neuron **83**(5): 1159-1171.

Rall, W. (1967). "Distinguishing theoretical synaptic potentials computed for different soma-dendritic distributions of synaptic input." J Neurophysiol **30**(5): 1138-1168.

Randall, A. and R. W. Tsien (1995). "Pharmacological dissection of multiple types of Ca2+ channel currents in rat cerebellar granule neurons." J Neurosci **15**(4): 2995-3012.

Rangel, A., S. Sanchez-Armass and U. Meza (2010). "Protein kinase C-mediated inhibition of recombinant T-type Cav3.2 channels by neurokinin 1 receptors." Mol Pharmacol **77**(2): 202-210.

Rehak, R., T. M. Bartoletti, J. D. Engbers, G. Berecki, R. W. Turner and G. W. Zamponi (2013). "Low voltage activation of KCa1.1 current by Cav3-KCa1.1 complexes." PLoS One **8**(4): e61844.

Reid, C. A., S. Xu and D. A. Williams (2008). "Spontaneous release from mossy fiber terminals inhibits Ni2+-sensitive T-type Ca2+ channels of CA3 pyramidal neurons in the rat organotypic hippocampal slice." Hippocampus **18**(7): 623-630.

Remy, S., J. Csicsvari and H. Beck (2009). "Activity-dependent control of neuronal output by local and global dendritic spike attenuation." Neuron **61**(6): 906-916.

Reuter, H., A. B. Cachelin, J. E. De Peyer and S. Kokubun (1983). "Modulation of calcium channels in cultured cardiac cells by isoproterenol and 8-bromo-cAMP." Cold Spring Harb Symp Quant Biol **48 Pt 1**: 193-200.

Rolls, E. T. (2007). "An attractor network in the hippocampus: theory and neurophysiology." Learn Mem **14**(11): 714-731.

Rouse, S. T., M. J. Marino, L. T. Potter, P. J. Conn and A. I. Levey (1999). "Muscarinic receptor subtypes involved in hippocampal circuits." Life Sci **64**(6-7): 501-509.

Sabatini, B. L. and K. Svoboda (2000). "Analysis of calcium channels in single spines using optical fluctuation analysis." Nature **408**(6812): 589-593.

Safiulina, V. F., P. Zacchi, M. Taglialatela, Y. Yaari and E. Cherubini (2008). "Low expression of Kv7/M channels facilitates intrinsic and network bursting in the developing rat hippocampus." J Physiol **586**(Pt 22): 5437-5453.

Sanchez, M. and O. B. McManus (1996). "Paxilline inhibition of the alpha-subunit of the high-conductance calcium-activated potassium channel." Neuropharmacology **35**(7): 963-968.

Santoro, B., S. Chen, A. Luthi, P. Pavlidis, G. P. Shumyatsky, G. R. Tibbs and S. A. Siegelbaum (2000). "Molecular and functional heterogeneity of hyperpolarization-activated pacemaker channels in the mouse CNS." J Neurosci **20**(14): 5264-5275.

Schiller, J., G. Major, H. J. Koester and Y. Schiller (2000). "NMDA spikes in basal dendrites of cortical pyramidal neurons." Nature **404**(6775): 285-289.

Schmidt-Hieber, C., P. Jonas and J. Bischofberger (2007). "Subthreshold dendritic signal processing and coincidence detection in dentate gyrus granule cells." J Neurosci **27**(31): 8430-8441.

Schoepp, D. D., J. Goldsworthy, B. G. Johnson, C. R. Salhoff and S. R. Baker (1994). "3,5-dihydroxyphenylglycine is a highly selective agonist for phosphoinositide-linked metabotropic glutamate receptors in the rat hippocampus." J Neurochem **63**(2): 769-772.

Schoepp, D. D., D. E. Jane and J. A. Monn (1999). "Pharmacological agents acting at subtypes of metabotropic glutamate receptors." Neuropharmacology **38**(10): 1431-1476.

Shah, M. M., Z. Huang and K. Martinello (2013). "HCN and KV7 (M-) channels as targets for epilepsy treatment." Neuropharmacology **69**: 75-81.

Shannon, H. E., S. C. Peters and A. E. Kingston (2005). "Anticonvulsant effects of LY456236, a selective mGlu1 receptor antagonist." Neuropharmacology **49 Suppl 1**: 188-195.

Shinoe, T., M. Matsui, M. M. Taketo and T. Manabe (2005). "Modulation of synaptic plasticity by physiological activation of M1 muscarinic acetylcholine receptors in the mouse hippocampus." J Neurosci **25**(48): 11194-11200.

Simms, B. A. and G. W. Zamponi (2012). "Trafficking and stability of voltage-gated calcium channels." Cell Mol Life Sci **69**(6): 843-856.

Simms, B. A. and G. W. Zamponi (2014). "Neuronal voltage-gated calcium channels: structure, function, and dysfunction." Neuron **82**(1): 24-45.

Skaggs, W. E., B. L. McNaughton, M. A. Wilson and C. A. Barnes (1996). "Theta phase precession in hippocampal neuronal populations and the compression of temporal sequences." Hippocampus **6**(2): 149-172.

Spruston, N. (2008). "Neuroscience: strength in numbers." Nature **452**(7186): 420-421.

Spruston, N. and C. McBain (2009). Structural and functional properties of hippocampal neurons. The Hippocampus Book. P. Andersen, R. Morris, D. G. Amaral, T. V. Bliss and J. O'Keefe. New York

, Oxford University Press.

Stadtman, E. R. (1993). "Oxidation of free amino acids and amino acid residues in proteins by radiolysis and by metal-catalyzed reactions." Annu Rev Biochem **62**: 797-821.

Stewart, M. and S. E. Fox (1990). "Do septal neurons pace the hippocampal theta rhythm?" Trends Neurosci **13**(5): 163-168.

Sun, M. K. and D. L. Alkon (2014). "The "memory kinases": roles of PKC isoforms in signal processing and memory formation." Prog Mol Biol Transl Sci **122**: 31-59.

Swartz, K. J. and B. P. Bean (1992). "Inhibition of calcium channels in rat CA3 pyramidal neurons by a metabotropic glutamate receptor." J Neurosci **12**(11): 4358-4371.

Tai, C., J. B. Kuzmiski and B. A. MacVicar (2006). "Muscarinic enhancement of R-type calcium currents in hippocampal CA1 pyramidal neurons." J Neurosci **26**(23): 6249-6258.

Talavera, K. and B. Nilius (2006). "Biophysics and structure-function relationship of T-type Ca2+ channels." Cell Calcium **40**(2): 97-114.

Tan, G. M., D. Yu, J. Wang and T. W. Soong (2012). "Alternative splicing at C terminus of Ca(V)1.4 calcium channel modulates calcium-dependent inactivation, activation potential, and current density." J Biol Chem **287**(2): 832-847.

Tang, A. H., M. A. Karson, D. A. Nagode, J. M. McIntosh, V. N. Uebele, J. J. Renger, M. Klugmann, T. A. Milner and B. E. Alger (2011). "Nerve terminal nicotinic acetylcholine receptors initiate quantal GABA release from perisomatic interneurons by activating axonal T-type (Cav3) Ca(2)(+) channels and Ca(2)(+) release from stores." J Neurosci **31**(38): 13546-13561.

Teles-Grilo Ruivo, L. M. and J. R. Mellor (2013). "Cholinergic modulation of hippocampal network function." Front Synaptic Neurosci **5**: 2.

Thomas, M. J., A. M. Watabe, T. D. Moody, M. Makhinson and T. J. O'Dell (1998). "Postsynaptic complex spike bursting enables the induction of LTP by theta frequency synaptic stimulation." J Neurosci **18**(18): 7118-7126.

Thuault, S. (2014). "A two-way street." Nat Neurosci **17**(10): 1297.

Todorovic, S. M. and V. Jevtovic-Todorovic (2006). "The role of T-type calcium channels in peripheral and central pain processing." CNS Neurol Disord Drug Targets **5**(6): 639-653.

Todorovic, S. M., V. Jevtovic-Todorovic, A. Meyenburg, S. Mennerick, E. Perez-Reyes, C. Romano, J. W. Olney and C. F. Zorumski (2001). "Redox modulation of T-type calcium channels in rat peripheral nociceptors." Neuron **31**(1): 75-85.

Todorovic, S. M. and C. J. Lingle (1998). "Pharmacological properties of T-type Ca2+ current in adult rat sensory neurons: effects of anticonvulsant and anesthetic agents." J Neurophysiol **79**(1): 240-252.

Toth, K., T. F. Freund and R. Miles (1997). "Disinhibition of rat hippocampal pyramidal cells by GABAergic afferents from the septum." J Physiol **500 (Pt 2)**: 463-474.

Traboulsie, A., J. Chemin, M. Chevalier, J. F. Quignard, J. Nargeot and P. Lory (2007). "Subunit-specific modulation of T-type calcium channels by zinc." J Physiol **578**(Pt 1): 159-171.

Tran-Van-Minh, A., R. D. Caze, T. Abrahamsson, L. Cathala, B. S. Gutkin and D. A. DiGregorio (2015). "Contribution of sublinear and supralinear dendritic integration to neuronal computations." Front Cell Neurosci **9**: 67.

Traub, R. D., R. Miles and G. Buzsaki (1992). "Computer simulation of carbachol-driven rhythmic population oscillations in the CA3 region of the in vitro rat hippocampus." J Physiol **451**: 653-672.

Tringham, E., K. L. Powell, S. M. Cain, K. Kuplast, J. Mezeyova, M. Weerapura, C. Eduljee, X. Jiang, P. Smith, J. L. Morrison, N. C. Jones, E. Braine, G. Rind, M. Fee-Maki, D. Parker, H. Pajouhesh, M. Parmar, T. J. O'Brien and T. P. Snutch (2012). "T-type calcium channel blockers that attenuate thalamic burst firing and suppress absence seizures." Sci Transl Med **4**(121): 121ra119.

Tsubokawa, H. and W. N. Ross (1997). "Muscarinic modulation of spike backpropagation in the apical dendrites of hippocampal CA1 pyramidal neurons." J Neurosci **17**(15): 5782-5791.

Ulrich, D. and J. R. Huguenard (1997). "GABA(A)-receptor-mediated rebound burst firing and burst shunting in thalamus." J Neurophysiol **78**(3): 1748-1751.

van der Staay, F. J., R. J. Fanelli, A. Blokland and B. H. Schmidt (1999). "Behavioral effects of apamin, a selective inhibitor of the SK(Ca)-channel, in mice and rats." Neurosci Biobehav Rev **23**(8): 1087-1110.

Waithe, D., L. Ferron, K. M. Page, K. Chaggar and A. C. Dolphin (2011). "Beta-subunits promote the expression of Ca(V)2.2 channels by reducing their proteasomal degradation." J Biol Chem **286**(11): 9598-9611.

Wang, B., D. B. Jaffe and R. Brenner (2014). "Current understanding of iberiotoxin-resistant BK channels in the nervous system." Front Physiol **5**: 382.

Wang, K., M. T. Lin, J. P. Adelman and J. Maylie (2014). "Distinct Ca2+ sources in dendritic spines of hippocampal CA1 neurons couple to SK and Kv4 channels." Neuron **81**(2): 379-387.

Wei, D. S., Y. A. Mei, A. Bagal, J. P. Kao, S. M. Thompson and C. M. Tang (2001). "Compartmentalized and binary behavior of terminal dendrites in hippocampal pyramidal neurons." Science **293**(5538): 2272-2275.

Welsby, P. J., H. Wang, J. T. Wolfe, R. J. Colbran, M. L. Johnson and P. Q. Barrett (2003). "A mechanism for the direct regulation of T-type calcium channels by Ca2+/calmodulin-dependent kinase II." J Neurosci **23**(31): 10116-10121.

Williams, S. R. and S. J. Mitchell (2008). "Direct measurement of somatic voltage clamp errors in central neurons." Nat Neurosci **11**(7): 790-798.

Wolfe, J. T., H. Wang, J. Howard, J. C. Garrison and P. Q. Barrett (2003). "T-type calcium channel regulation by specific G-protein betagamma subunits." Nature **424**(6945): 209-213.

Wolfe, J. T., H. Wang, E. Perez-Reyes and P. Q. Barrett (2002). "Stimulation of recombinant Ca(v)3.2, T-type, Ca(2+) channel currents by CaMKIIgamma(C)." J Physiol **538**(Pt 2): 343-355.

Yao, J. A. and G. N. Tseng (1994). "Modulation of 4-AP block of a mammalian A-type K channel clone by channel gating and membrane voltage." Biophys J **67**(1): 130-142.

Yassa, M. A. and C. E. Stark (2011). "Pattern separation in the hippocampus." Trends Neurosci **34**(10): 515-525.

Yasuda, R., B. L. Sabatini and K. Svoboda (2003). "Plasticity of calcium channels in dendritic spines." Nat Neurosci **6**(9): 948-955.

Young, S. R., S. C. Chuang and R. K. Wong (2004). "Modulation of afterpotentials and firing pattern in guinea pig CA3 neurones by group I metabotropic glutamate receptors." J Physiol **554**(Pt 2): 371-385.

Young, S. Z., J. C. Platel, J. V. Nielsen, N. A. Jensen and A. Bordey (2010). "GABA(A) Increases Calcium in Subventricular Zone Astrocyte-Like Cells Through L- and T-Type Voltage-Gated Calcium Channels." Front Cell Neurosci **4**: 8.

Zamponi, G. W., E. Bourinet, D. Nelson, J. Nargeot and T. P. Snutch (1997). "Crosstalk between G proteins and protein kinase C mediated by the calcium channel alpha1 subunit." Nature **385**(6615): 442-446.

Zamponi, G. W., E. Bourinet and T. P. Snutch (1996). "Nickel block of a family of neuronal calcium channels: subtype- and subunit-dependent action at multiple sites." J Membr Biol **151**(1): 77-90.

Zhang, Y., X. Jiang, T. P. Snutch and J. Tao (2013). "Modulation of low-voltage-activated T-type Ca(2)(+) channels." Biochim Biophys Acta **1828**(7): 1550-1559.

Zhang, Y., L. Zhang, F. Wang, Y. Zhang, J. Wang, Z. Qin, X. Jiang and J. Tao (2011). "Activation of M3 muscarinic receptors inhibits T-type Ca(2+) channel currents via pertussis toxin-sensitive novel protein kinase C pathway in small dorsal root ganglion neurons." Cell Signal **23**(6): 1057-1067.